IMPACTS OF MIDPOINT FACTS CONTROLLERS ON THE COORDINATION BETWEEN GENERATOR PHASE BACKUP PROTECTION AND GENERATOR CAPABILITY LIMITS

A Thesis

Submitted to the College of Graduate Studies and Research

in Partial Fulfillment of the Requirements

For the Degree of Doctor of Philosophy

in the Department of Electrical and Computer Engineering

University of Saskatchewan

Saskatoon, Saskatchewan

By

Mohamed Salah Kamel Elsamahy

PERMISSION TO USE

I agree that the Library, University of Saskatchewan, may make this thesis freely available for inspection. I further agree that permission for copying of this thesis for scholarly purpose may be granted by the professor or professors who supervised the thesis work recorded herein or, in their absence, by the Head of the Department or the Dean of the College in which the thesis work was done. It is understood that due recognition will be given to me and to the University of Saskatchewan in any use of the material in this thesis. Copying or publication or any other use of this thesis for financial gain without approval by the University of Saskatchewan and my written permission is prohibited.

Request for permission to copy or to make any other use of the material in this thesis in whole or part should be addressed to:

Head of the Department of Electrical and Computer Engineering
57 Campus Drive
University of Saskatchewan
Saskatoon, Saskatchewan
Canada S7N 5A9

ABSTRACT

The thesis reports the results of comprehensive studies carried out to explore the impact of midpoint FACTS Controllers (STATCOM and SVC) on the generator distance phase backup protection in order to identify important issues that protection engineers need to consider when designing and setting a generator protection system. In addition, practical, feasible and simple solutions to mitigate the adverse impact of midpoint FACTS Controllers on the generator distance phase backup protection are explored.

The results of these studies show that midpoint FACTS Controllers have an adverse effect on the generator distance phase backup protection. This adverse effect, which can be in the form of underreach, overreach or a time delay, varies according to the fault type, fault location and generator loading. Moreover, it has been found that the adverse effect of the midpoint FACTS Controllers extends to affect the coordination between the generator distance phase backup protection and the generator steady-state overexcited capability limit.

The Support Vector Machines classification technique is proposed as a replacement for the existing generator distance phase backup protection relay in order to alleviate potential problems. It has been demonstrated that this technique is a very promising solution, as it is fast, reliable and has a high performance efficiency. This will result in enhancing the coordination between the generator phase backup protection and the generator steady-state overexcited capability limit in the presence of midpoint FACTS Controllers.

The thesis also presents the results of investigations carried out to explore the impact of the generator distance phase backup protection relay on the generator overexcitation thermal capability. The results of these investigations reveal that with the relay settings according to the current standards, the generator is over-protected and the generator distance phase backup protection relay restricts the generator overexcitation thermal capability during system disturbances. This restriction does not allow the supply of the maximum reactive power of the generating unit during such events. The restriction on the generator overexcitation thermal capability caused by the generator distance phase backup protection relay highlights the necessity to revise the relay settings. The proposed solution in this thesis is to reduce the

generator distance phase backup protection relay reach in order to provide secure performance during system disturbances.

ACKNOWLEDGMENTS

My first, and most earnest, acknowledgment must go to my supervisor, Dr. Sherif O. Faried. Since my arrival in Saskatoon nearly three years ago, Dr. Faried has been instrumental in ensuring my academic, professional and moral well-being ever since. In every sense, none of this work would have been possible without him. I attribute the level of my doctoral degree to his encouragement and effort and without him this thesis, too, would not have been completed. Dr. Faried is the one professor/teacher who has truly made a difference in my life. The joy and enthusiasm he has for his research was contagious and motivational for me. One simply could not wish for a better or friendlier supervisor.

I am also deeply indebted to the members of the Ph.D. Advisory Committee, Professors Ha Nguyen, M. Boulfiza, A.M. El-Serafi and N. Chowdhury for their valuable advices and encouragement.

I would like also to express my deeply-felt thanks to Professor Mohamed Mansour of Ain Shams University, Egypt who put me on the track of power system protection, for his continuous warm encouragement and thoughtful guidance.

I dedicate this work to

my father, ***Professor | Salah Kamel Elsamahy,***

my beloved mother, ***Professor | Mona Ahmed Sadek,***

for their absolute and infinite love, moral support and encouragements

and

my son, ***Adham Mohamed Salah Elsamahy***

to inspire him to be a great man

TABLE OF CONTENTS

LIST OF FIGURES

LIST OF TABLES

LIST OF SYMBOLS

$\boldsymbol{\alpha}$	Lagrangian multiplier vector
ANN	Artificial Neural Network
b	Bias
B_{ref}	Susceptance p.u. signal (IEEE basic model 1 for SVC)
B_{max}	Maximum limit of susceptance p.u. signal (IEEE basic model 1 for SVC)
B_{min}	Minimum limit of susceptance p.u. signal (IEEE basic model 1 for SVC)
C	Control parameter for the trade-off between the slack variable penalty and the size of the margin.
Class A	Group containing the red balls
Class B	Group containing the black balls
C_a	Capacitor
CT	Current transformer
CI	Coordination Index
DWT	Discrete Wavelet Transform
δ	Phase angle difference between the receiving and the sending ends in Figure 1.2(a)
$E_{STATCOM}$ (E_s)	STATCOM three-phase output voltage
$E_{utitlity}$ (E_t)	Utility bus voltage
E_f	Internal or rotor field excitation voltage
E	Generator internal voltage
$\eta_{training}$	SVM training performance efficiency
$\eta_{testing}$	SVM testing performance efficiency
$\eta_{21\text{-}perf}$	Relay (21) performance efficiency
$\eta_{SVM\text{-}D}$	SVM_D module performance efficiency
$\eta_{SVM\text{-}reach}$	SVM_Reach module performance efficiency
$\eta_{21\text{-}Coord}$	Coordination efficiency between Relay (21) and GOEC
$\eta_{generalization}$	SVM scheme generalization efficiency
$\eta_{overall\text{-}testing}$	SVM scheme overall efficiency during testing
$\eta_{overall\text{-}generalization}$	SVM scheme overall efficiency during generalization

ξ	Slack variable
FOR	False Overreach
FUR	False Underreach
GCC	Generator capability curve
GOEC	Generator steady-state overexcited capability limit
GUEC	Generator steady-state underexcited capability limit
GSU transformer	Generator step up transformer
G_1	A hydrogenerator in System I
G_2	A turbogenerator in System II
γ	Gaussian Kernel control parameter
$\boldsymbol{H_P}$, $\boldsymbol{H_{P\ new}}$	Separating hyperplanes
$\boldsymbol{H_{P1}}$, $\boldsymbol{H_{P1}}$ $\boldsymbol{H_{P1\ new}}$, $\boldsymbol{H_{P1\ new}}$	Decision boundaries
$\boldsymbol{H}$	Hessian matrix
I_{SVC}	SVC current
$I_{STATCOM}$	STATCOM current
I_{dc}	Capacitor dc current
I_{CC}	SVC/STATCOM capacitive current
$I_{CC\ max}$	SVC/STATCOM maximum capacitive current
I_{LL}	SVC/STATCOM inductive current
$I_{LL\ max}$	SVC/STATCOM maximum inductive current
I_A, I_B, I_C	Phase currents
I_0, I_1, I_2	Sequence components of the phase currents
I_{21}	Relay (21) current
I_f	Fault current
i	i^{th} attributes of training vector
I_{FD}	Field current
$I_{FD\ RATED}$	Rated field current
I_{FF}	Maximum field current limit
I_{safe}	Safe field current value
I_{Pickup}	Field current pickup value
K_R	Static gain (IEEE basic model 1 for SVC)
K_{Idc}	STATCOM dc capacitor voltage control integration gain

K_{pdc}	Proportional gain (STATCOM controller)
K_{mv}	STATCOM voltage control gain
k	Polynomial Kernel parameter
$K(x_i, x_j)$	Kernel function
$K_{n,k}^{polynomial}(\boldsymbol{x_i}, \boldsymbol{x_j})$	Polynomial Kernel function
$K_{\boldsymbol{\gamma}}^{Gaussian}(\boldsymbol{x_i}, \boldsymbol{x_j})$	Gaussian Kernel function
L_D	Dual Lagrangian expression
L_P	Primal Lagrangian expression
L_a	Inductor
MTA	Relay (21) Maximum Torque Angle
MLPs	Multi Layer Perceptrons
M	Midpoint of transmission lines during investigations
m	Modulation ratio
m_{min}	Maximum limit of the STATCOM modulation ratio
m_{max}	Minimum limit of STATCOM modulation ratio
m_r	Separating margin
max_i	Maximum value of the i^{th} attributes of a training vector
min_i	Minimum value of the i^{th} attributes of a training vector
$\boldsymbol{\mu}$	Lagrangian multiplier for error control
n	Polynomial Kernel degree
N	Number of elements in the training vector $\boldsymbol{x}$
$N_{correct\text{-}testing}$	Number of cases where SVM_D and SVM_Reach produced simultaneously correct decisions during testing.
$N_{correct\text{-}generalization}$	Number of cases where SVM_D and SVM_Reach produced simultaneously correct decisions during generalization.
OEL	Overexcitation Limiter
P	Active (real) power
PEMI (Error, %)	Percentage error in the measured impedance by Relay (21)
$\emptyset(\boldsymbol{x})$	Mapping function
Q	Reactive power (MVAR)
Q_{Comp}	Reactive power injected by an ideal midpoint compensator
QP	Quadratic Programming

R_{21}	Relay (21)
R_c	Current transformation ratio
R_v	Voltage transformation ratio
RPFA	Rated Power Factor Angle
SCR	Short Circuit Ratio
S_1, S_2, S_3	System 1, System 2 and System 3 (System II)
S	Set of indices of the support vectors
Set_1	Main training data set obtained during three-phase faults
Set_2	Reduced training data set obtained during three-phase faults
Set_t	Testing data set obtained during three-phase faults
Set_g	Generalization data set obtained during line-to-line faults
SVM_D	SVM fault detection module
SVM_Reach	SVM zone identification module
SV	Support Vector
T_{mv}	STATCOM voltage control time constant
TOR	True Overreach
TSA	Transient Stability Analysis
TUR	True Underreach
T_{Idc}	STATCOM dc capacitor voltage control time constant
T_R	Transient time constant (IEEE basic model 1 for SVC)
T_1, T_2	Time constants (SVC/STATCOM controllers)
Trip	Relay (21) trip signal
T_{FF}	Field forcing time
$\Delta\theta_{dc}$	Phase lag angle change (STATCOM controller)
$\Delta\theta_{dcmax}$	Maximum phase lag angle change (STATCOM controller)
$\Delta\theta_{dcmin}$	Minimum phase lag angle change (STATCOM controller)
θ_{corr}	Phase angle of the impedance corresponding to the measured impedance by Relay (21) with STATCOM in service on the Z_{GCC} circumference
UEL	Underexcitation limiter
V_t	Generator terminal voltage
V_{21}	Measured voltage at Relay (21) location

V_m	Ideal FACTS Controller voltage of Figure 1.2(a)
V_{sm}	Voltage of the midpoint between the sending end and the transmission line midpoint of Figure 1.2(a)
V_{mr}	Voltage of the midpoint between the midpoint and the receiving end of Figure 1.2(a)
V_{ref}	Reference voltage signal (IEEE basic model 1 for SVC)
V_{meas}	Measured voltage signal (IEEE basic model 1 for SVC)
V_e	Error voltage signal (IEEE basic model 1 for SVC)
VT	Voltage transformer
V_A, V_B, V_C	Phase voltages
V_0, V_1, V_2	Sequence components of the phase voltages
V_{dc}	Capacitor dc voltage
$V_{midpoint}$	Transmission line midpoint voltage
v_{inj}	Injected voltage by series FACTS Controllers
$\boldsymbol{w}$	Weight vector
$\boldsymbol{x}$	Training sample vector $\boldsymbol{x}$
$\boldsymbol{x_1}$	Input vector to the SVM fault detection module
$\boldsymbol{x_2}$	Input vector to the SVM fault zone identification module
$\boldsymbol{x_{norm}}$	Normalized training vector
$\boldsymbol{x_S}$	Support vector
$\boldsymbol{x_{unknown}}$	Unknown sample
X_{g2}	Generator negative-sequence reactance
X_d	Generator direct-axis synchronous reactance
$X_d^{/}$	Generator direct-axis transient reactance
X_{tr}	Transformer reactance
y	Label vector associated with a sample vector $\boldsymbol{x}$
y_{unkown}	Classification of an unknown sample
Z_{Sys1}, Z_{Sys2}, Z_{Sys3}	System equivalent impedance
Z_{AB}, Z_{BC}, Z_{CA}	Phase impedances measured by Relay (21)
Z_{s1}, Z_{s2}	Sequence components of the phase impedances
Z_S	Impedance measured by Relay (21) with STATCOM/SVC in service
Z_N	Impedance measured by relay (21) without

	STATCOM/SVC
Z_{GCC}	Maximum setting of Relay (21) to keep the coordination with GOEC limit
Z_{21}	Impedance measured by Relay (21)
Z_{corr}	Magnitude of the impedance corresponding to the measured impedance by Relay (21) with STATCOM/SVC in service on the Z_{GCC} circumference

1. INTRODUCTION

1.1 General

Growth of electric power transmission facilities is restricted despite the fact that bulk power transfers and use of transmission systems by third parties are increasing. Transmission bottlenecks, non-efficient utilization of transmission capacity and unwanted parallel-path or loop flows are not uncommon. Transmission system expansion is needed, but not easily accomplished. Factors that contribute to this situation include a variety of environmental, land-use and regulatory requirements. As a result, the utility industry is facing the challenge of the efficient utilization of the existing AC transmission lines. Thus, the transmission systems are being pushed to operate closer to their stability and thermal limits.

Flexible AC Transmission Systems (FACTS) technology is an important tool for permitting existing transmission facilities to be loaded, at least under contingency situations, up to their thermal limits without degrading system security [1]-[4]. FACTS Controllers provide the flexibility of controlling both real (active) and reactive power which could result in an excellent capability for improving power system dynamics.

1.2 FACTS Controllers

FACTS Controllers are power electronic based controllers which can influence transmission system voltages, currents, impedances and/or phase angles rapidly. Thus, such controllers can improve both the security and flexibility of a power system. System security may be improved by enhancing its small signal stability and transient stability as well as by damping subsynchronous resonance oscillations. System flexibility may be improved by the control of the active and reactive power flow, loop flow, voltage and short-circuit level.

In general, FACTS Controllers can be divided into four categories [2]:

1. Series controllers: In principle, all these controllers inject voltage in series with the line (Figure 1.1(b)). Even a variable impedance multiplied by the current flow through it, represents an injected series voltage in the line. As long as the voltage is in phase

quadrature with the line current, the series controller only supplies or consumes variable reactive power. The two series FACTS Controllers that have been in use in the transmission grid are the Thyristor Controlled Series Capacitor (TCSC) and the Static Synchronous Series Compensator (SSSC) [2], [4].

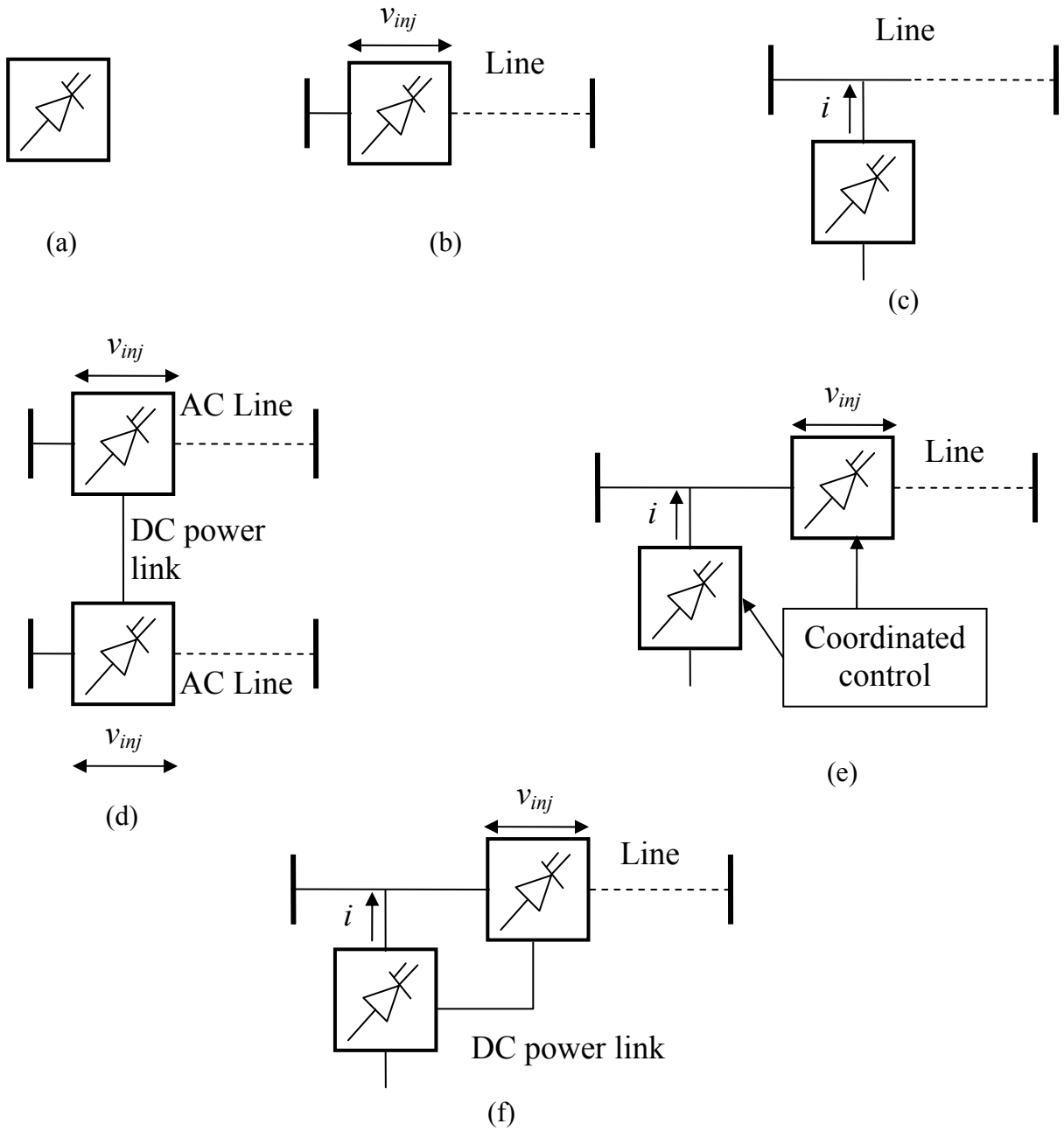

Figure 1.1. Basic types of FACTS Controllers: (a) general symbol for a FACTS Controller, (b) series controller, (c) shunt controller, (d) unified series-series controller, (e) coordinated series and shunt controller, (f) unified series-shunt controller.

2. Shunt controllers: In principle, all these controllers inject current into the system at the point of connection (Figure 1.1(c)). Even a variable shunt impedance connected to the line causes a variable current flow and, hence, represents injection of current into the line. The two shunt FACTS Controllers that have been in use in the transmission grid are the Static Var Compensator (SVC) and the Static Synchronous Compensator (STATCOM) [2], [4].
3. Combined series-series controllers: These could be a combination of separate series controllers, which are controlled in a coordinated manner, in a multiline transmission system. Or it could be a unified controller in which the series controllers provide independent series reactive compensation for each line but also transfer real power among the lines via a dc power link (Figure 1.1(d)). The real power transfer capability of the unified series-series controller, referred to as the Interline Power Flow Controller (IPFC), makes it possible to balance both the real and reactive power flow in the lines and, thereby, maximize the utilization of the transmission system. The term "unified" here means that the dc terminals of all controllers are all connected together for real power transfer.
4. Combined series-shunt controllers: These could be a combination of separate shunt and series controllers, which are controlled in a coordinated manner (Figure 1.1(e)), or a Unified Power Flow Controller (UPFC) with series and shunt controllers connected through a dc link (Figure 1.1(f)). In principle, combined shunt and series controllers inject current into the system with the shunt part of the controller and voltage in series in the line with the series part of the controller. However, when the shunt and series controllers are unified, there can be a real power exchange between the series and shunt controllers via the dc power link.

FACTS Controllers may be based on thyristor devices with no gate turn-off (only with gate turn-on), or on power devices with gate turn-off capability. In general, the principal controllers with gate turn-off devices are based on the dc to ac converters, which can exchange active and/or reactive power with the ac system.

1.3 Transmission Line Midpoint Shunt Compensation

It has long been recognized that the steady-state transmittable power can be increased and the voltage profile along the line can be controlled by appropriate reactive shunt compensation. The ultimate objective of applying reactive shunt compensation in a transmission system is to increase the transmittable power [1], [2], [4], [5]. This may be required to improve the steady-state transmission characteristics as well as the stability of the system. Var compensation is, thus, used for voltage regulation at the midpoint (or some intermediate) to segment the transmission line and at the end of the (radial) line to prevent voltage instability as well as for dynamic voltage control to increase transient stability and damp power oscillations.

1.3.1 Principle of midpoint shunt compensation

Consider the simple two-machine (two-bus) transmission model in which an ideal var compensator is shunt connected at the midpoint of the transmission line as shown in Figure 1.2(a). For simplicity, the line is represented by its series inductive reactance. The compensator is represented by a sinusoidal ac voltage source (of the fundamental frequency) in phase with the midpoint voltage, V_m and with an amplitude identical to that of the sending and receiving end voltages ($V_m = V_s = V_r = V$). The midpoint compensator in effect segments the transmission line into two independent parts; the first segment, with an impedance of $\frac{X}{2}$, carries power from the sending end to the midpoint and the second segment, also with an impedance of $\frac{X}{2}$, carries power from the midpoint to the receiving end. The relationship between the voltages V_s, V_r, V_m (together with V_{sm}, V_{mr}) and the line segment currents I_{sm} and I_{mr} is shown by the phasor diagram in Figure 1.2(b).

For the lossless system assumed, the real power is the same at each terminal (sending end, midpoint and receiving end) of the line and it can be derived readily from the phasor diagram of Figure 1.2(b) as follows

$$\text{With } V_{sm} = V_{mr} = V\cos\frac{\delta}{4}; \quad I_{sm} = I_{mr} = I = \frac{4V}{X}\sin\frac{\delta}{4}, \tag{1.1}$$

the transmitted power is

$$P = V_{sm}I_{sm} = V_{mr}I_{mr} = V_sI_{sm}\cos\frac{\delta}{4} = VI\cos\frac{\delta}{4} = 2\frac{V^2}{X}\sin\frac{\delta}{2}. \tag{1.2}$$

Similarly, it can be shown that the reactive power injected by the midpoint compensator is

$$Q_{Comp} = 4\frac{V^2}{X}\left(1 - \cos\frac{\delta}{2}\right). \tag{1.3}$$

It can be seen from Eqs. (1.2) and (1.3) that the midpoint shunt compensation can significantly increase the transmittable power (doubling its maximum value) at the expense of a rapidly increasing reactive power demand on the midpoint compensator (and also on the end generators). It is also evident that for the system of Figure 1.2, the midpoint of the transmission line is the best location for the compensator. This is because the voltage sag along the uncompensated transmission line is the largest at the midpoint.

The two shunt FACTS Controllers that are installed and operated by utilities for transmission line midpoint compensation are the SVC and the STATCOM. The basic construction, principle of operation and control of each controller are discussed in the next chapter.

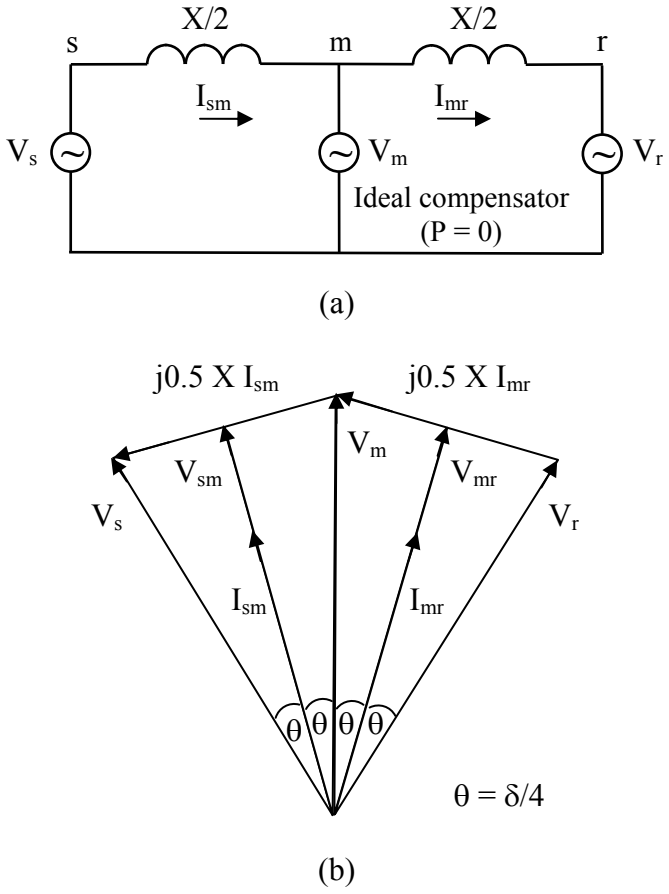

Figure 1.2. A simple model of a two-machine power system with an ideal midpoint reactive compensator: (a) schematic diagram, (b) corresponding phasor diagram.

1.4 Impact of FACTS Controllers on Power System Protection

One of the most important equipment employed in the protection of power systems are protective relays. These are one of the most flexible, economic and well-known devices that provide reliable, fast and inexpensive protection.

The IEEE defines a protective relay as "a device whose function is to detect defective lines or apparatus or other power system condition of an abnormal or dangerous nature and to initiate appropriate control action [6]. Reference [6] defines power system protection as "the science, skill and art of applying and setting relays and/or fuses to provide maximum sensitivity to system faults and undesirable conditions, but to avoid their operation on all permissible or tolerable conditions". The basic idea is to define the undesirable conditions and look for differences between the undesirable and permissible conditions that relays and fuses can sense. It is also important to remove only the faulted equipment from the system while maintaining as much of the unfaulted system as possible in service in order to continue to supply as much of the load as possible.

As the power system voltages, currents and impedances are the variables involved in power system protective relay settings and operations, the power system protection system may be affected by the presence of FACTS Controllers due to their ability to rapidly change these variables. It is, therefore, important to investigate the impact of FACTS Controllers on the power system protective system.

The impact of FACTS Controllers on the performance of distance protection of transmission lines has been investigated and reported during the last two decades. The studies reported in [7]-[12] showed that the TCSC and the UPFC have a significant impact on the distance protection causing serious problems such as relay overreach (a relay operates during faults located out of its set reach), miscoordination between zones of distance protection and directional integrity malfunction (a relay operates for faults in the reverse direction). References [13]-[15] reported the results of comprehensive investigations on the impact of midpoint STATCOM and SVC on the performance of ***distance based transmission line protection***. The results of these investigations, which are one of the main motivations to conduct this research, can be summarized as follows:

1. The performance of stand-alone and channel-aided distance protection schemes will be adversely affected by midpoints STATCOM and SVC. The two controllers affect both the steady-state and the transient trajectory of the apparent impedance seen by the distance relay. The adverse effects of these controllers on the distance relay performance cause relay mal-operations (as a result of impedance measurement error due to severe underreaching and overreaching effects), delayed response and incorrect phase selection.
2. The amount of impedance error varies depending on factors such as fault type and location.
3. The underreaching (a relay sees an impedance greater than its reach setting) effect of the midpoint STATCOM is more severe compared to that of the SVC which results in more cases of relay mal-operation. This is attributed to the distinct difference between the V-I characteristics of the two controllers which is discussed in detail in the next chapter.
4. Both the stand-alone and the channel-aided distance protection schemes fail to provide secure operation for external faults as a result of the overreaching effect of the STATCOM.

Virtually, no research work has been reported on the impact of midpoint FACTS Controllers on the performance of ***generator distance phase backup protection***. The function of such a protection is to disconnect the generator if a symmetrical or unsymmetrical phase fault outside of the generator zone of protection has not been cleared by other protective devices after a sufficient time delay (typically between 1 to 2 s) has elapsed. As the transmission line distance relay and the generator distance phase backup relay are in tandem, the midpoint FACTS Controllers will definitely have an adverse effect on the performance of the generator distance phase backup protection relay.

1.5 Distance Relay Fundamentals [16]-[19]

Distance relays utilize a combination of the voltage and current at the relay location to determine the apparent impedance seen by the relay under all conditions. In this context, the apparent impedance is defined as the relay phasor voltage divided by the relay phasor current, where both quantities are in per unit and are measured at the relay location. When there is no fault present, the relay will see normal voltages and currents, resulting in rather large values of the apparent impedance magnitude, with an impedance angle corresponding to the load power

factor. When plotted on the complex impedance (Z) plane, the apparent impedance for this type of normal condition will usually lie near the real axis, but can be either positive or negative, depending on the direction of power flow. Reactive power flow will move the apparent impedance off the real axis in either direction, depending again on the direction of flow.

It should be recognized immediately that, because the distance relay uses both the current and voltage signals at the relay location, it is inherently directional. Viewed as fundamental frequency phasor quantities, a positive direction of power flow is indicated when the current phase is within 90^{o} of the voltage.

Under fault conditions, the impedance viewed at a relay location will change drastically. First, the voltage will usually be depressed to some degree and the current will be much greater than the normal condition. This translates into a much smaller apparent impedance, which is largely reactive because the transmission line impedance between the relay and the fault point is largely reactive, except for possible arc resistance. This means that low values of impedance can be interpreted as a fault condition, with the direction to the fault point being known, as well as the approximate ohmic value, which can be interpreted as a distance to the fault.

Distance relays are designed such that a maximum impedance seeing can be adjusted to form a threshold for tripping. These relay thresholds are often plotted in the complex Z plane and may take the form of straight lines, circular arcs or complete circles. An example of a relay with three zones of protection is shown in Figure 1.3, which illustrates a circular characteristic passing through the origin, which is commonly known as a “mho” characteristic. Measurements taken by the relay that fall close to the origin and inside of the specified threshold setting are identified as faults for which the relay should operate. Measurements taken that result in impedance outside the threshold settings are conditions for which the relay should not operate. Timers are used to delay clearing if the fault is observed to fall in Zone 2 or Zone 3, with increasing delays for the more remote zones. This allows the distance relay to act as backup protection for adjacent lines.

In most cases, distance relays are set to “reach” a given distance along the protected transmission line, that is, the threshold setting is translated into a given ohmic value that is converted into the desired distance. A common reach setting might be 80 or 90% of the total length of the protected line. There is an obvious danger of trying to reach exactly 100% of the

line length, as any small error may cause an incorrect line trip due to reaching beyond the remote bus. Many distance relays offer two or more "zones" of protection, so that measurements of more distant faults will be cleared, but with a given time delay. An example of a protected transmission line with time graded settings is shown in Figure 1.4.

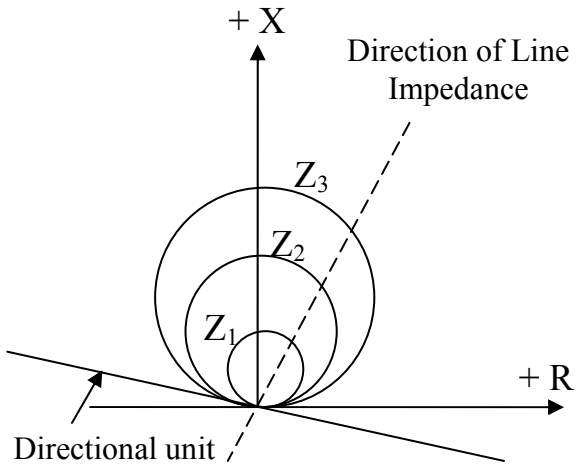

Figure 1.3. Distance protection zones in the Z plane.

Using time-graded distance protection, as shown in Figure 1.4, there is a portion of the transmission line for which all faults are within the Zone 1 setting of relays at both ends and, therefore, will be cleared without intentional time delay. Consider a line that has relays set for Zone 1 reach of 80% of the line length. This condition results in 40% of all faults being cleared following a time delay, i.e. Zone 2 clearing. This time delay may not be acceptable, especially on EHV lines that often are relied upon for high power transfer. Thus, distance protection alone may be considered inadequate for "some" transmission lines.

1.6 Generator Protection [16]-[18]

There are many different types of faults that synchronous generators may experience and, therefore, many different types of protection. All generators will not have the same level of protection, however. As a general rule, the larger, more expensive machines will have the greatest number of different protective systems simply because serious damage of these units is very costly, both in terms of the repair and also the cost due to the unavailability of the unit. Generally, all generators will have basic protection against stator short circuit, but not all

generators will have all of the other protective measures described concisely in this section. Table 1.1 provides an overview of the "major" synchronous generator protections.

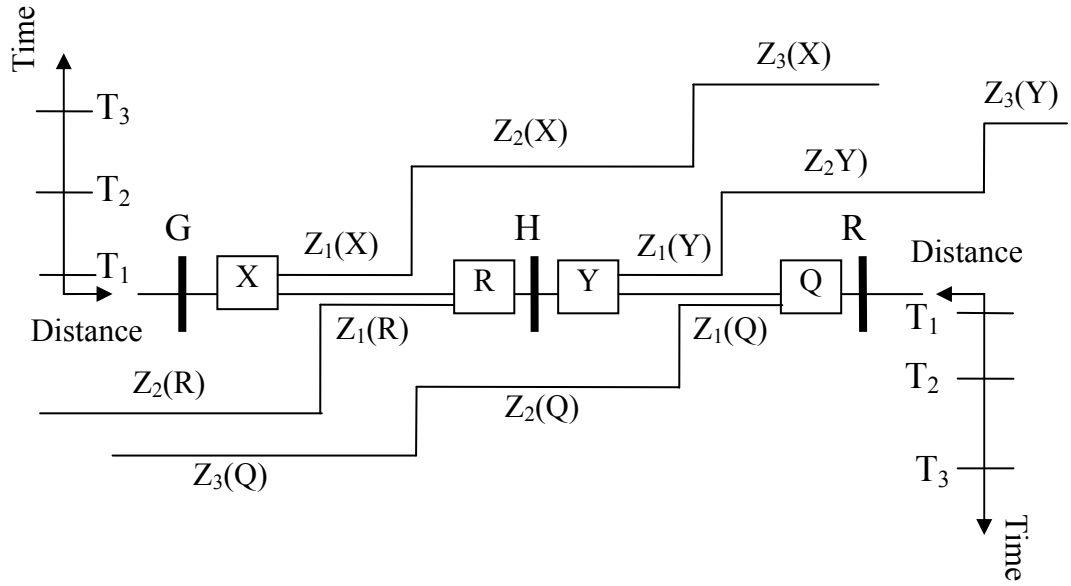

Figure 1.4. Zoned distance protection on adjacent transmission lines.

Table 1.1. An overview of major synchronous generator protections [18].

Problem Location	Type of Problem
Stator winding	Phase fault
	Ground fault
	Turn-to-turn fault
	Open circuit
	Overheating
	Overvoltage
	Unbalanced current
	Generator fault backup
	External fault backup
Field winding	Shorted winding
	Grounded winding
	Overheating
	Motoring
	Loss of excitation
	Loss of synchronism

1.6.1 Phase and ground faults protection

Stator faults result from insulation breakdown that causes an arc to develop, either from phase to phase (phase fault) or from the phase conductor to the grounded magnetic steel laminations of the stator (phase-to-ground fault). The standard method of protection against phase faults is the differential relay, and usually the percentage differential type of relay. The differential relay will not respond, however, to phase-to-ground faults occurring in generators with high grounding impedances as the fault current levels are low. A separate relay in the grounded neutral will provide sensitive protection, since it can be set without regard to the load current.

1.6.2 Turn-to-turn faults protection

Differential stator winding protection will not detect turn-to-turn faults until they become shorted to ground. Turn-to-turn faults are rare, but they can have high currents and produce significant core damage. Since the probability of occurrence of such faults is low, protection is usually not provided. There is always the back-up protection provided by ground fault relaying, since turn-to-turn faults will eventually develop into ground faults.

1.6.3 Stator open-circuit protection

Stator open-circuit protection is usually not provided, since no permanent damage is likely although it is possible that damage will accumulate due to a high resistance connection. An open circuit in one of the stator winding will cause single phasing of the generator and high negative - sequence currents. This will cause an alarm to alert the operator of the condition. Open circuits are highly unlikely in a generator and any possible damage will develop slowly, hence, there is no need for prompt tripping of the unit.

1.6.4 Overheating protection

Overheating of a synchronous generator may occur due to overload, failure of the ventilation or hydrogen cooling system, shorted laminations in the stator iron or core bolt insulation failures in the stator iron. Excessive overload is not likely since the prime mover rating is usually not much greater than the generator rating. There is a possibility of overload due to high active power load coupled with high excitation. If the power factor is below rating, this will give an

alarm for high excitation. Failure of the cooling system is also likely to be detected by operator alarms. The other failures, involving core failures and heating will develop slowly and must be detected by temperature measurements of some kind. Temperature detection is often accomplished using embedded thermocouples in the stator winding slots.

1.6.5 Overvoltage protection

Overvoltage usually occurs in a generator due to transient surges caused by lightning or switching surges. These transient are protected by surge protective devices that are designed for this purpose.

1.6.6 Unbalanced current protection

Unbalanced loading of a synchronous generator causes negative-sequence currents to flow in the stator winding. These currents are reflected in the rotor as double-frequency currents in the rotor iron, which can cause severe rotor heating and may soften or weaken the slot edges and the retaining rings. These harmful conditions may be caused by one open phase of a line, one open pole of a circuit breaker, a close-in unbalanced fault that is not promptly cleared or a stator winding fault. Negative-sequence relays are used for such unbalanced current protection.

1.6.7 Backup protection

There are two types of backup protection that might be applied to a generator; backup of relays protecting the generator protection zone and backup of relays protecting external zones. The negative-sequence relay discussed in the previous subsection might be considered a form of backup protection, since most faults should be cleared by the stator differential protection with the negative-sequence relay acting as backup. For protecting the external zones, two types of relays are commonly used; a distance type of relay (21) or a voltage restrained/voltage-controlled time-overcurrent relay (51 V). The choice of the relay type in such an application is usually a function of the type of relaying used on the lines connected to the generator. In order to simplify zones coordination, the distance backup relay is used where distance relaying is used for line protection, while the overcurrent type of backup relay is used where overcurrent relaying is used for line protection.

1.6.8 Shorted field winding protection

Shorted turns in the generator field winding have the potential for distorting the magnetic field across the air gap. This is due to the unsymmetrical ampere turns of the mmf in different parts of the field winding. If the air gap flux is badly distorted, there can be high magnitude distorted forces acting on the rotor, since the forces vary with the square of the flux density. These forces tend to wrap the rotor and, in some cases, the rotor may be displaced enough to contact the stator iron core. Vibration detectors are usually installed to alarm the operator or trip the unit.

1.6.9 Grounded field winding protection

The field winding of a synchronous machine is usually floating with respect to ground. A single ground fault, therefore, does not draw any fault current. The real danger is a second ground (shorted turns exist between the two grounds), which can set up significant forces as discussed above in subsection 1.6.8. The best way to prevent this from occurring is to detect the first ground fault. There are several methods of detecting a rotor circuit ground (e.g. potentiometer method, ac and dc injection methods).

1.6.10 Overheating of the field winding protection

The temperature of the field winding can be monitored by an ohmmeter type detector that measures the winding resistance of the field. Such an instrument is often calibrated in temperature, rather than ohms, for a direct estimation of the winding temperature.

1.6.11 Loss of excitation protection

Loss of excitation can occur as a result of loss of field to the main exciter, accidental tripping of the field breaker, short circuits in the field circuits or loss of ac supply to the excitation system. A distance relay with a mho characteristic is usually used for loss of excitation protection.

1.6.12 Loss of synchronism protection

Out-of-step protection, which is also called loss-of-synchronism protection, is typically applied on large generators to trip the machine, thereby protecting it from shaft torque damage and avoiding a system cascading event.

1.6.13 Generator motoring protection

Generator motoring (sometimes referred to as reverse active power) protection is designed for the prime mover rather than the generator. Motoring is not harmful to the generator in any way. The protection is usually considered as part of the generator protective relay system since it uses electrical quantities, usually in the form of sensitive power relays.

1.6.14 Volts per Hz protection

From the fundamental expression for the induced e.m.f. (E) in a coil, it can be shown that the flux density (B) is proportional to (E/f), where f is the frequency. Hysteresis and eddy current losses are each proportional to a power of the flux density. Therefore, impending overheating can be recognized by measuring volts per Hertz. An inverse-time volts-per-Hertz relay is used for such a protection.

1.6.15 Unit generator-transformer protection

An overview of the protection that would be expected for a unit generator-transformer system is summarized in Figure 1.5 and Table 1.2 [18]. The protective relays shown in these figure and table are the minimum recommended protection for turbogenerators, hydrogenerators and combustion turbine generators where the generator uses a unit transformer for stepping up to transmission voltages. Table 1.2 lists all of the protections illustrated, giving the generic type of relay and the action taken by each device.

1.7 Coordination of Generator Capability, Generator Control and Transmission System Protection

Recent misoperations of generating unit protection during major power system disturbances have highlighted the need for secure coordination of generator protection with generator capability, generator control, and transmission system protection. As a result of recent significant disturbances (the 1996 outages in the Western U.S. and the 2003 U.S. East Coast blackout), the North Electric Reliability Council (NERC) has mandated tests and is demanding users to verify the coordination between generator protection and generator control. The recent reports of the Working Groups J-5 and J-6 of the IEEE Power System Relaying Committee identified the need to improve the coordination between the generator protection and control

[20], [21]. More specific, it is necessary to coordinate between the generator protection, excitation control, system protection, and other control strategies in order to avoid system collapse. The impact of major disturbances on the performance of generator control and generator protection systems is reported in [22]. It is concluded that proper coordination of generator protection relays and excitation control systems is of paramount importance to provide the needed system support during stressed system conditions.

1.8 Research Objective and Scope of the Thesis

Power system protection is considered as the first line of defense against system disturbances. Therefore, fast, accurate and reliable operation of the power system protective system is vital to power system security. Studies of past major disturbances and blackouts in North America showed that protective relay mal-operation either caused or aggravated the situation. As a result, it is very important to study the performance of the protection system for different operating conditions and system configurations.

As noted earlier, no research work has been reported on the impact of midpoint FACTS Controllers on the performance of generator distance phase backup protection. As the generator distance phase backup relay is next in line to the transmission line distance relay (which is already affected by the presence of the midpoint FACTS Controllers), its performance would be definitely adversely affected too.

The objective of this research is to carry out extensive studies to explore the effect of midpoint FACTS Controllers on the generator distance phase backup protection in order to identify the important issues that protection engineers need to consider when designing and setting the generator protection system. In addition, practical, feasible and simple solutions to mitigate the adverse impact of midpoint FACTS Controllers on generator distance phase backup protection need to be explored. The research objective is accomplished through the following three studies:

1. Investigating the impact of midpoint FACTS Controllers on the coordination between generator distance phase backup protection and generator capability limits.

2. Investigating the use of a pattern classification technique (Support Vector Machines) for enhancing the coordination between generator phase backup protection and generator capability limits in the presence of midpoint FACTS controllers.
3. Investigating the impact of generator distance phase backup protection on generator overexcitation thermal capability in the presence of a midpoint STATCOM.

The thesis is organized in five chapters, a list of references section and four appendices. Chapter 1 provides a brief introduction on the concept and application of FACTS Controllers with emphasis on their role in transmission line midpoint compensation. A brief introduction on distance relaying and generator protection is also included. Important conclusions and the objectives of the research are drawn from the literature review on the impact of FACTS Controllers on the performance of distance protection of transmission lines.

The principle of operation and control of SVC and STATCOM are presented in Chapter 2. The capability curves for different turbine driven generators and the generator distance phase backup protection are also discussed. The remainder of Chapter 2 is devoted to reporting the studies conducted to explore the impact of midpoint FACTS Controllers on the performance of generator distance phase backup protection as well as on the coordination between generator distance phase backup protection and generator capability limits.

Chapter 3 presents the proposed Support Vector Machines pattern classification technique to enhance the coordination between generator phase backup protection and generator capability limits.

Chapter 4 presents the studies concerned with the impact of generator distance phase backup protection on generator overexcitation thermal capability. The impact of a midpoint STATCOM on the behavior of such a protection is also investigated.

Chapter 5 summarizes the thesis and presents the conclusions.

The data of the systems under investigations are given in Appendix A and the principles of the voltage source converter are presented in Appendix B. Appendix C illustrates the calculation steps of generator distance phase backup protection relay reach. Appendix D illustrates an example of a classification problem with hard limit Support Vector Machines.

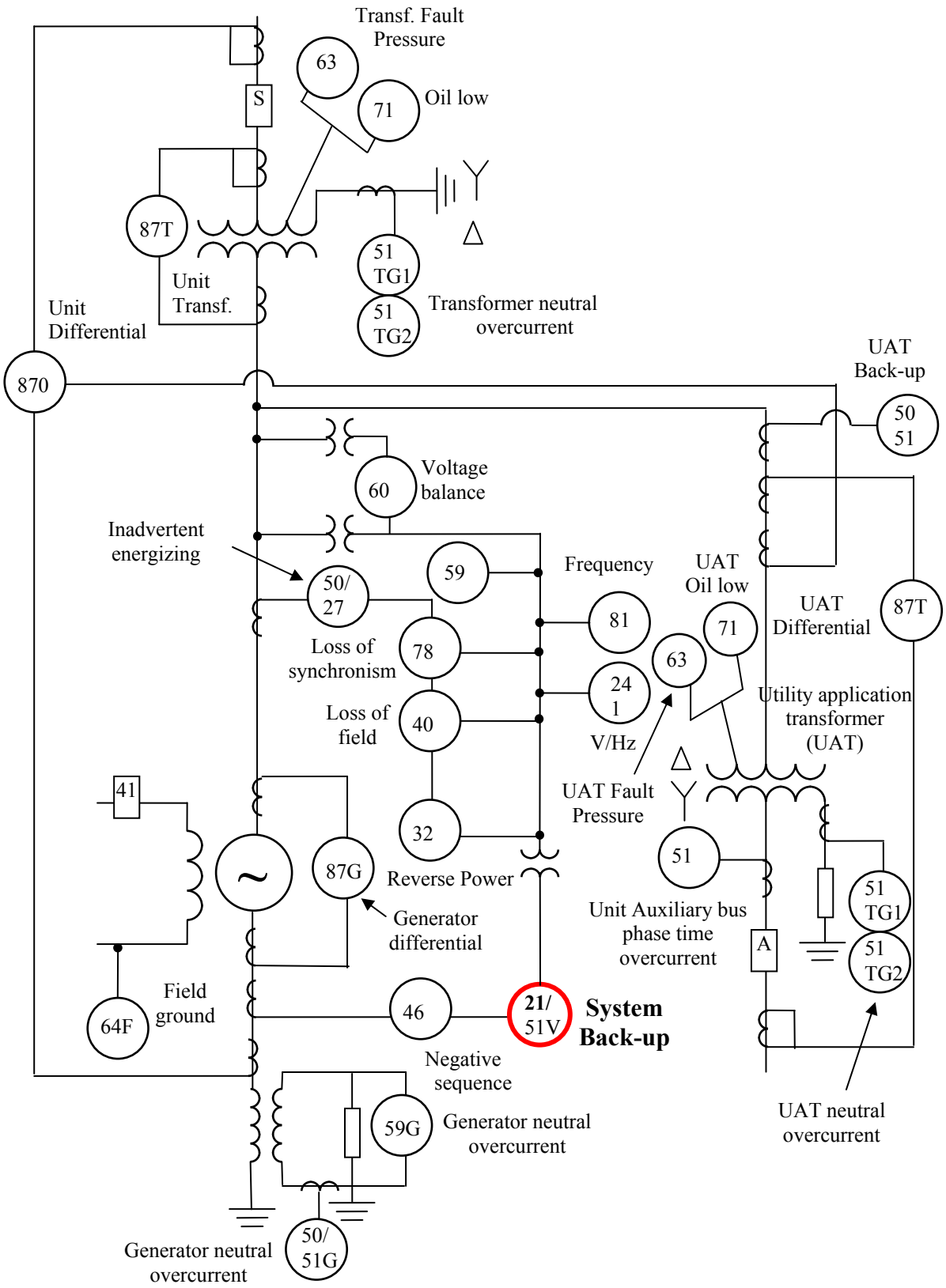

Figure 1.5. Unit generator-transformer protection configuration.

Table 1.2. Synchronous generator protective devices [18].

Device	Function
21	Distance relay. Backup for system and generator zone phase faults. Device 21 requires a time delay for coordination.
24	V/Hz protection for the generator.
50/27	Inadvertent energizing protection using voltage supervised overcurrent relaying.
32	Reverse power relay. Motoring protection.
40	Loss-of-field protection.
46	Stator unbalanced current protection. Negative-sequence relay.
50/51	Time current relays with instantaneous element. High-side bank overcurrent relays providing phase fault protection for utility application transformer (UAT) and backup protection for failure of UAT low-side bank breaker.
50G/51G	Time-overcurrent relay with instantaneous element. Primary and/or backup protection for generator ground faults.
51	Time-overcurrent relay. Detection of turn-to-turn faults in generator windings.
51TG1	Time-overcurrent relay. Provides backup protection for transmission ground faults when applied to generator step up (GSU) transformer neutral. Protects for ground faults on the unit auxiliary bus when applied to UAT neutral.
51TG2	Time-overcurrent relay. Provides backup protection for GSU transformer ground faults when applied to GSU transformer neutral. Protects for faults in the low side of the UAT down to the low-side bank breaker when applied to UAT neutral. Provides backup for failure of low-side breaker to trip.
51 UAT	Time-overcurrent relays connected to CTs in UAT low-side bank breaker. Protects for phase faults on unit auxiliary bus.
51V	Voltage controlled or voltage-restrained time-overcurrent relay. Backup for system and generator zone phase faults.
59	Overvoltage protection.
59G	Voltage relay. Primary ground fault protection for a generator.
60	Voltage balance relay. Detection of blown potential transformer fuses.
63	Fault pressure relay. Detects transformer faults.
64F	Voltage relay. Primary protection for rotor ground faults.
71	Transformer oil or gas level.
78	Loss of synchronism protection. This protection is optional. Applied when, during a loss of synchronism, the electrical center is in the step-up transformer or in the generator zone. Alternate locations are shown for this protection. A study should be made to determine which location is best for the detection of an out-of-step condition.
81	Frequency relay. Both underfrequency and overfrequency protection may be required.

Table 1.2. , Continued.

87G	Differential relay. Primary phase fault protection for the generator.
87T	Differential relay. Primary protection for the GSU or UAT transformer. May be used to provide phase fault backup for the generator in some station arrangements. The zone may be extended to cover the generator bus using CTs from the generator and UAT when low side CTs are not available.
870	Differential relay for overall unit and transformer.

2. IMPACTS OF MIDPOINT FACTS CONTROLLERS ON THE COORDINATION BETWEEN GENERATOR DISTANCE PHASE BACKUP PROTECTION AND GENERATOR CAPABLITY LIMITS

2.1 Introduction

This chapter begins by introducing the systems used in the investigations of this thesis. It then presents an overview of the principle of operation and control of the Static Var Compensator (SVC) and the Static Synchronous Compensator (STATCOM). The important difference between these FACTS Controllers during transient conditions is discussed. The capability curves for different turbine driven generators and their transformation to the impedance plane are also discussed in this chapter. The generator distance phase backup protection, the analysis of its measured impedance and the setting of its relay are also presented. Finally, the impacts of midpoint FACTS Controllers on the performance of generator distance phase backup protection as well as on the coordination between such a protection and the generator steady-state overexcited capability (GOEC) limits are addressed.

2.2 Systems under Investigations

The two systems used in the investigations of this thesis are designated as Systems I and II. System I, shown in Figure 2.1, consists of a hydrogenerator (G_1, salient-pole synchronous machine) which is connected via a transformer to an infinite bus system through a 230 kV, 300 km transmission line. A STATCOM/SVC is installed at the middle of the transmission line for the purpose of increasing its power transfer capability. System II, shown in Figure 2.2, consists of a turbogenerator (G_2, cylindrical-rotor synchronous machine) which is connected via a transformer to three large systems through three 230 kV transmission lines. A STATCOM/SVC is installed at the middle of Line 1 for the purpose of increasing its power transfer capability. The transmission lines in Systems I and II are protected by distance relays. The phase backup protection for G_1 and G_2 is provided by distance relays which are shown in Figures 2.1 and 2.2 as

R_{21}. The data of Systems I and II are given in Appendix A. The time domain simulation studies are carried out using the PSCAD/EMTDC simulation package [23].

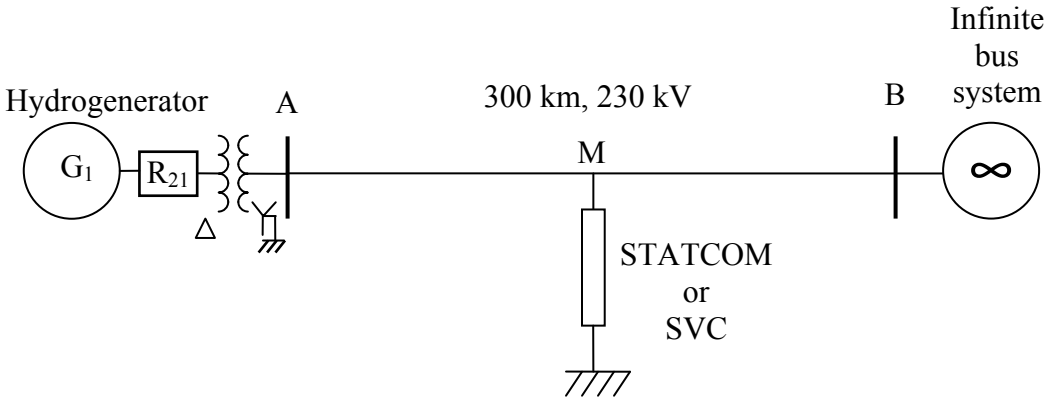

Figure 2.1. First system under investigations: System I

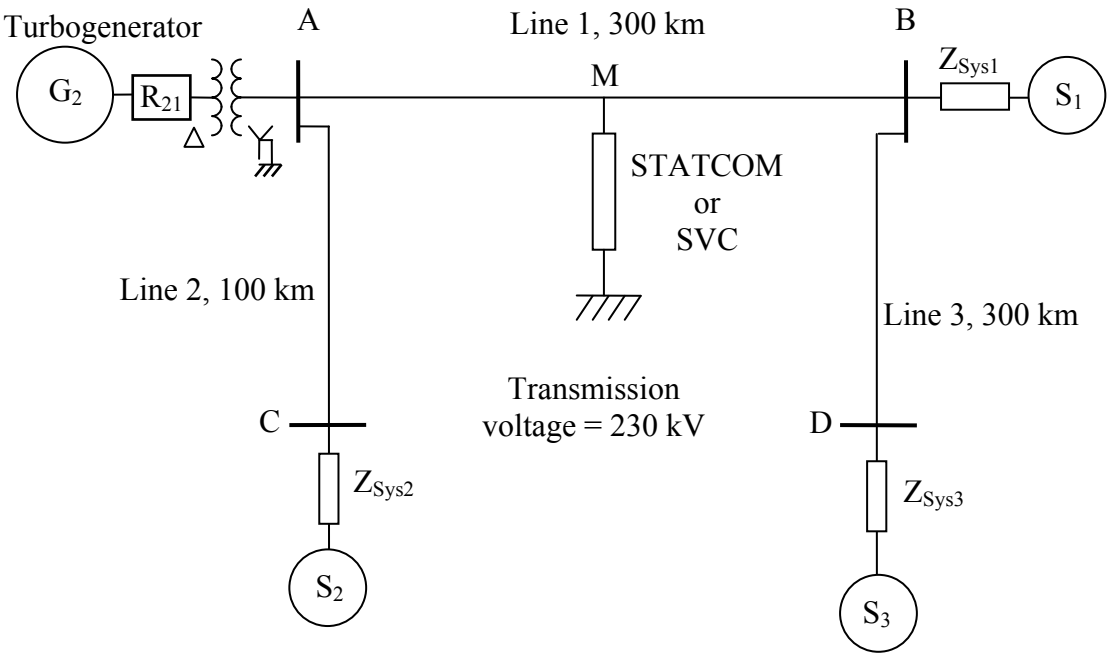

Figure 2.2. Second system under investigations: System II.

2.3 The Static Var Compensator

The SVC is a shunt-connected static generator/absorber of reactive power in which the output is varied to maintain or control specific parameters of an electrical power system. It is generally composed of a combination of thyristor-switched capacitors and reactors in which the outputs are coordinated. Figure 2.3 shows a Thyristor-Switched Capacitor (TSC)-Thyristor-

Controlled Reactor (TCR) SVC [2], [4]. The capacitors can be switched in discrete steps, whereas continuous control within the reactive power span of each step is provided by the TCR. Thus, the maximum inductive range of the SVC corresponds to the rating of the relatively small interpolating TCR.

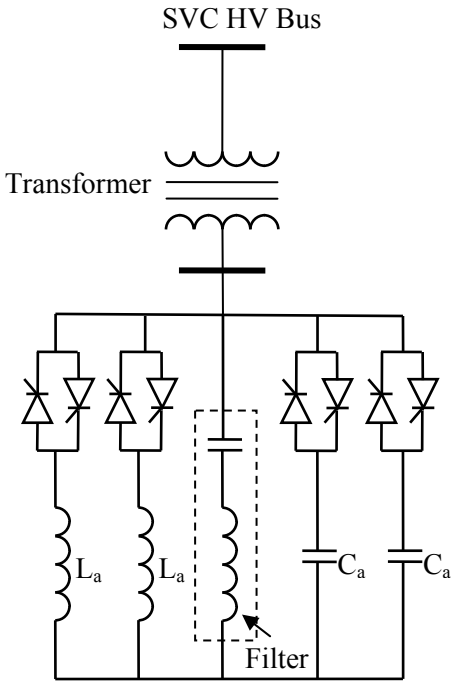

Figure 2.3. A general TSC-TCR SVC.

As the size of the TCR is small, the harmonic generation is also substantially reduced. The TSC branches are tuned with the series reactor to different dominant harmonic frequencies. To avoid a situation in which all TSC and, consequently, the associated filters are switched off (with only the TCR in operation), an additional non-switchable capacitive-filter is provided.

A typical V-I characteristic of a TSC-TSR SVC is shown in Figure 2.4 [2], [4]. It can be seen from this figure that the maximum attainable compensation current of the SVC decreases linearly with the ac system voltage. This major drawback in the SVC does not exist in the STATCOM.

The IEEE Basic SVC Model 1, which corresponds to the gain-time-constant format, is shown with its voltage regulator model in Figure 2.5. The gain K_R (inverse of the current slope) is typically between 20 p.u. (5% slope) and 100 p.u. (1% slope) on the base of the SVC rated reactive power. The time constant T_R usually lies between 20 and 150 ms, and the time constants

T_1 and T_2 are zero in most cases [4]. The phase-lead shown in Figure 2.5(b) can, however, be provided to enhance the damping contribution of the SVC. The maximum and minimum limits on the susceptance output B_{ref} are given by B_{max} and B_{min} respectively.

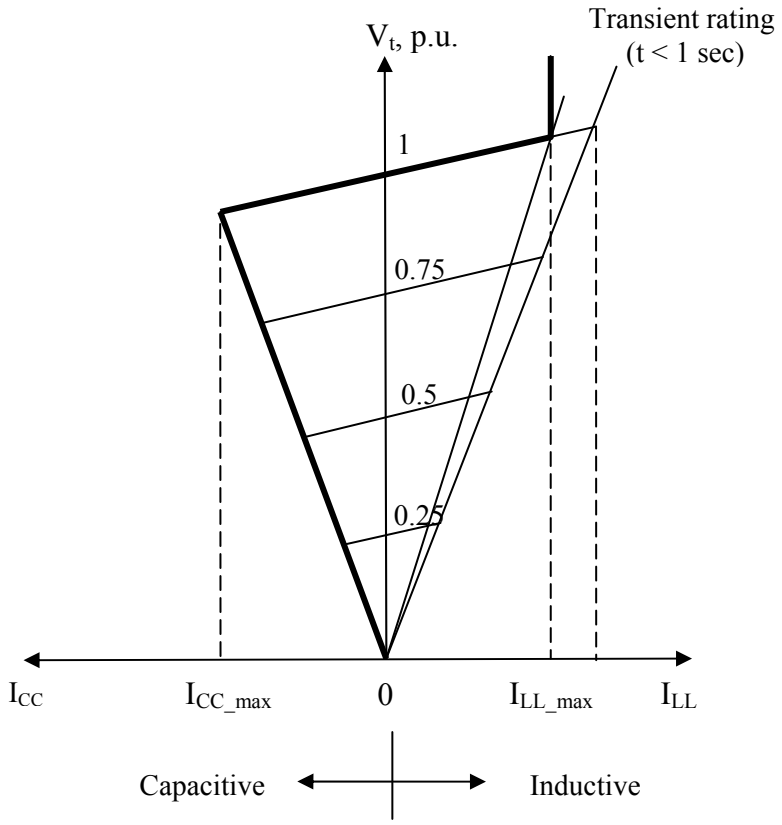

Figure 2.4. The SVC V-I characteristic.

2.4 The Static Synchronous Compensator

The STATCOM is a shunt connected reactive power compensation FACTS Controller that is capable of generating and/or absorbing reactive power and in which the output can be varied to control specific parameters of an electric power system. It is, in general, a solid-state switching converter capable of generating or absorbing independently controllable real and reactive power at its output terminals when it is fed from an energy source or energy-storage device at its input terminals. More specific, the STATCOM is a voltage-source converter (VSC) that, from a given input of dc voltage, produces a set of three-phase ac output, each in phase and coupled to the corresponding ac system voltage through a relatively small reactance (which is provided by either an interface reactor or the leakage inductance of a coupling transformer). The dc voltage

is provided by an energy storage capacitor. The principle of operation of VSCs is discussed in Appendix B [24].

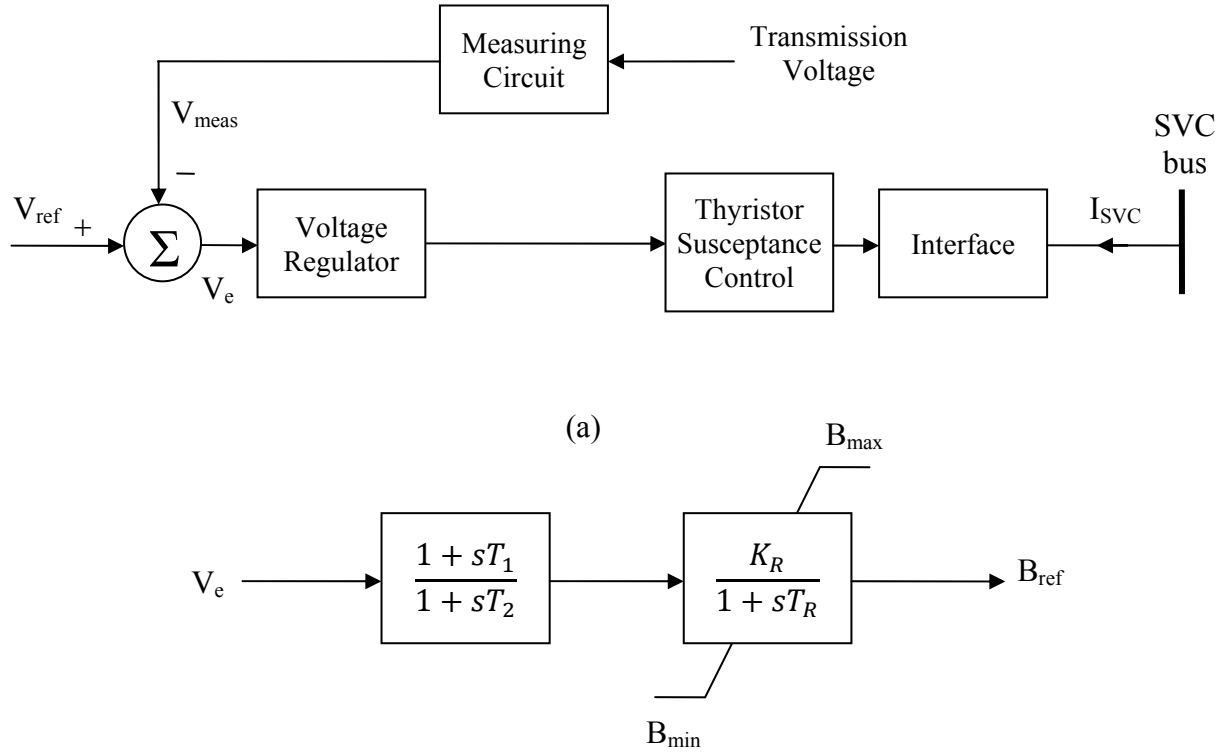

Figure 2.5. The IEEE Basic Model 1 for the SVC [4]: (a) SVC control system, (b) voltage regulator model.

2.4.1 STATCOM principle of operation

The STATCOM is a controlled reactive power source. It provides the desired reactive power generation or absorption entirely by means of electronic processing of the voltage and current waveforms in a VSC. A single-line diagram of a STATCOM power circuit is shown in Figure 2.6(a), where a VSC is connected to a utility bus through a transformer.

The exchange of the reactive power between the converter and the ac system can be controlled by varying the amplitude of the three-phase output voltage, E_s, of the converter, as illustrated in Figure 2.6(b). That is, if the amplitude of the output voltage is increased above that of the utility bus voltage, E_t, then a current flows through the reactance from the converter to the ac system and the converter generates capacitive-reactive power for the ac system. If the amplitude of the output voltage is decreased below the utility bus voltage, then current flows

from the ac system to the converter and the converter absorbs inductive-reactive power from the ac system. If the output voltage equals the ac system voltage, the reactive power exchange becomes zero, in which case, the STATCOM is said to be in a floating state.

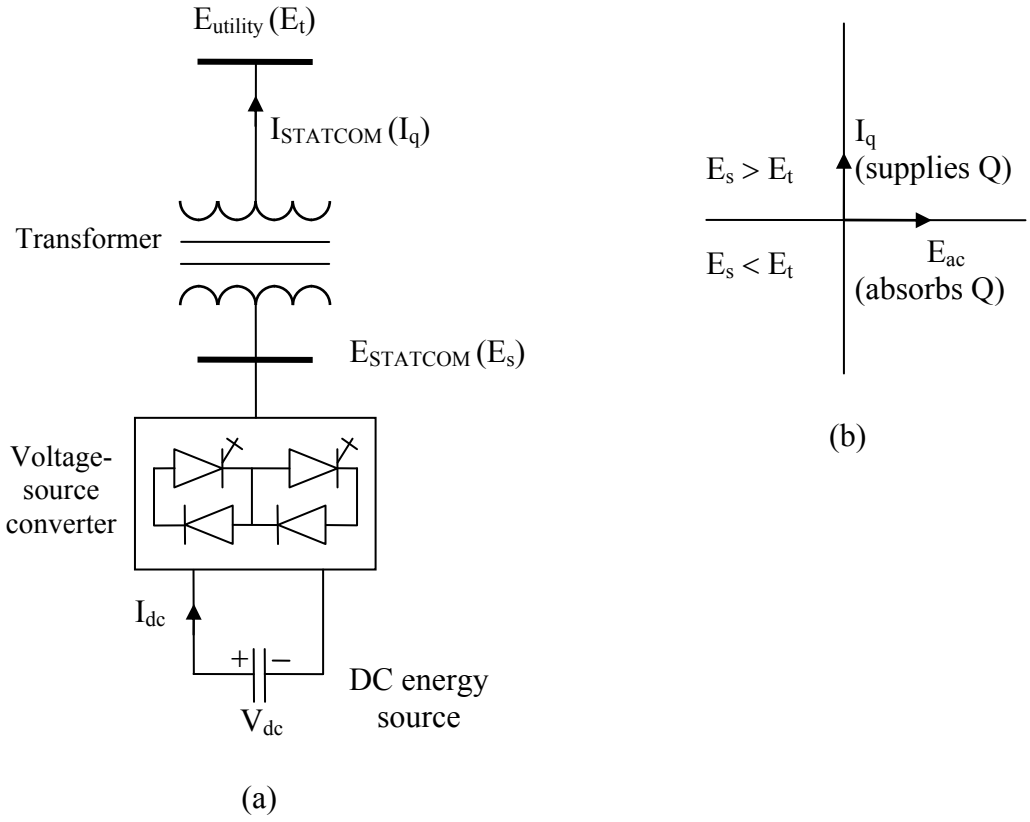

Figure 2.6. The STATCOM principle diagram: (a) power circuit, (b) reactive power exchange.

The VSC has the same rated current capacity when it operates with the capacitive or inductive current. Therefore, a VSC having a certain MVA rating gives the STATCOM twice the dynamic range in MVAR. The magnitude of the capacitor is chosen so that the dc voltage across its terminal remains fairly constant to prevent it from contributing to the ripples in the dc current.

The VSC may be a 2- level or 3-level type, depending on the required output power and voltage [2], [4]. A number of VSCs are combined in a multi-pulse connection to form the STATCOM. At steady-state, the VSCs operate with fundamental frequency switching to minimize converter losses. However, during transient conditions caused by line faults, a Pulse

Width Modulation (PWM) mode is used to prevent the fault current from entering the VSCs. In this way, the STATCOM is able to withstand transients on the ac side without blocking.

2.4.2 STATCOM V-I characteristic

A typical V-I characteristic of a STATCOM is depicted in Figure 2.7. As can be seen, the STATCOM can be operated over its full output current range even at very low system voltage levels (typically 0.15 p.u. and is known as the ***threshold***). In other words, the maximum capacitive or inductive output current of the STATCOM can be maintained independently of the ac system voltage. Moreover, the STATCOM maximum Var generation or absorption changes linearly with the ac system voltage.

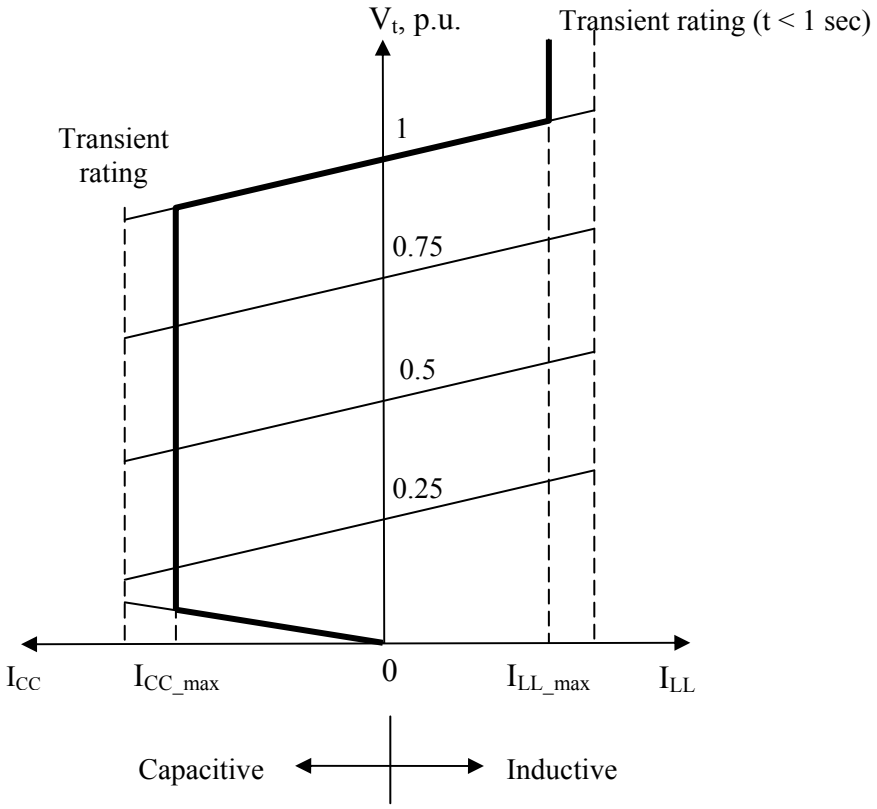

Figure 2.7. The STATCOM V-I characteristic.

2.4.3 STATCOM controller

The main function of a STATCOM, as with an SVC, is to regulate the transmission line voltage at the point of connection. Figure 2.8(a) shows the block diagram of a STATCOM voltage controller where E_s is controlled by varying the modulation ratio m (Appendix B).

For a proper operation of the STATCOM, the dc bus voltage must be maintained within a pre-specified range. At steady-state, E_s lags E_t by a small angle (less than one degree) in order to charge the dc capacitor and supply the VSC losses. The control of the dc capacitor voltage is achieved by implementing a proportional-integral (PI) controller as shown in Figure 2.8(b). The output of this controller, "$\Delta\theta_{dc}$" is added to the phase angle between E_s and E_t.

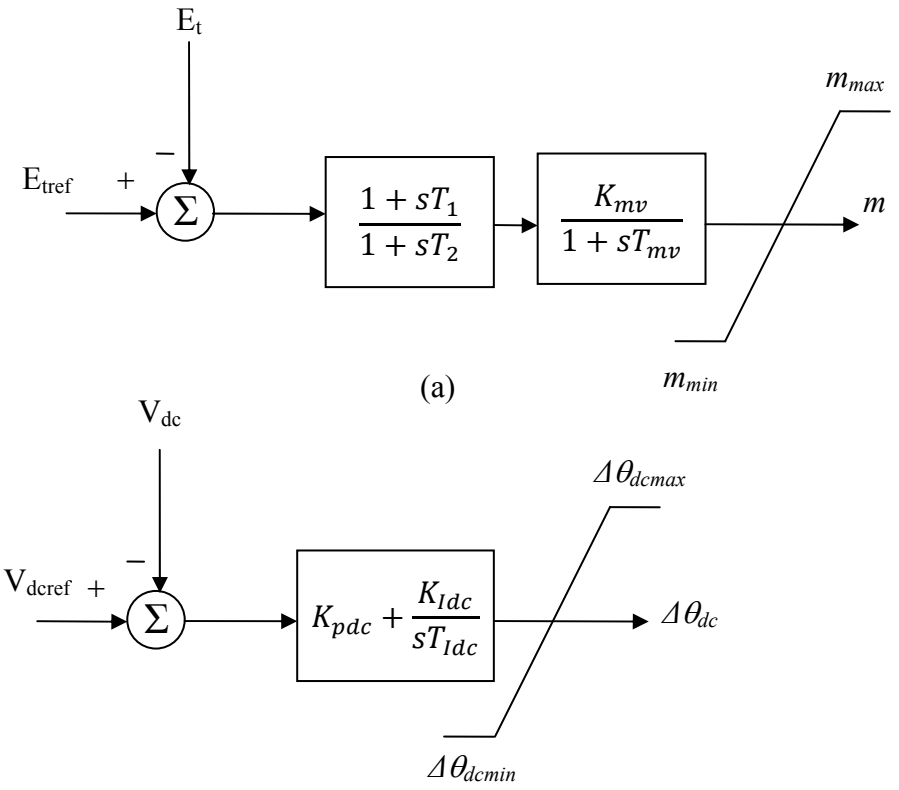

Figure 2.8. A STATCOM controller: (a) voltage control, (b) dc capacitor voltage control.

2.5 Comparison between the STATCOM and the SVC

In contrast to the STATCOM, the SVC, being composed of thyristor-switched capacitors and reactors, becomes a fixed capacitive admittance at full output. Thus, the maximum attainable compensation current of the SVC decreases linearly with the ac system voltage (Figure 2.4) and the maximum var output decreases with the square of this voltage. The STATCOM is, therefore, superior to the SVC in providing voltage support under large system disturbances during which the voltage excursions would be well outside the linear operating range of the compensator. The capability of providing maximum compensating current at reduced voltage enables the

STATCOM to perform in a variety of applications the same dynamic compensation as an SVC of considerably higher rating.

2.6 Generator Capability Curves

The need to coordinate generator protection with generator control and load capability requires the knowledge of generator steady-state and dynamic characteristics. The nameplate ratings of a generator define only one limiting point of operation for the machine. It is logical to assume that a reduction in the MVAR output would allow some increase in the MW output and that a reduction in the MW would allow a higher MVAR output. These allowable variations are defined by the generator capability limits, which are usually provided by the manufacturer [17], [25]. These limits, when plotted in the P (MW) – Q (MVAR) plane, form the Generator Capability Curve (GCC). Figure 2.9 shows the capability curves for turbogenerators and hydrogenerators. The operating terminal voltage range allowed by standards is 95% – 105% of rated voltage, but generator capability curves are normally plotted for the rated terminal voltage. The capability curve contains two or more boundaries for MW and MVAR limits.

The capability curve of a turbogenerator (cylindrical rotor synchronous machine) is a composite of three distinct limits (A-B, B-D and D-E). The upper boundary of the curve (A-B) is the rotor field thermal limit specified at a dc current rating. This boundary is often approximated by an arc with a center at a value equal to the short circuit ratio (SCR) in per unit on the negative y axis (the MVAR axis) and a radius of E_f/X_d where E_f is the internal or rotor field excitation voltage given that the synchronous generator terminal voltage is one per unit. The right hand boundary (B-D) is the synchronous generator stator current limit. The center of the arc defining this limit is the origin. The curve (A-C) is termed as the generator steady-state overexcited capability (GOEC) limit which ensures the operation of the generator within the overexcited region. The lower boundary (D-E) is the end iron heating limit (heating in the end laminations of the stator core) which occurs during leading power factor, underexcited operating conditions. The curve (C-E) is termed as the generator steady-state underexcited capability (GUEC) limit which ensures the operation of the generator within the underexcited region.

The capability curve for a hydrogenerator is different from that of a turbogenerator. Hydro units are of salient-pole construction and have negligible end core losses. Thus, their capability

curves have only two distinct limits. The field circuit imposed lagging Vars limit from A to B and the stator winding current limit which extends as a continuous arc from B to F. Therefore, the leading VAR limit is determined by the current rating of the stator winding. Similarly, the boundary (A-C) represents the generator steady-state overexcited capability (GOEC) limit while the boundary (C-F) represents the generator steady-state underexcited capability (GUEC) limit.

The utility application engineer will design some additional limitations in both the overexcited and underexcited regions for generator control purposes. The overexcitation limiter (OEL) which is discussed in detail in Chapter 4 limits the generator operation in the overexcited region within generator capability curve. Some users set the OEL just under the machine capability curve, while others set it just over the machine capability as shown in Figure 2.9 to allow full machine capability.

In the underexcited region, every machine will have a steady-state stability limit which is a function of both the synchronous generator characteristics and the stiffness of the electrical system to which the machine is paralleled. A loss-of-field relay can be set to trip the machine before this limit is exceeded. An acceptable margin is computed in order to make an underexcitation alarm relay setting and additional margin is provided in order to set either a minimum excitation limiter (MEL) or underexcitation reactive ampere limiter (UEL) in the automatic voltage regulator. The capability curves of the two generators (G_1 and G_2, Figures. 2.1 and 2.2) used in the investigations of this thesis are shown in Figure 2.10.

2.7 Generator Distance Phase Backup Protection (Relay (21))

The function of the generator distance phase backup protection (Relay (21))[1] is to protect the generator from supplying prolonged fault current to a fault on the power system to which the generator is connected. One zone of distance relaying with a mho characteristic (Figure 2.11) is commonly used for system distance phase fault backup. The origin of the plot in Figure 2.11 is defined by the location of the voltage transformer (VT). The angle between the R-axis and the line drawn through the center of the characteristic circle and the origin is the maximum torque angle (MTA) of the relay. The relay reach is the length of the vector drawn from the origin with an angle equal to the MTA to the circumference of the circle (*OL*, Fig. 2.11). Both of the relay reach and the MTA are settable parameters.

[1] The "generator distance phase backup protection" is referred to it also in this thesis as "Relay (21)".

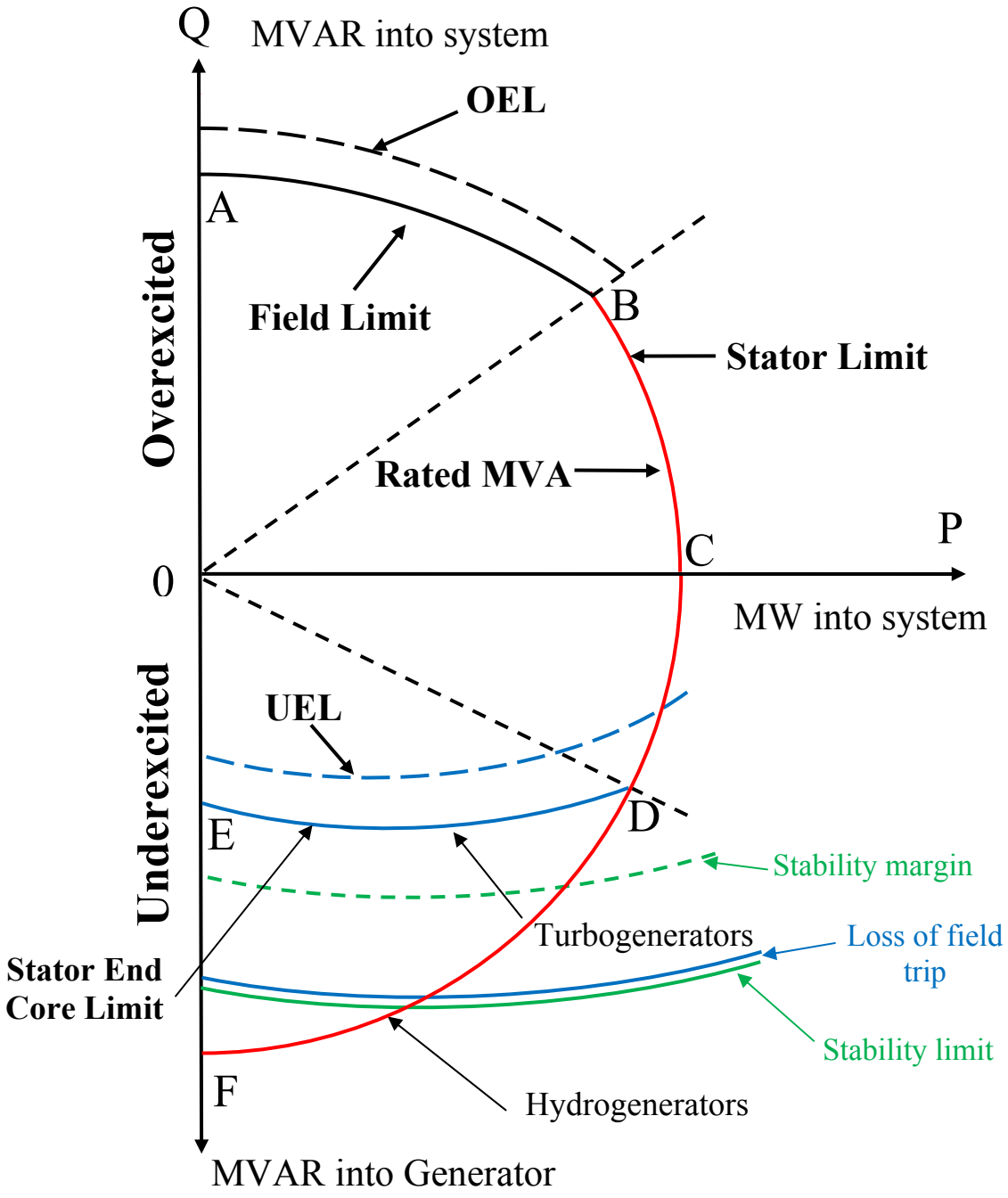

Figure 2.9. Generator capability curves for turbogenerators and hydrogenerators.

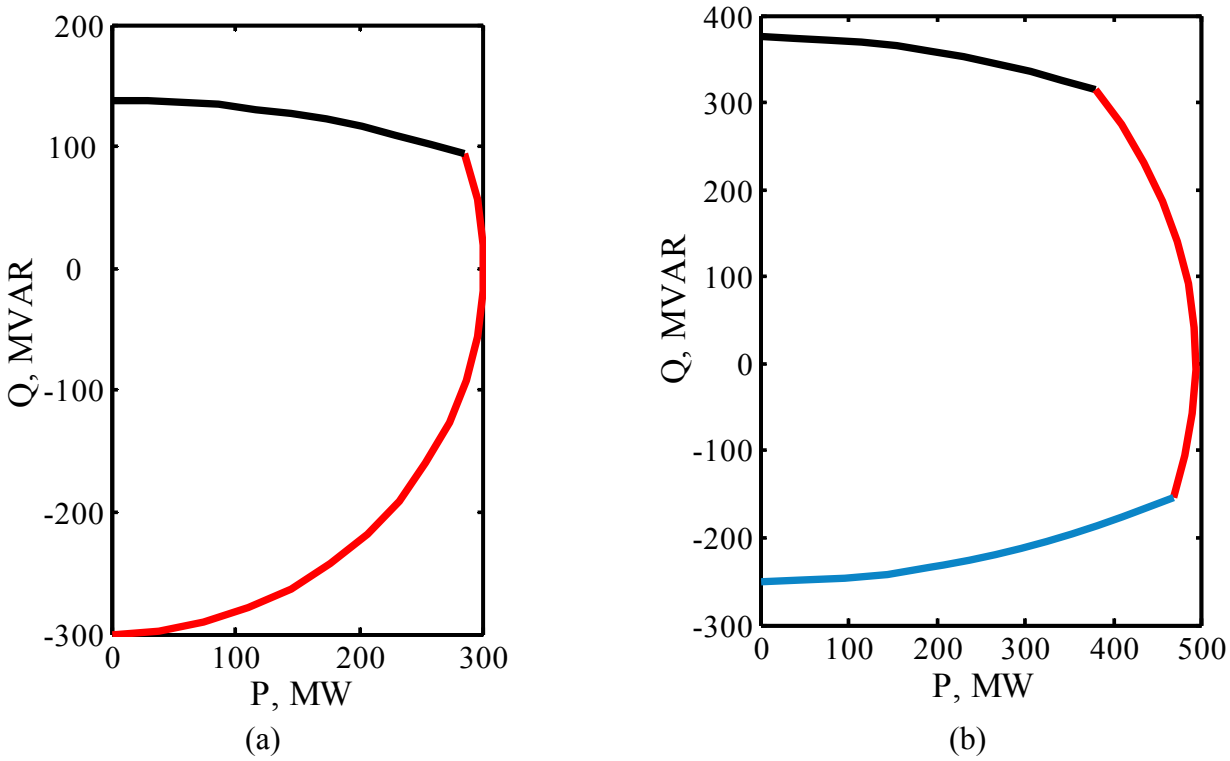

Figure 2.10. G_1 and G_2 capability curves: (a) G_1, (b) G_2.

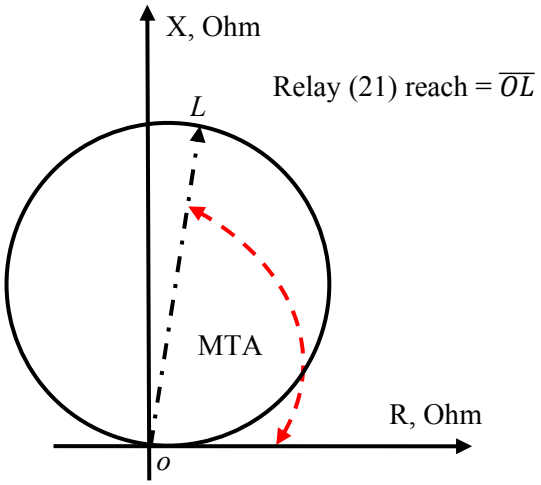

Figure 2.11. A mho distance relay characteristic.

In some cases, Relay (21) is connected to receive currents from current transformers (CTs) in the neutral ends of the generator phase windings and potentials from the voltage transformers (VTs) at the terminals of the generator as shown in Figure 2.12. For this connection, the relay will not only provide backup for system faults but it will also provide some backup protection for phase faults in the generator and generator zone since faults at these two locations are detected in the first quadrant. This is because the direction of the relay current and the polarity of the relay

voltage are the same in both conditions. This connection will trip the breaker on the high voltage side of the generator step up (GSU) transformer, the generator field breaker, the auxiliary transformer breaker and initiates prime mover shut down. If the station configuration includes a generator breaker, it would be tripped instead of the high voltage breaker [17], [26].

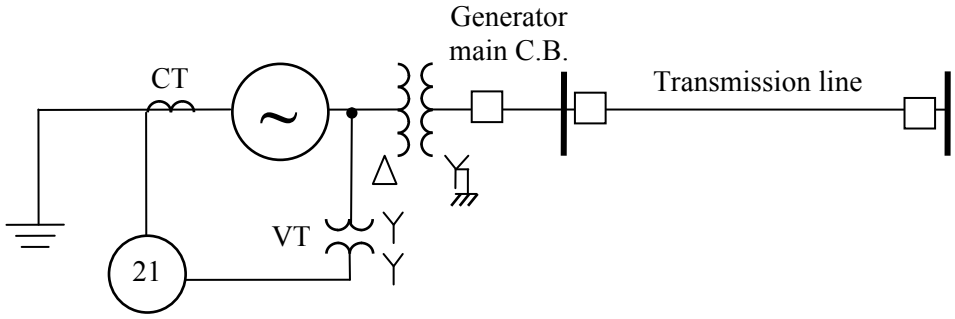

Figure 2.12. Application of Relay (21) to a generator-transformer unit (current transformer is connected at the neutral end of the generator).

In other cases, the distance relay is connected looking toward the system receiving both current and potential from the terminals of the generator as shown in Figure 2.13 (this is the case considered in the investigations of this thesis). This connection will only provide backup for system phase faults and will not provide any backup for phase faults in the generator and the generator zone [17]. This is because a fault in the stator winding will produce a relay current in the opposite direction of that of a system fault. The stator fault impedance will appear in the third quadrant of the R – X plot and will not be detected, while the impedance of the system fault will appear in the first quadrant and will be detected. In this connection, the GSU transformer or the generator breaker need to be tripped. This would allow a faster generator re-synchronization after the failure has been isolated [17], [26].

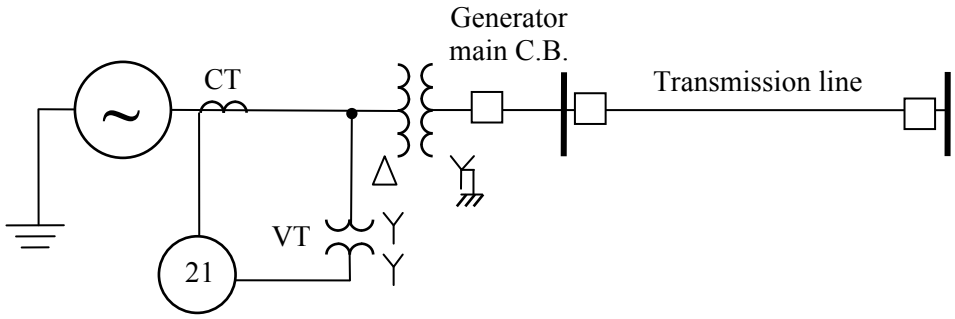

Figure 2.13. Application of Relay (21) to a generator-transformer unit (current transformer is connected at the terminals of the generator).

2.7.1 Impedance measured by Relay (21)

There are several different algorithms used in distance relays, but in all cases, the common goal is to measure the positive-sequence impedance from the relay to the fault. When phase faults protection is provided by distance relaying, three elements are required, phase elements A–B, B–C and C–A [17], [18]. The following analysis is based on the simple power system shown in Figure 2.14. It consists of an unloaded synchronous generator connected to a radial transmission line through a step up transformer. Since the time delay of Relay (21) is between 1 and 2 s, the positive-sequence reactance of the synchronous machine is taken as the direct-axis transient reactance, $X_d^{'}$. Moreover, in the following analysis, E is the internal e.m.f, X_{g2} is the synchronous machine negative-sequence reactance and Z_{s1} and Z_{s2} are the positive- and negative-sequence phase impedances respectively defined as

$$Z_{s1} = Z_{T1} + Z_{sl1} \tag{2.1}$$

$$Z_{s2} = Z_{T2} + Z_{sl2} \tag{2.2}$$

where Z_{sl} is the transmission line impedance from bus A to the fault point and Z_T is the generator step up transformer impedance ($Z_{T1} = Z_{T2}$ and $Z_{sl1} = Z_{sl2}$).

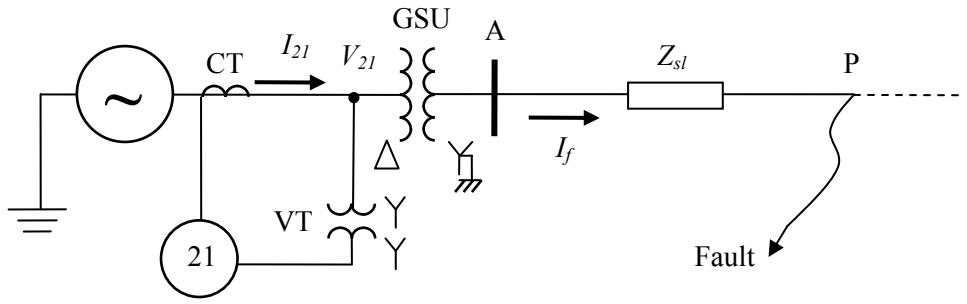

Figure 2.14. A single-line diagram of a synchronous generator connected to a radial transmission line through a step up transformer.

The equations governing the conversion of the symmetrical component quantities to the phase quantities (for a phase sequence ABC) are as follows, where $a = 1\angle 120^{o}$

$$V_A = V_1 + V_2 + V_0 \tag{2.3}$$

$$V_B = a^2 V_1 + aV_2 + V_0 \tag{2.4}$$

$$V_C = \ aV_1 + a^2V_2 + V_0 \tag{2.5}$$

$$I_A = \ I_1 + I_2 + I_0 \tag{2.6}$$

$$I_B = \ a^2I_1 + aI_2 + I_0 \tag{2.7}$$

$$I_C = \ aI_1 + a^2I_2 + I_0. \tag{2.8}$$

Therefore, the phase-to-phase voltages and the delta currents (defined here as the differences between the line currents, which are also the currents in the delta winding of the GSU transformer) are in the following form

$$V_A - V_B = \sqrt{3}\,(V_1 \angle 30^o + V_2 \angle -30^o) \tag{2.9}$$

$$V_B - V_C = \sqrt{3}\,(V_1 \angle 270^o + V_2 \angle 90^o) \tag{2.10}$$

$$V_C - V_A = \sqrt{3}\,(V_1 \angle 150^o + V_2 \angle -150^o) \tag{2.11}$$

$$I_A - I_B = \sqrt{3}\,(I_1 \angle 30^o + I_2 \angle -30^o) \tag{2.12}$$

$$I_B - I_C = \sqrt{3}\,(I_1 \angle 270^o + I_2 \angle 90^o) \tag{2.13}$$

$$I_C - I_A = \sqrt{3}\,(I_1 \angle 150^o + I_2 \angle -150^o). \tag{2.14}$$

There are also many different techniques for phase distance measurement. The analysis presented here is for self-polarized distance elements, because the polarizing voltage is taken from the same phases as the current [16]-[18]. Each phase distance element measures the impedance defined by phase-to-phase voltages and delta currents as

$$Z_{AB} = \frac{V_A - V_B}{I_A - I_B} \tag{2.15}$$

$$Z_{BC} = \frac{V_B - V_C}{I_B - I_C} \tag{2.16}$$

$$Z_{CA} = \frac{V_C - V_A}{I_C - I_A}. \tag{2.17}$$

Neglecting the effect of the phase shift in the wye-delta transformer (which is discussed in the next subsection), the circuit impedance measured by each relay element for the various fault conditions can be found by substituting Eqs. (2.9) to (2.14) into Eqs. (2.15) to (2.17), which imply the following results

$$Z_{AB} = \frac{V_1 \angle 30^o + V_2 \angle -30^o}{I_1 \angle 30^o + I_2 \angle -30^o} \quad (2.18)$$

$$Z_{BC} = \frac{V_1 \angle 270^o + V_2 \angle 90^o}{I_1 \angle 270^o + I_2 \angle 90^o} \quad (2.19)$$

$$Z_{CA} = \frac{V_1 \angle 150^o + V_2 \angle -150^o}{I_1 \angle 150^o + I_2 \angle -150^o}. \quad (2.20)$$

1. Three-phase fault

Only the positive-sequence current and voltage exist during this symmetrical fault. Figure 2.15 shows the positive-sequence network during such a fault. Substituting $V_2 = 0$ and $I_2 = 0$ into Eqs. (2.18) to (2.20) results

$$Z_{AB} = Z_{BC} = Z_{CA} = \frac{V_1}{I_1}. \quad (2.21)$$

It can be seen from Figure 2.15 that the voltage at the generator terminals where the relay VTs are located is $V_1 = Z_{s1} I_1$. Substituting this value in Eq. (2.21) yields

$$Z_{AB} = Z_{BC} = Z_{CA} = Z_{s1}. \quad (2.22)$$

Hence, for a three-phase fault, each relay element will see the positive-sequence impedance of the circuit from the relay to the fault point.

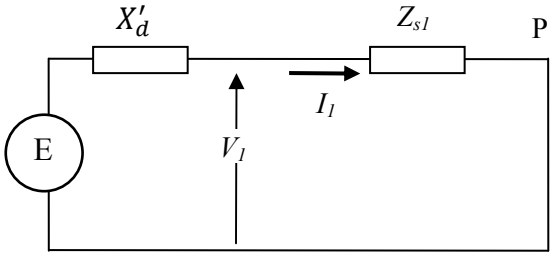

Figure 2.15. Positive-sequence network for the system of Fig. 2.14 during a three-phase fault at point P.

2. Phase-to-phase fault

Figure 2.16 shows the connection of the positive-and negative sequence networks for the system of Fig. 2.14 to simulate a phase-to-phase fault (phases B and C) at point P. The positive- and negative-sequence currents and voltages are defined as

$$I_1 = -I_2 \tag{2.23}$$

$$V_1 = E - I_1 X_d^{'} \tag{2.24}$$

$$V_2 = -I_2 X_{g2} \tag{2.25}$$

$$I_1 = \frac{E}{X_d^{'}+X_{g2}+Z_{s1}+Z_{s2}} = \frac{E}{X_d^{'}+X_{g2}+2Z_{s1}}. \tag{2.26}$$

Substituting Eqs. (2.23) to (2.26) into Eqs. (2.18) to (2.20) yields

$$Z_{AB} = 2Z_{s1}\angle -60^{o} + \sqrt{3}\, X_{g2}\angle -90^{o} \tag{2.27}$$

$$Z_{BC} = Z_{s1} \tag{2.28}$$

$$Z_{CA} = 2Z_{s1}\angle 60^{o} + \sqrt{3}\, X_{g2}\angle 90^{o}. \tag{2.29}$$

As it can be seen from Eqs. (2.27) to (2.29), the B-C phase element, will see the correct circuit impedance from the relay to the fault point while the other phase elements (A-B and C-A) will see impedances with significantly higher value and angular displacement.

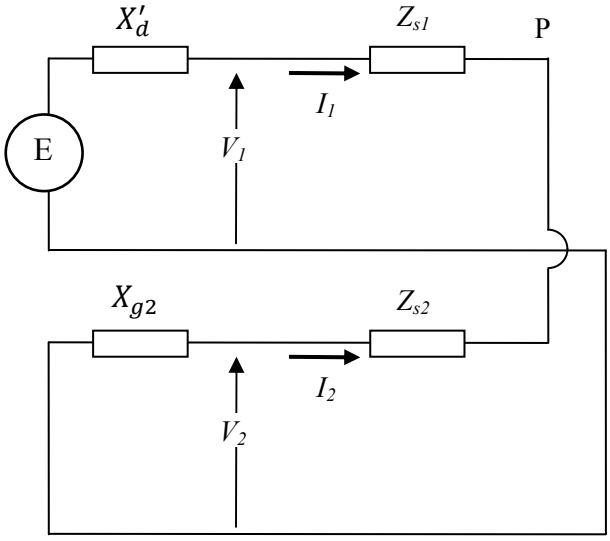

Figure 2.16. Connection of the positive-and negative-sequence networks for the system of Fig. 2.14 to simulate a phase-to-phase fault at point P.

2.7.2 Relay (21) setting

As it is noted before, the task of the generator distance phase backup protection is to isolate the generator from the power system for a phase fault that is not cleared by the transmission line

breakers. In addition, Relay (21) has to operate within the GOEC limit with an adequate margin for overload and stable power swings. Therefore, it is recommended that the setting of this relay be evaluated by the generator and system protection engineers to optimize the coordination while still protecting the generator. In order to achieve a correct operation in terms of satisfying the basic requirements of any protection system, the following considerations must be taken into account [17], [26]:

2.7.2.1 Load limits for stable power swings

The load at the generator terminals can be represented as an equivalent impedance. If this load impedance falls within the generator distance phase backup protection relay's characteristic, the relay will operate. Network transients such as faults and line switching necessitate generators connected to the power system to adjust to the new system configuration.

A power swing is defined as a variation in the system power flow that occurs when the generator load angles are advancing or retarding relative to each other in response to changes in the system load, line switching, loss of generation, faults and other system disturbances. A power swing is said to be stable if the system reach a new state of equilibrium after the transient period. During these transients, the generator Watt/Var output can substantially exceed the generator rating. These power swings will appear as points on the R–X diagram with a circular or spiral trajectory. If the impedance swing enters and remains within Relay (21) characteristic for a period of time exceeding the relay's trip delay, the relay will operate. This is the worst-case scenario for a misoperation of a generator protective relay. The resulting loss of generation will tend to amplify the system transient, with the potential to initiate tie line trips and cascading loss of generation and system collapse. To avoid misoperation on stable power system swings, Relay (21) reach should not be less than twice the generator load impedance (Z_{load}) at the rated power factor angle (RPFA).

2.7.2.2 Effect of system infeed current on the apparent impedance

When a distance relay is required to provide phase backup protection for transmission system faults, the effect of the infeed current must be considered. The infeed current increases the impedance of the faulted line seen by Relay (21). This increase occurs because Relay (21) and the faulted line currents are not the same. The effect of the system infeed current is incorporated in the power system of Figure 2.14 and is shown in the Figure 2.17.

With the infeed current, the voltage at the relay, V_{21}, during a three-phase fault at point P is

$$V_{21} = Z_T I_{21} + Z_{sl} I_f \,. \tag{2.30}$$

The impedance seen by the relay, Z_{21} is given by

$$Z_{21} = \frac{V_{21}}{I_{21}} = \frac{X_{tr} I_{21} + Z_{sl} I_f}{I_{21}} = X_{tr} + Z_{sl} \frac{I_f}{I_{21}}. \tag{2.31}$$

The "apparent impedance" of the line is determined by the ratio of the fault current to the relay current. Therefore, this configuration apparent impedance would necessitate a much larger reach for Relay (21) to detect a line end fault than that calculated for a radial system (with no infeed current, Figure 2.14).

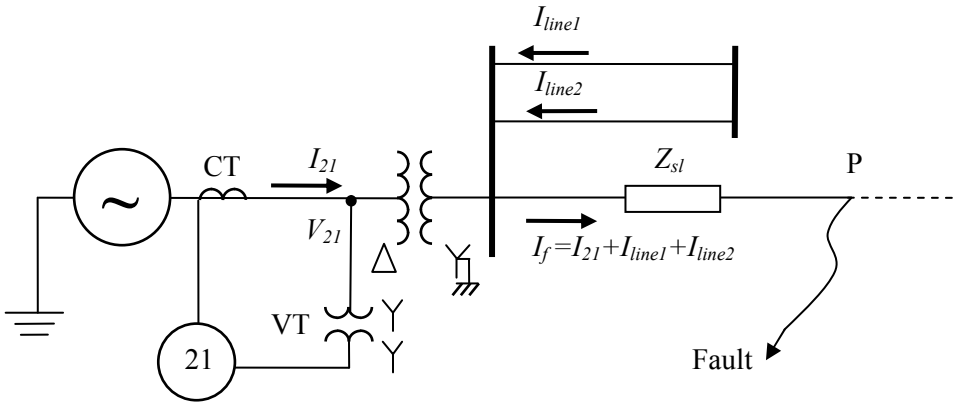

Figure 2.17. Apparent impedance measurement with system infeed currents.

2.7.2.3 Influence of an interposing wye-delta transformer

When Relay (21) is required to detect faults through a wye-delta transformer, the 30° phase shift (resulting from the wye-delta connection) will alter the impedance measured by the relay elements. Therefore, distance relays whose response is defined by Eqs. (2.18) to (2.20) will not measure the true positive-sequence impedance for phase-to-phase faults.

The installation of wye-delta auxiliary VTs and CTs to correct the 30° phase shift is advocated by many texts including standards [26]. These VTs and CTs, when phased properly, will negate the voltage and current phase shifts caused by the GSU transformer. The resulting voltages and currents seen by the distance relays are equivalent to those seen for a fault through a wye-wye or a delta-delta transformer.

2.7.2.4 Relay (21) setting criteria

As it is mentioned before, Relay (21) is set within the generator steady-state overexcited capability (GOEC) with adequate margin overload and stable power swings. Therefore, Relay (21) elements are, generally, set at the smallest of the following three criteria [26], [27]:

1. 120% of the longest line with system infeed currents.
2. 50% to 67% of the generator load impedance (Z_{load}) at the rated power factor angle (RPFA) of the generator. This provides a 150% to 200% margin over the generator full load.
3. 80% to 90% of the generator load impedance at the maximum torque angle (typically 85°).

A time delay of 1 second for the relay element is considered in the investigations reported in this chapter as well as in Chapter 3 to provide the proper coordination with the transmission line backup relays.

2.8 Coordination between Relay (21) and GOEC

Figure 2.9 shows that the generator steady-state overexcited capability (GOEC) limit is plotted on a P-Q (MW - MVAR) plane (curve ABC). On the other hand, the generator distance phase backup protection relay measures impedance and its characteristic is typically displayed on an R – X (ohm) plane as shown in Figure 2.11. To coordinate the GOEC limit with Relay (21) characteristic, it is necessary to convert the GOEC limit to an R - X plot. Figure 2.18 illustrates this conversion where the current transformer (CT) and the voltage transformer (VT) ratios (R_c/R_v) convert the primary ohms to the secondary side quantities that are set within the relay and the kV is the rated voltage of the generator [28], [16]. The GOEC limits of G_1 and G_2 in the R - X plane are shown in Figure 2.19.

2.9 Impacts of the Midpoint STATCOM and SVC on the Performance of Relay (21) of System I

The results of the time-domain simulation studies conducted on System I are analyzed with respect to the following points:

2.9.1 The relationship between the measured impedance by Relay (21) and the generator loading

The injected current of a midpoint STATCOM/SVC is a function of both the transmission line loading and length. The transmission line loading is directly related to the generator output

MVA while the line length affects its series impedance. Therefore, the measured impedance by the generator distance phase backup protection relay varies with the fault location in a nonlinear manner.

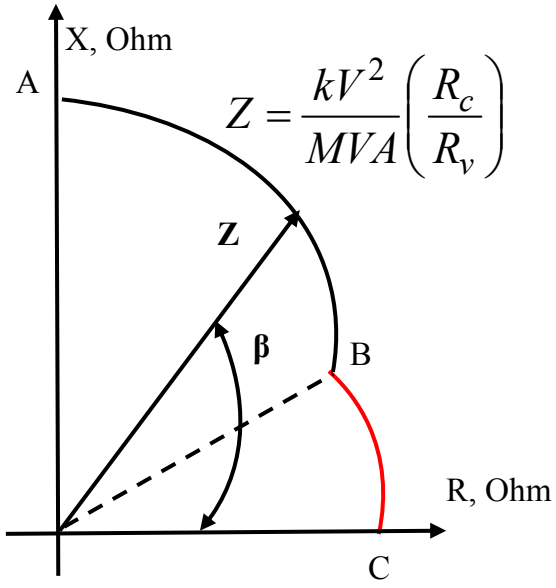

Figure 2.18. Transformation of a P-Q plot to an R-X plot.

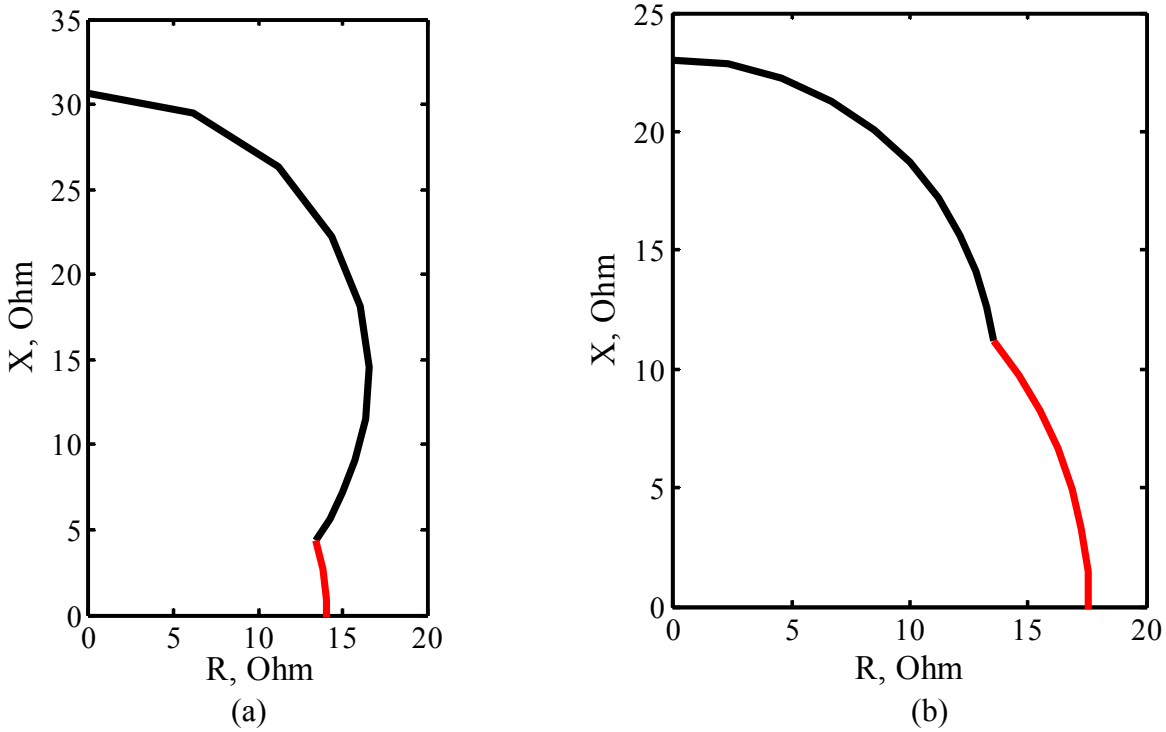

Figure 2.19. G_1 and G_2 GOEC limits in the R-X plane: (a) G_1, (b) G_2.

2.9.2 Midpoint STATCOM/SVC response to line-to-line faults

The midpoint STATCOM/SVC is designed to operate in a balanced mode. During unsymmetrical transmission line phase faults (i.e. line-to-line faults), the faulted phases experience a severe voltage collapse compared to the healthy phase. The midpoint STATCOM/SVC would, however, still inject three-phase balanced current in the three phases. This could result in a significant increase in the voltage of the healthy phase.

2.9.3 Effect of the midpoint STATCOM/SVC control circuit transient response during faults on Relay (21) operating time

The transient response of the midpoint STATCOM/SVC control circuit during three-phase and line-to-line faults causes the impedance trajectory seen by the generator distance phase backup protection relay to take a longer time to converge to a new steady-state value. This results in delaying the relay operating time.

2.9.4 Performance of Relay (21) during system phase faults and the definition of the percentage error in the measured impedance

In order to illustrate the adverse impacts of the midpoint STATCOM and SVC on the performance of Relay (21), the relay protective zone reach is set according to Section 2.7.2.4 (120% of the transmission line). This yields to $Z_{21} = 16.1\ \Omega$ at MTA = 85° (Appendix C).

The percentage error in the measured impedance (*PEMI*) by Relay (21) is defined as

$$PEMI, \%\ (Error, \%) = \frac{|Z_S| - |Z_N|}{|Z_N|} \times 100 \tag{2.32}$$

where $|Z_N|\angle\theta_N$ and $|Z_S|\angle\theta_S$ are respectively, the measured impedances by the relay without/with the STATCOM/SVC.

Figures 2.20 and 2.21 illustrate the effect of the midpoint STATCOM/SVC on the performance of Relay (21) during three-phase and line-to-line faults at different generator loadings and fault locations. The fault location on the transmission line is measured from bus A towards bus B (0%: fault is at bus A and 100%: fault is at bus B). The following observations are worth noting.

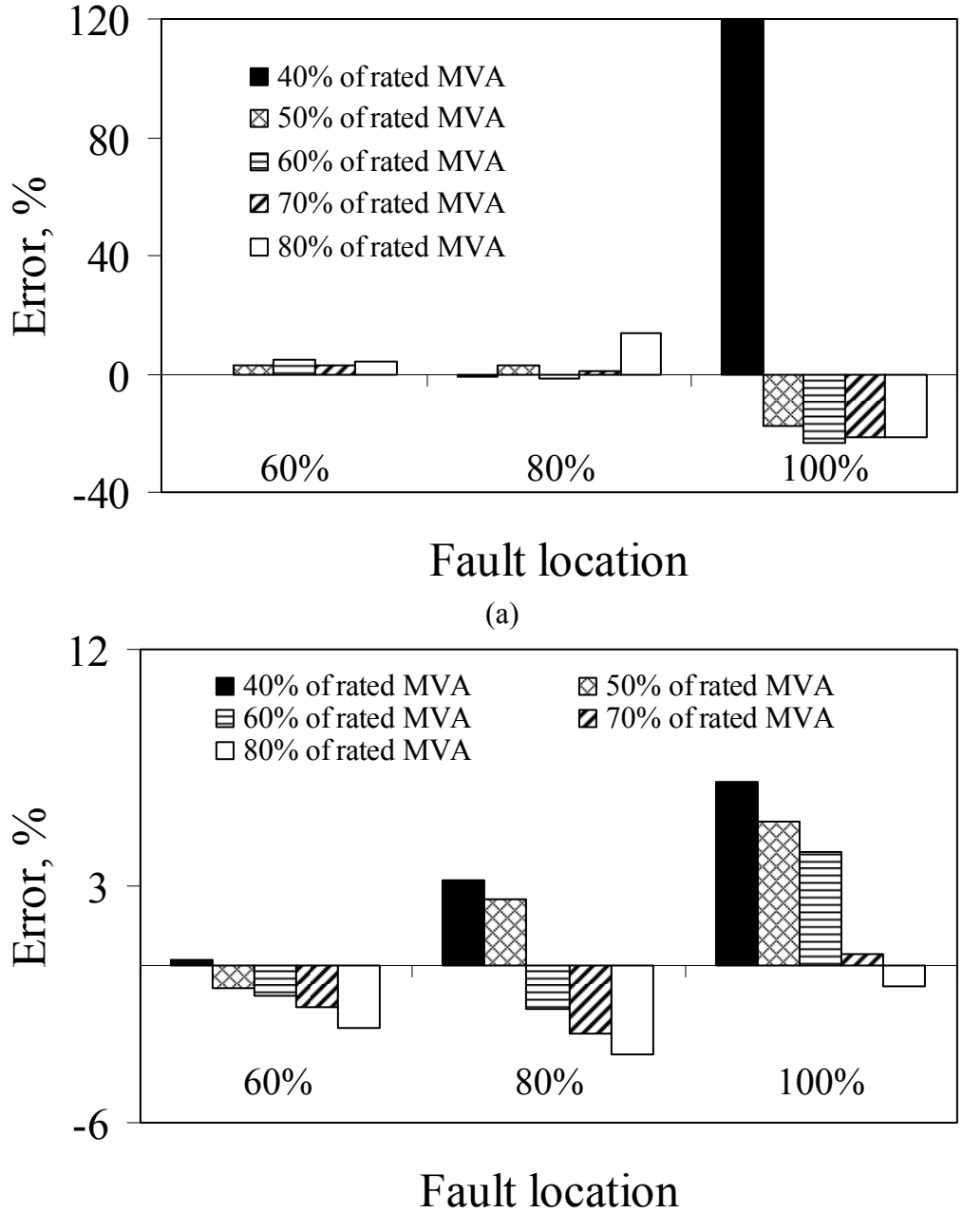

Figure 2.20. *PEMI* for three-phase faults in System I: (a) with a midpoint STATCOM, (b) with a midpoint SVC.

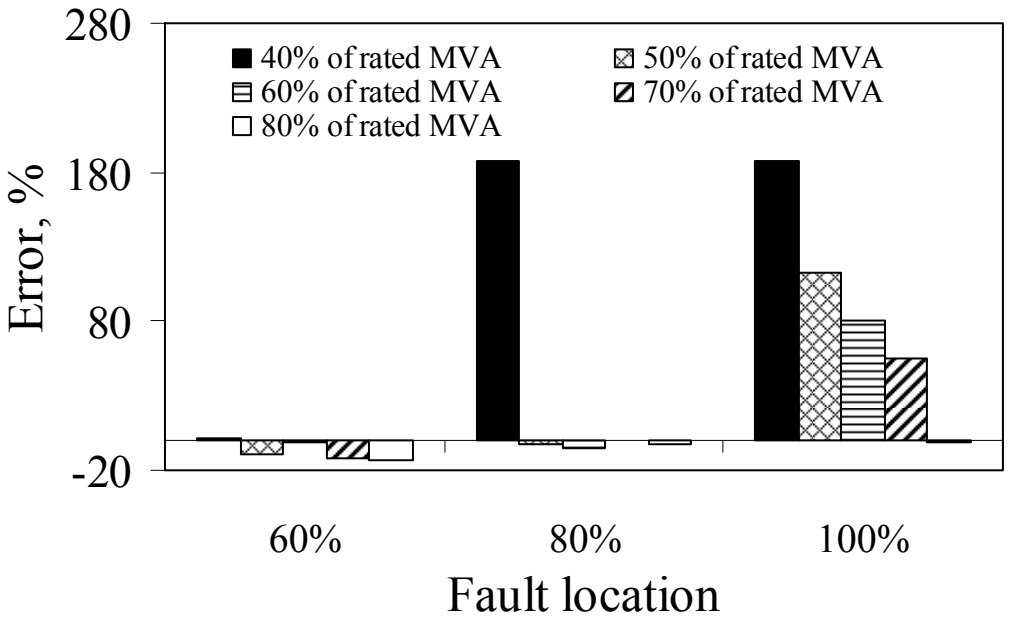

(a)

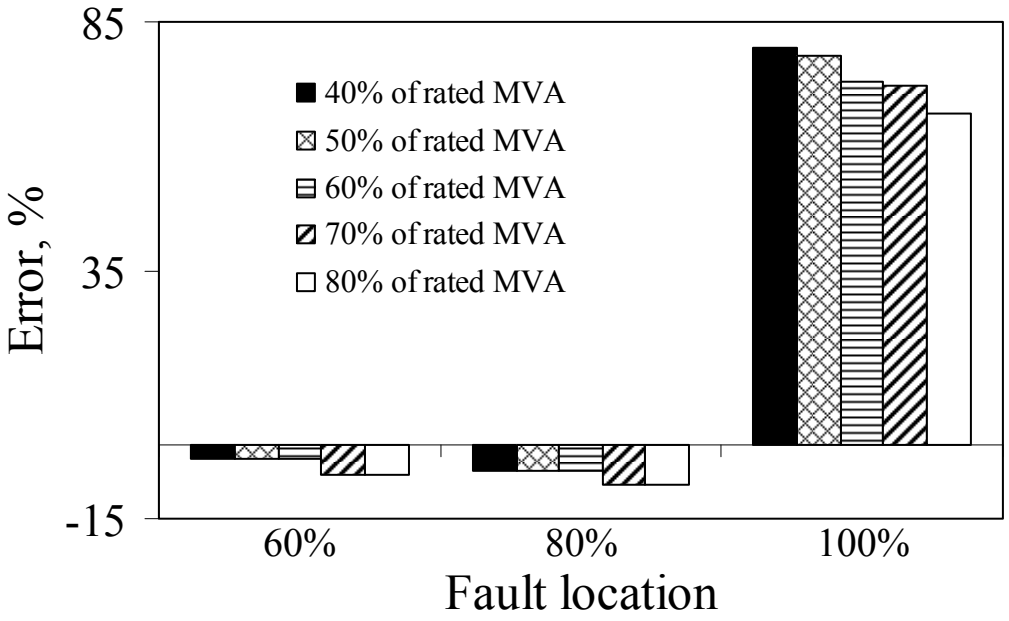

(b)

Figure 2.21. *PEMI* for line-to-line faults in System I: (a) with a midpoint STATCOM, (b) with a midpoint SVC.

2.9.4.1 Performance of Relay (21)

According to the value of *PEMI*, Relay (21) performance can be classified into the following categories:

- True underreach (TUR) (the relay does not pick up for faults inside the protected zone): where the fault (three-phase or line-to-line) is inside the protected zone and the measured impedance by Relay (21) with the midpoint STATCOM/SVC in service is greater than Relay (21) reach (and *PEMI* is equal or greater than 52.5% and 66.72% for the midpoint STATCOM and SVC respectively).
- False underreach (FUR) (Relay (21) picks up for a fault with a time delay): where the fault (three-phase or line-to-line) is inside the protected zone and the measured impedance with the midpoint STATCOM/SVC in service is smaller than Relay (21) reach (and *PEMI* is positive and less than 52.5% and 66.72% for the midpoint STATCOM and SVC respectively).
- True overreach (TOR) (Relay (21) picks up for faults outside the protected zone): where the fault is outside the protected zone and the measured impedance with the midpoint STATCOM/SVC in service is smaller than the relay reach. (this case, however, does not exist in System I).
- False overreach (FOR): (Relay (21) picks up with a time delay) where the fault is inside the protected zone and *PEMI* is negative.
- A time delay in Relay (21) element response has occurred (during FUR and FOR) for both the midpoint STATCOM and SVC. This time delay increases as the fault location varies from the midpoint of the transmission line to its end at bus B. The maximum time delays are obtained in the case of three-phase faults during FOR (0.167 s and 0.072 s with the midpoint STATCOM and SVC respectively).

Tables 2.1 and 2.2 show the time delays in Relay (21) response during FUR and FOR cases for three-phase and line-to-line faults at bus B. The relay malfunctions (TUR cases) are also shown in the same tables.

2.9.4.2 Effect of the generator loading

- The highest values of *PEMI* occurred at the lowest generator loading considered in the investigations of System I, namely 40%. The highest values of *PEMI* due to the midpoint STATCOM are 119.8% and 187.5% for the cases of three-phase and line-to-line faults respectively. On the other hand, the highest values of *PEMI* due to the midpoint SVC are 6.97% and 79.87% for the cases of three-phase and line-to-line faults respectively.
- For the same fault location, the response of the midpoint STATCOM/SVC to the variation in the generator loading may cause Relay (21) to experience TUR, FUR or FOR.

Table 2.1. Time delays in Relay (21) response and TUR cases during three-phase and line-to-line faults (with a midpoint STATCOM in System I).

		Faults at bus B	
		Line-to-line faults	Three-phase faults
Generator loading (% of rated MVA)	40%	TUR	TUR
	50%		0.167 s (FOR)
	60%		0.158 s (FOR)
	70%		0.156 s (FOR)
	80%	0.0533 s (FUR)	0.155 s (FOR)

Table 2.2. Time delays in Relay (21) response and TUR cases during three-phase and line-to-line faults (with a midpoint SVC in System I).

		Faults at bus B	
		Line-to-line faults	Three-phase faults
Generator loading (% of rated MVA)	40%	TUR	0.072 s (FOR)
	50%		0.063 s (FOR)
	60%		0.03 s (FOR)
	70%		–
	80%		–

2.9.4.3 Effect of the fault type

- As the midpoint STATCOM/SVC control circuits operate normally in a balanced mode (injecting three-phase balanced current), the severest impact of these FACTS Controllers

on Relay (21) is obtained during line-to-line faults, at all generator loadings and fault locations.

- In the case of the midpoint STATCOM, the maximum number of TUR cases (5 cases) is obtained for line-to-line faults; one case at 80% fault location and 40% generator loading and the other 4 cases at bus B at 40%, 50%, 60%, and 70% generator loadings. For three-phase faults, a TUR case at the end of the transmission line at 40% generator loading is obtained.
- In the case of the midpoint SVC, the maximum number of TUR cases (5 cases) is obtained for line-to-line faults at bus B for all of the generator loadings. For three-phase faults, no TUR cases occurred (only FUR and FOR cases).

2.9.4.4 Effect of the fault location

- In the case of three-phase faults, the highest value of *PEMI* is obtained for faults at the end of the transmission line (bus B) for both the midpoint STATCOM and SVC. In the case of line-to-line faults, the highest value of *PEMI* is obtained at 80% fault location and at bus B for only the midpoint STATCOM.
- The midpoint STATCOM and SVC have no impact (*PEMI* = 0) on the generator distance phase backup protection for faults occurring from bus A to the midpoint of the transmission line regardless of the generator loading or the type of fault. This finding is in a complete agreement with the results reported in [14], [15].

2.10. Impacts of the Midpoint STATCOM and SVC on the Coordination between Relay (21) and GOEC Limit for System I

The analysis in this section is based on the following basic points:

2.10.1 Coordination between Relay (21) and GOEC limit

In order to perform such coordination, the GOEC limit shown in Figure 2.19(a) is plotted with Relay (21) characteristic as shown in Figure 2.22.

2.10.2 Maximum setting of Relay (21)

The first factor which should be defined is the maximum setting of Relay (21) characteristic required to maintain the coordination with the GOEC limit at different generator loadings. This maximum setting, designated as Z_{GCC}, is selected in the investigations reported in this chapter at

90% of the generator load impedance at MTA = 85°. This yields Z_{GCC} =*27.54* Ω for G_1 (Appendix C) as shown in Figure 2.22.

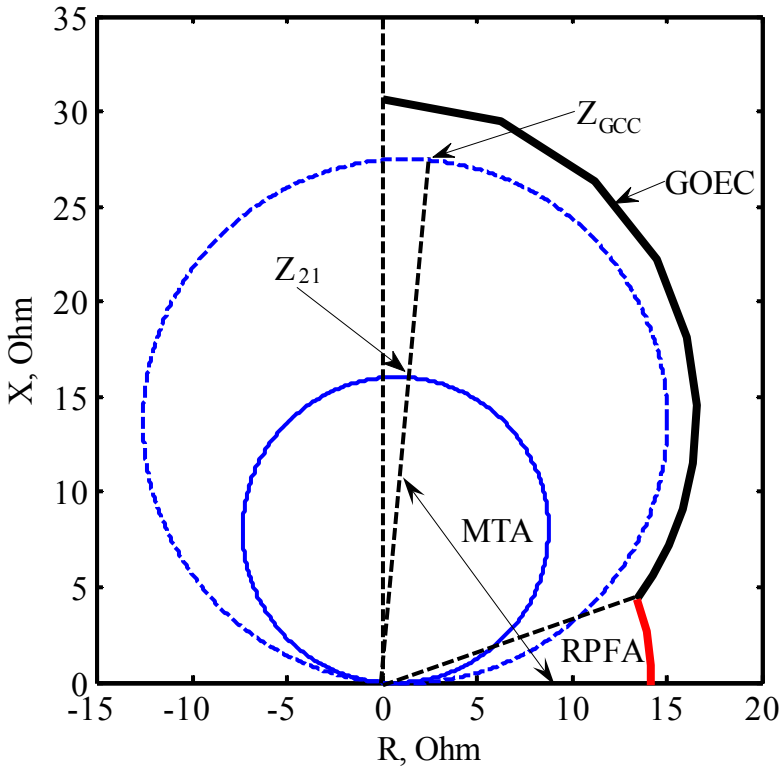

Figure 2.22. Coordination between Relay (21) and the GOEC limit in System I.

2.10.3 The Coordination Index *(CI)*

The second factor which would give an insight on the impact of the midpoint STATCOM/SVC on the coordination between Relay (21) characteristic and the GOEC limit is the coordination index. This index, designated as *CI*, is defined as

$$CI, \% = \frac{|Z_S|}{|Z_{Gcc}|} \times 100. \tag{2.33}$$

The impact of the midpoint STATCOM/SVC is explained with respect to the variation of *CI*. If *CI* is greater than 100%, the coordination is lost between Relay (21) and the GOEC limit. The results presented in Figures 2.23 and 2.24 show the effects of the midpoint STATCOM/SVC on the coordination between Relay (21) characteristic and the GOEC limit for three-phase and line-to-line faults respectively. The following observations are worth noting.

2.10.3.1 Effect of the generator loading

- For the same fault location, *CI* increases as the generator loading decreases. This is true in the case of the midpoint STATCOM/SVC for both three-phase and line-to-line faults.

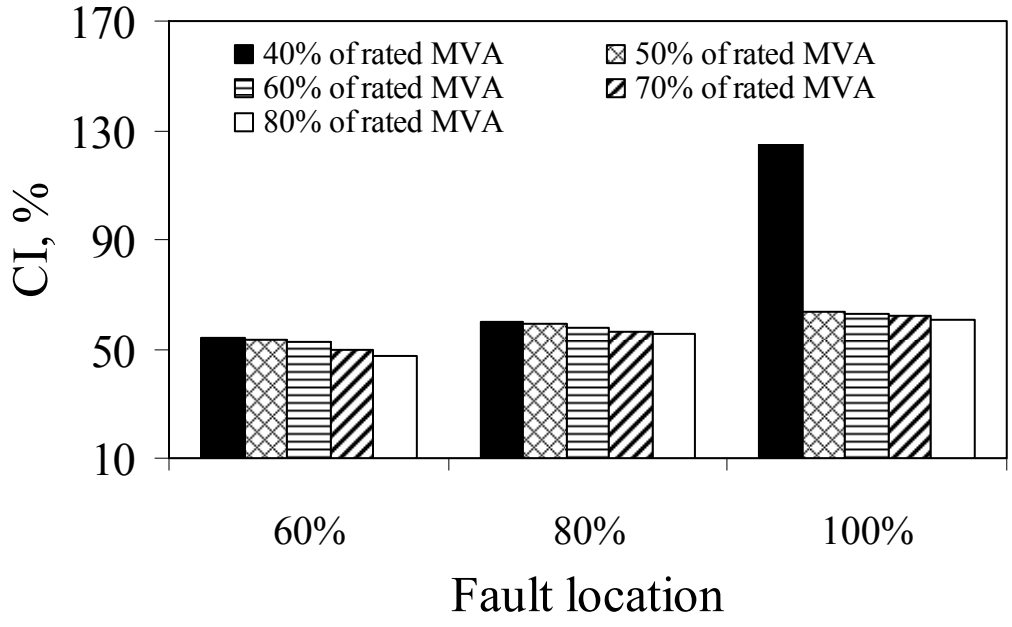

(a)

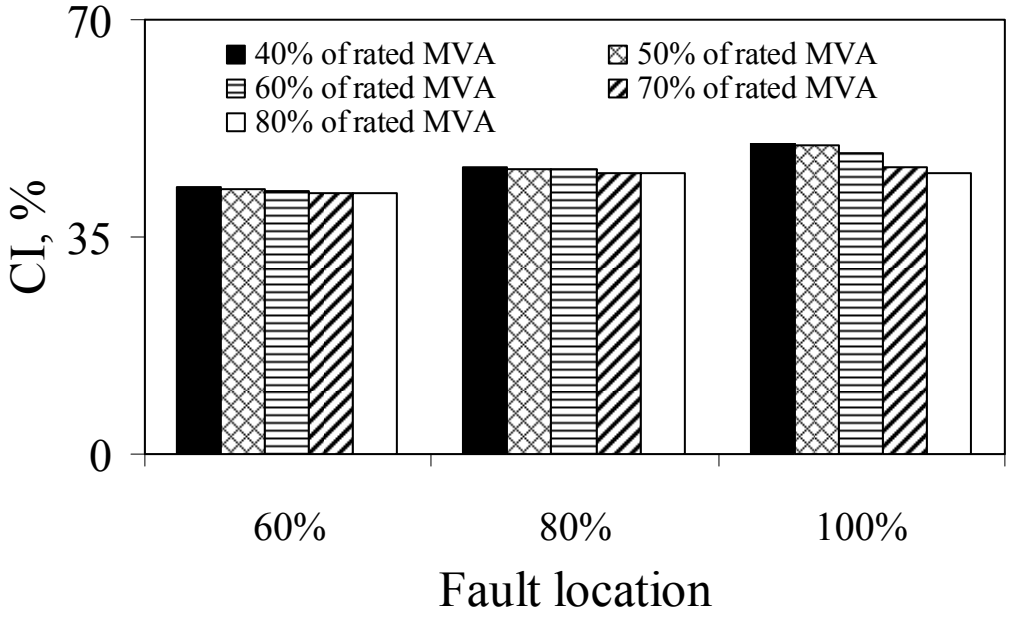

(b)

Figure 2.23. Coordination index, *CI* for three-phase faults in System I: (a) with a midpoint STATCOM, (b) with a midpoint SVC.

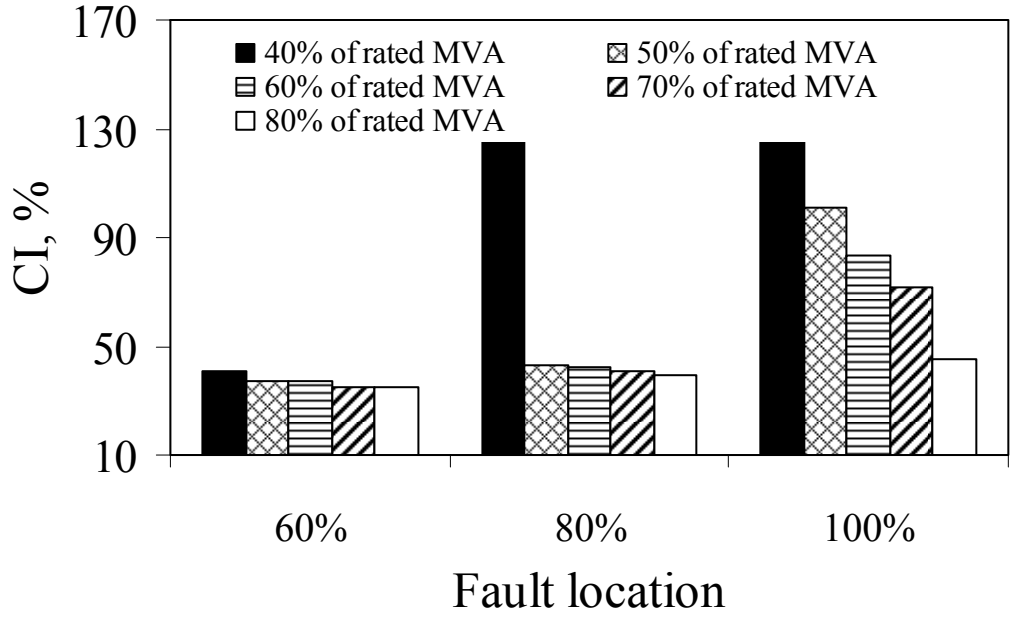

(a)

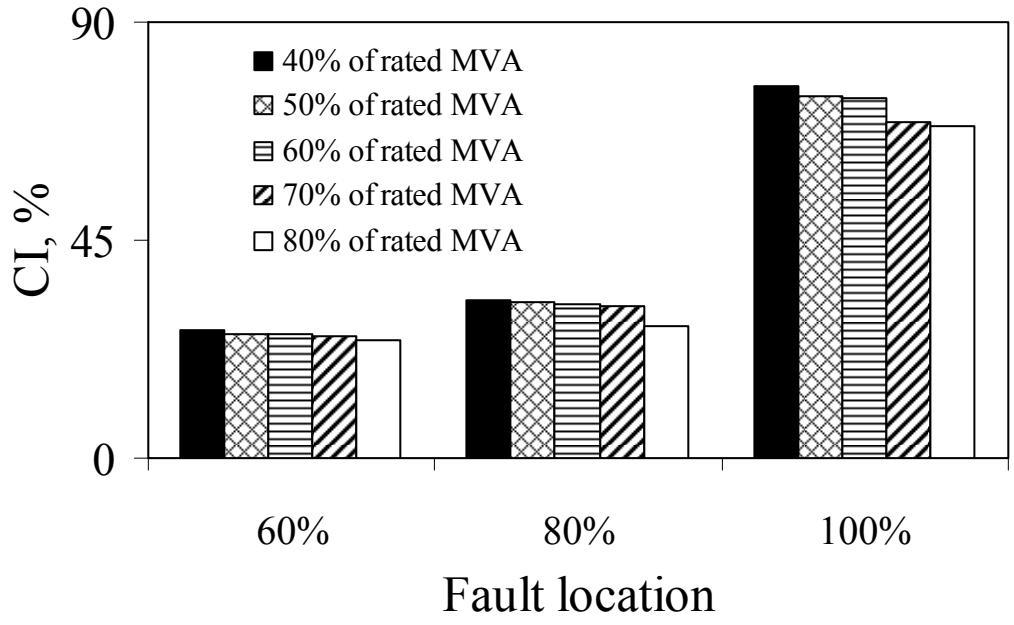

(b)

Figure 2.24. Coordination index, *CI* for line-to-line faults in System I: (a) with a midpoint STATCOM, (b) with a midpoint SVC.

- Regardless of the fault type or its location, the highest *CI* is obtained at the lowest generator loading (40%). This is true for both midpoint FACTS Controllers.

2.10.3.2 Effect of the fault type

In the case of the midpoint STATCOM, the ratio of the loss of coordination cases due to line-to-line faults to those due to three-phase faults is 3 to 1. On the other hand, the midpoint SVC has no impact on the coordination between Relay (21) and GOEC limit, regardless of the fault type (i.e. *CI* is always less than 100%).

2.10.3.3 Effect of the fault Location

- In the case of the midpoint STATCOM, the number of loss of coordination cases decreases as the fault location varies from bus B to the midpoint of the transmission line. This is true for both fault types. Moreover, the midpoint STATCOM has no impact on the coordination between Relay (21) and the GOEC limit for faults occurring from bus A to the midpoint of the transmission line regardless of the generator loading or the type of fault.
- The midpoint SVC has no impact on the coordination between the Relay (21) and the GOEC limit regardless of the fault location (i.e. *CI* is always less than 100%).

A comparison between the impacts of the midpoint STATCOM and SVC on the coordination between Relay (21) and the GOEC limit at bus B is illustrated graphically in the R-X plane in Figures 2.25 and 2.26 for three-phase and line-to-line faults respectively.

Table 2.3 shows a comparison between the impacts of the midpoint STATCOM and SVC on the performance and coordination efficiencies of Relay (21) of System I for all case studies. The performance efficiency ($\eta_{21\text{-}perf}$) and the coordination efficiency ($\eta_{21\text{-}coord}$) are defined as

$$\eta_{21-perf},\% = \left(1 - \frac{Number\ of\ TUR\ cases}{Total\ number\ of\ cases}\right) \times 100 \tag{2.34}$$

$$\eta_{21-Coord},\% = \left(1 - \frac{Number\ of\ loss\ of\ coordination\ cases}{Total\ number\ of\ cases}\right) \times 100. \tag{2.35}$$

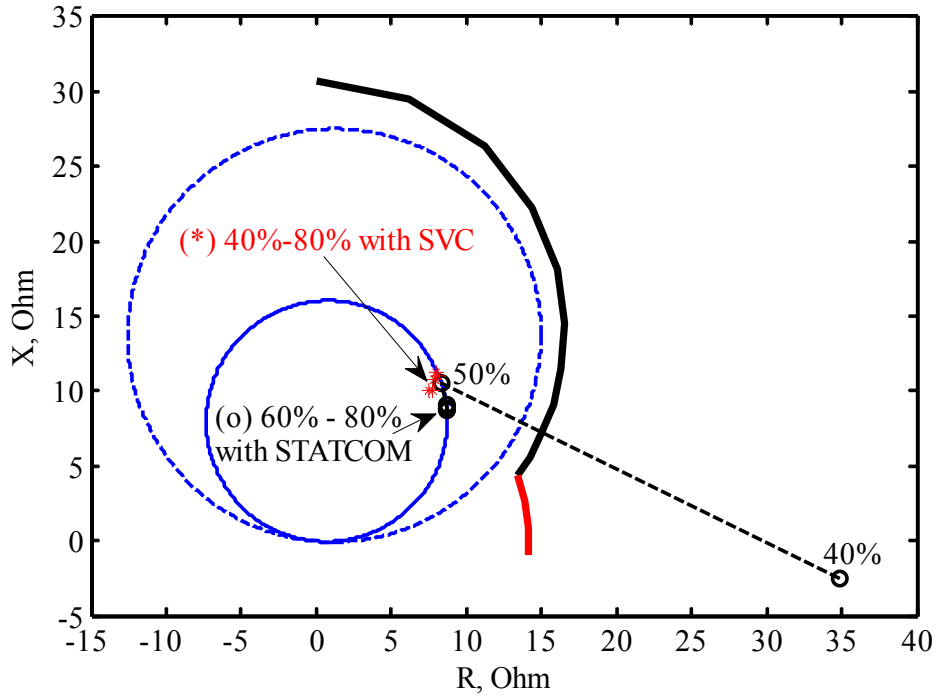

Figure 2.25. Impacts of the midpoint STATCOM and SVC on the coordination between Relay (21) and GOEC limit for three-phase faults in System I at bus B (the percentages are the generator loading).

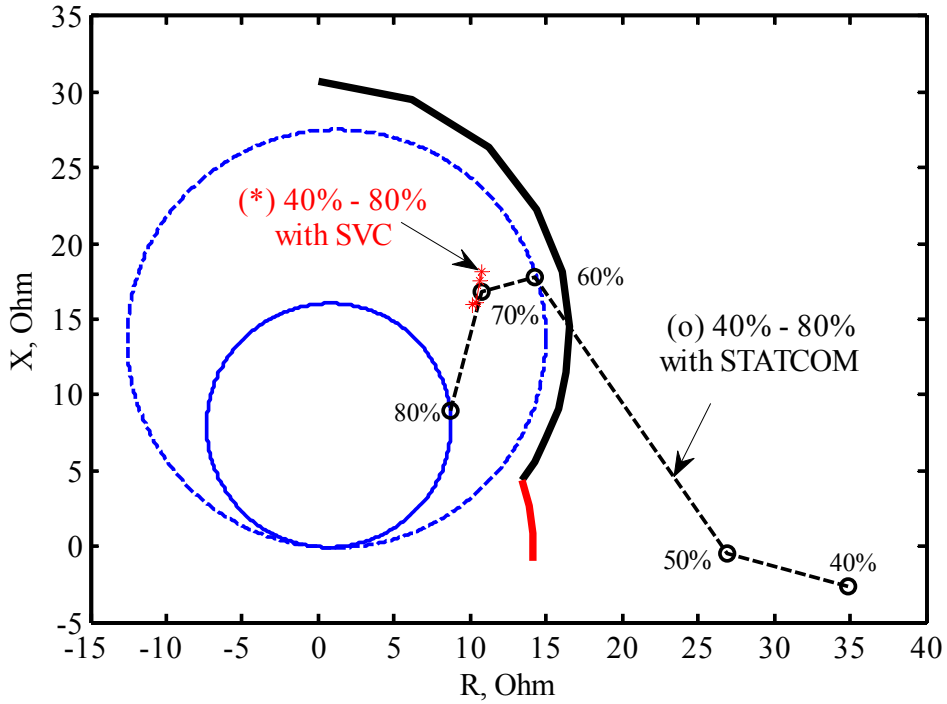

Figure 2.26. Impacts of the midpoint STATCOM and SVC on the coordination between Relay (21) and GOEC limit for line-to-line faults in System I at bus B (the percentages are the generator loading).

Table 2.3. Relay (21) of System I performance and coordination efficiencies for all case studies.

Fault type	Relay (21) performance efficiency		Relay (21) coordination efficiency	
	With a midpoint STATCOM	With a midpoint SVC	With a midpoint STATCOM	With a midpoint SVC
Three-phase	93.33%	100%	93.33%	100%
Line-to-line	66.67%	66.67%	80%	100%

As an example, with a midpoint STATCOM, the performance and coordination efficiencies of Relay (21) during line-to-line faults are calculated as follows

$$\eta_{21-perf},\% = \left(1 - \frac{5}{15}\right) \times 100 = 66.67\%$$

(total number of cases = 15 and number of TUR cases = 5)

and

$$\eta_{21-Coord},\% = \left(1 - \frac{3}{15}\right) \times 100 = 80\%$$

(total number of cases = 15 and number of loss of coordination cases = 3).

2.11 Impacts of the Midpoint STATCOM and SVC on Relay (21) of System II

The two advantages that System II configuration has over that of System I are:

1. It allows exploring the effect of faults on a transmission line (Line 2) adjacent to the midpoint shunt compensated transmission line (Line 1) on the performance of Relay (21).
2. It incorporates infeed currents during system faults.

The procedures for conducting the investigations on System II and the analysis of the results are very similar to those used for System I. However, due to the nature of System II configuration, the percentage error in the measured impedance (*PEMI)* by Relay (21) must be redefined in order to obtain accurate analysis. In this regard, *PEMI* is redefined as

$$PEMI,\%\ (Error,\%) = \frac{|Z_S| - |Z_N| \times \cos(\theta_N - \theta_S)}{|Z_N| \times \cos(\theta_N - \theta_S)} \times 100 \qquad (2.36)$$

where $|Z_N|\angle\theta_N$ and $|Z_S|\angle\theta_S$ are respectively, the measured impedances by the relay without/with the STATCOM/SVC.

Consequently, the modified definition of the coordination index is

$$CI, \% = \frac{|Z_S| \cos \theta_s}{|Z_{corr}| \cos \theta_{corr}} \times 100 \quad (2.37)$$

where $|Z_{corr}| \angle \theta_{corr}$ is the impedance corresponding to $|Z_S| \angle \theta_S$ on Z_{GCC} circumference.

The impact of the midpoint STATCOM/SVC is still explained with respect to the variation of *CI*. If *CI* is greater than 100%, the coordination is lost between Relay (21) and the GOEC limit.

2.11.1 Performance of Relay (21) of System II

Relay (21) protective zone reach is set according to Section 2.7.2.4 (at 67% of the generator load impedance (Z_{load}) at RPFA). This yields to Z_{21} = 16.8 Ω at MTA = 85° (Appendix C). Figures 2.27 to 2.29 illustrate the effect of the midpoint STATCOM/SVC on the performance of Relay (21) during three-phase and line-to-line faults on Lines 1 and 2 at different generator loadings and fault locations. The fault location on the transmission lines is expressed in terms of the relay reach (0%: fault is at bus A, 100%: fault is on Line 1 at the relay reach; 200 km from bus A and 50% fault: fault is on either line; 100 km from bus A). According to the value of *PEMI*, Relay (21) performance can be classified into the following categories:

- True underreach (TUR) (the relay does not pick up for faults inside the protected zone): where the fault (three-phase or line-to-line) is inside the protected zone and the measured impedance by Relay (21) with the midpoint STATCOM in service is greater than Relay (21) reach and *PEMI* is equal or greater than 4.41%. On the other hand, where the fault is inside the protected zone and the measured impedance by Relay (21) with the midpoint SVC in service is greater than Relay (21) reach and *PEMI* is equal or greater than 3.6% and 15.54% for three-phase and line-to-line faults respectively.
- False underreach (FUR) (Relay (21) picks up for a fault with a time delay): where the fault (three-phase or line-to-line) is inside the protected zone and the measured impedance with the midpoint STATCOM in service is smaller than Relay (21) reach and *PEMI* is positive and less than 4.41%. On the other hand, where the fault is inside the protected zone and the measured impedance by Relay (21) with the midpoint SVC in service is greater than Relay (21) reach and *PEMI* is positive and less than 3.6% and 15.54% for three-phase and line-to-line faults respectively.

- True overreach (TOR) (Relay (21) picks up for faults outside the protected zone): where the fault is outside the protected zone and the measured impedance with the midpoint STATCOM/SVC in service is smaller than the relay reach. (this case, however, does not exist in System II).
- False overreach (FOR): (Relay (21) picks up with a time delay) where the fault is inside the protected zone and *PEMI* is negative.

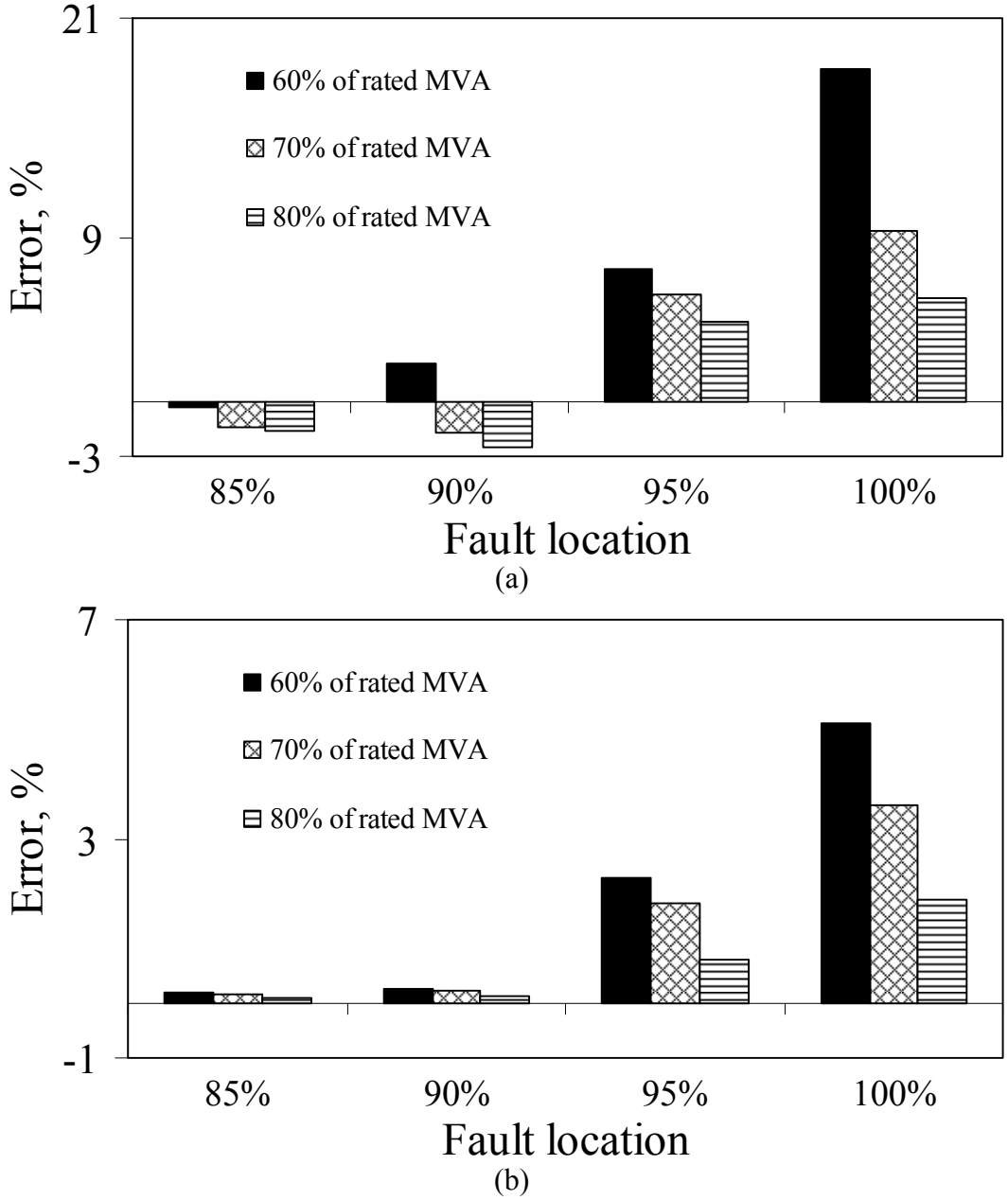

Figure 2.27. *PEMI* for three-phase faults on Line 1 in System II: (a) with a midpoint STATCOM, (b) with a midpoint SVC.

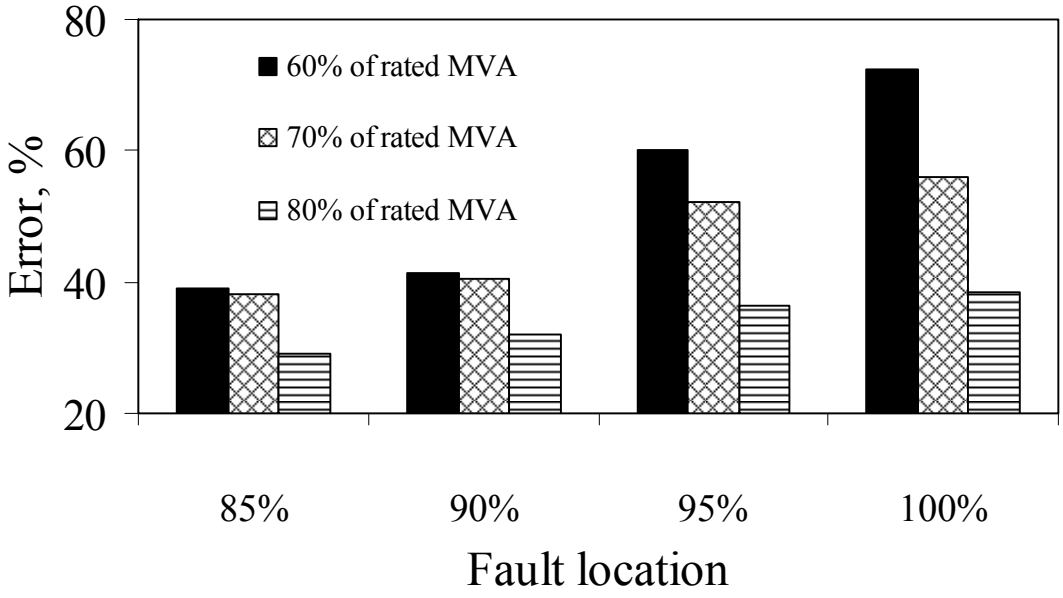

(a)

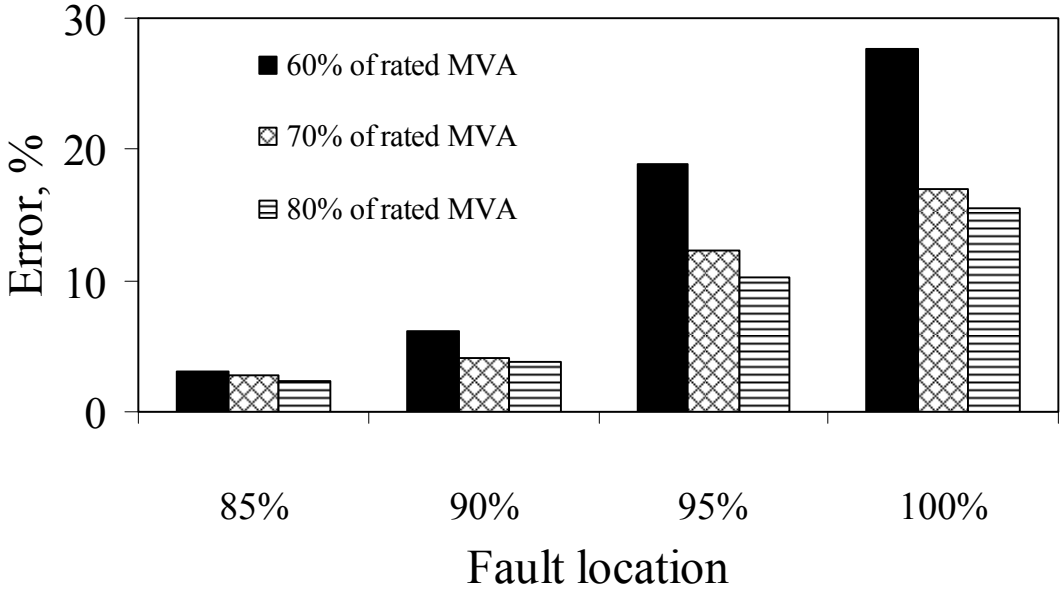

(b)

Figure 2.28. *PEMI* for line-to-line faults on Line 1 in System II: (a) with a midpoint STATCOM, (b) with a midpoint SVC.

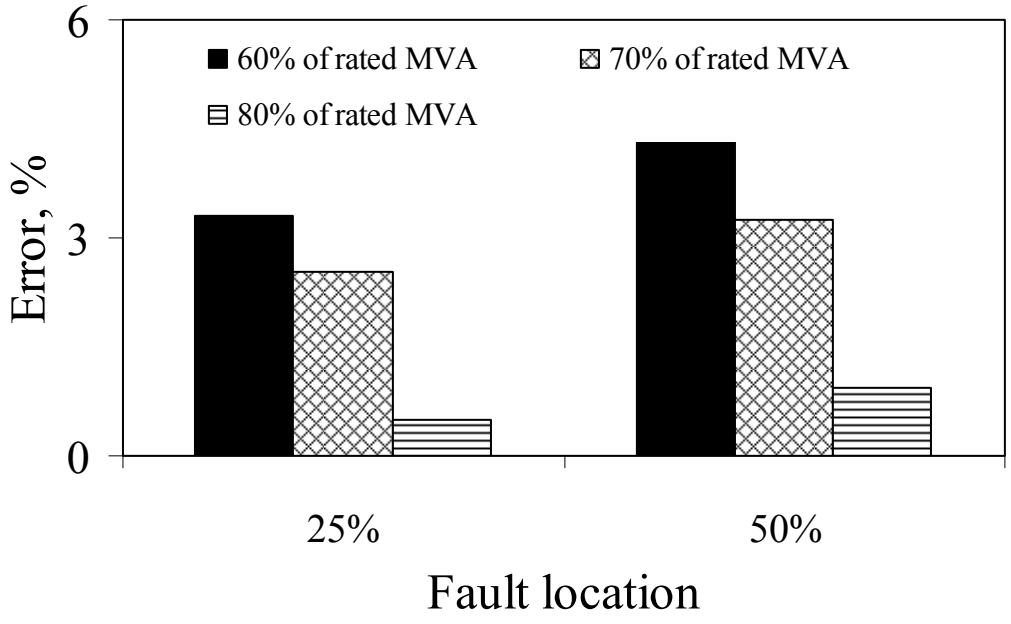

(a)

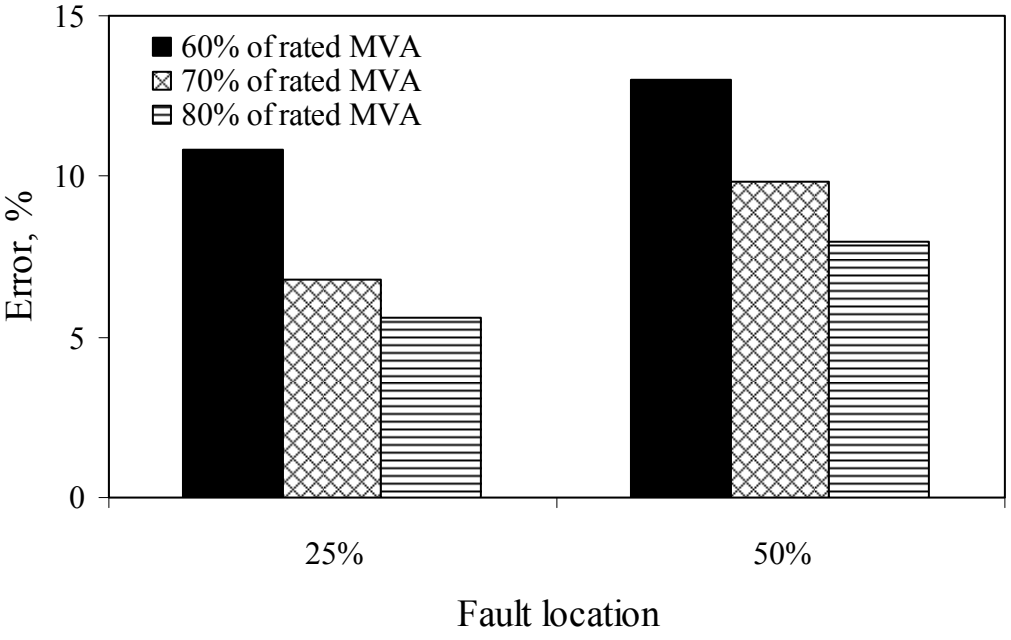

(b)

Figure 2.29. *PEMI* due to the midpoint STATCOM for faults on Line 2 in System II: (a) three-phase faults, (b) line-to-line faults.

- A time delay in Relay (21) element response has occurred (during FOR) in the case of the midpoint STATCOM. This time delay increases as the fault location varies from the midpoint of the transmission line to the relay reach. The maximum time delay (3.95 s with the midpoint STATCOM) is obtained in the case of a three-phase fault at 90% fault location and 60% loading.

Tables 2.4 and 2.5 show the relay malfunction (TUR cases) for three-phase and line-to-line faults at the relay reach.

Table 2.4. TUR cases during three-phase and line-to-line faults on Line 1 (with a midpoint STATCOM in System II).

		Faults on Line 1 at the relay reach	
		Line-to-line faults	Three-phase faults
Generator loading (% of rated MVA)	60%	TUR	TUR
	70%		
	80%		

Table 2.5. TUR cases during three-phase and line-to-line faults on Line 1 (with a midpoint SVC in System II).

		Faults on Line 1 at the relay reach	
		Line-to-line faults	Three-phase faults
Generator loading (% of rated MVA)	60%	TUR	TUR
	70%		
	80%		0.725 s

2.11.2 Effect of the generator loading

- The highest values of *PEMI* occurred at the lowest generator loading considered in the investigations of System II, namely 60%. The highest values of *PEMI* due to the midpoint STATCOM are 18.25% and 72.4% for the cases of three-phase and line-to-line faults respectively. On the other hand, the highest values of *PEMI* due to the midpoint SVC are 5.12 % and 27.6% for the cases of three-phase and line-to-line faults respectively.
- For the same fault location, the response of the midpoint STATCOM to the variation in the generator loading may cause Relay (21) to experience TUR, FUR or FOR. On the other hand, in the case of a midpoint SVC, Relay (21) may experience only TUR and FUR.

2.11.3 Effect of the fault type

- As the midpoint STATCOM/SVC control circuits operate normally in a balanced mode (injecting three-phase balanced current), the severest impact of these FACTS Controllers on Relay (21) is obtained during line-to-line faults, at all generator loadings and fault locations.
- In the case of the midpoint STATCOM, the maximum number of TUR cases (12 cases) is obtained for line-to-line faults on Line 1 for all generator loadings and fault locations. For three-phase faults on the same line, 6 TUR cases occurred (95% and 100% fault locations at all generator loadings).
- In the case of the midpoint SVC, the maximum number of TUR cases (4 cases) is obtained for line-to-line faults on Line 1 (3 at 100% fault location and 1 at 95% fault location and 60% loading). For three-phase faults on the same line, no TUR cases occurred (only FUR cases).

2.11.4 Effect of the fault location

- In the case of three-phase and line-to-line faults on Line 1, the highest value of *PEMI* is obtained for faults at the relay reach for both the midpoint STATCOM and SVC.
- The midpoint STATCOM and SVC have no impact (*PEMI* = 0) on the generator distance phase backup protection for faults occurring from bus A to the midpoint of Line 1 regardless of the generator loading or the type of fault. Here again, this finding is in a complete agreement with the results reported in [14], [15].
- In the case of three-phase and line-to-line faults on Line 2, the highest value of *PEMI* is obtained for faults at the end of the line for the case of the midpoint STATCOM. On the other hand, no effect is observed (*PEMI* is zero) for the case of the midpoint SVC.

2.12 Impacts of the Midpoint STATCOM and SVC on the Coordination between Relay (21) and GOEC Limit for System II

The maximum setting of Relay (21) characteristic required to maintain the coordination with the GOEC limit at different generator loadings, Z_{GCC}, is selected at 90% of the generator load impedance at MTA = 85°. This yields $Z_{GCC} = 20.8\ \Omega$ (Appendix C) as shown in Figure 2.30.

Figures 2.31 and 2.32 show the effects of the midpoint STATCOM/SVC on the coordination between Relay (21) characteristic and the GOEC limit for three-phase and line-to-line faults on

Line 1 respectively (no loss of coordination cases occurred due to faults on Line 2). The following observations are worth noting.

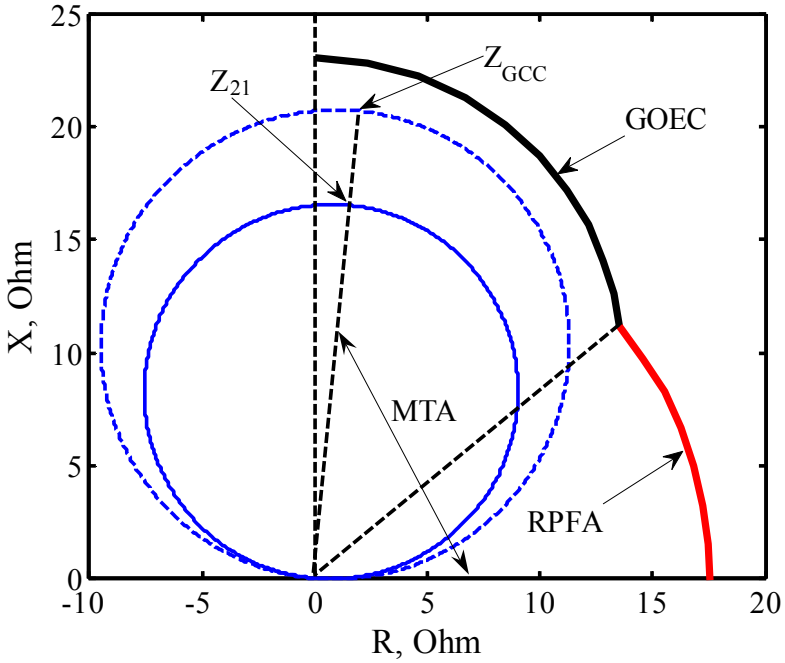

Figure 2.30. Coordination between Relay (21) and the GOEC limit in System II.

2.12.1 Effect of the generator loading

For the same fault location, *CI* increases as the generator loading decreases. This is true in the case of the midpoint STATCOM/SVC for both three-phase and line-to-line faults.

2.12.2 Effect of the fault type

In the case of the midpoint STATCOM, the ratio of the loss of coordination cases due to line-to-line faults to those due to three-phase faults is 2 to 1. On the other hand, in the case of the midpoint SVC, all the three cases of loss of coordination occurred due to line-to-line faults.

2.12.3 Effect of the fault Location

- In the case of the midpoint STATCOM/SVC, *CI* decreases as the fault location varies from the relay reach to the midpoint of the transmission line. Moreover, the number of loss of coordination cases decreases as the fault location varies from the end of the relay reach to the midpoint of the transmission line. This is true for both fault types. Moreover, the midpoint STATCOM/SVC has no impact on the coordination between Relay (21) and the GOEC limit

for faults occurring from bus A to the midpoint of the transmission line regardless of the generator loading or the type of fault.

A comparison between the impacts of the midpoint STATCOM and SVC on the coordination between Relay (21) of System II and the GOEC limit at the relay reach is illustrated graphically in the R-X plane in Figures 2.33 and 2.34 for three-phase and line-to-line faults respectively.

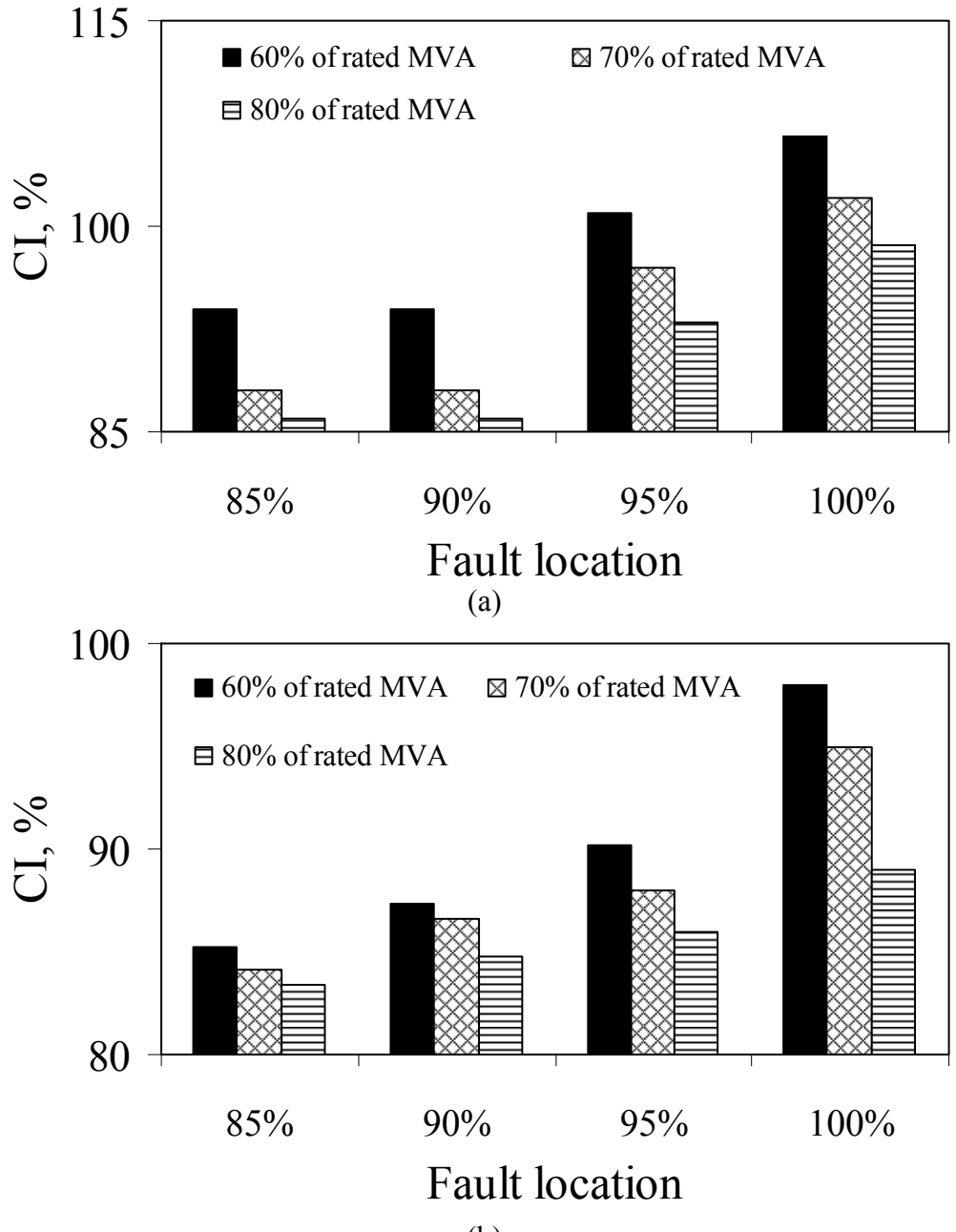

Figure 2.31. Coordination index, *CI* for three-phase faults on Line 1 in System II: (a) with a midpoint STATCOM, (b) with a midpoint SVC.

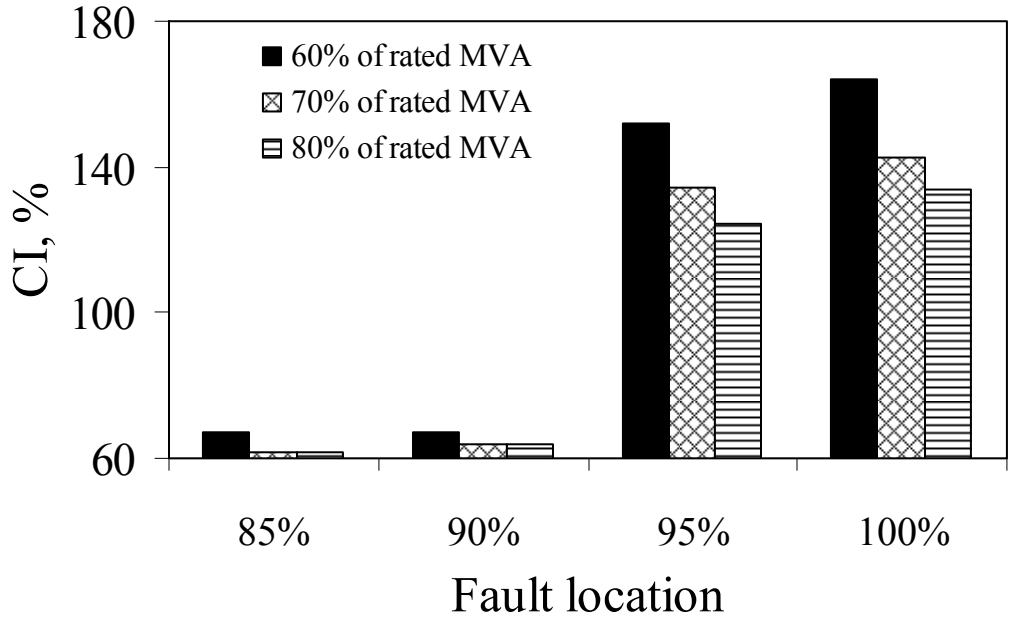

(a)

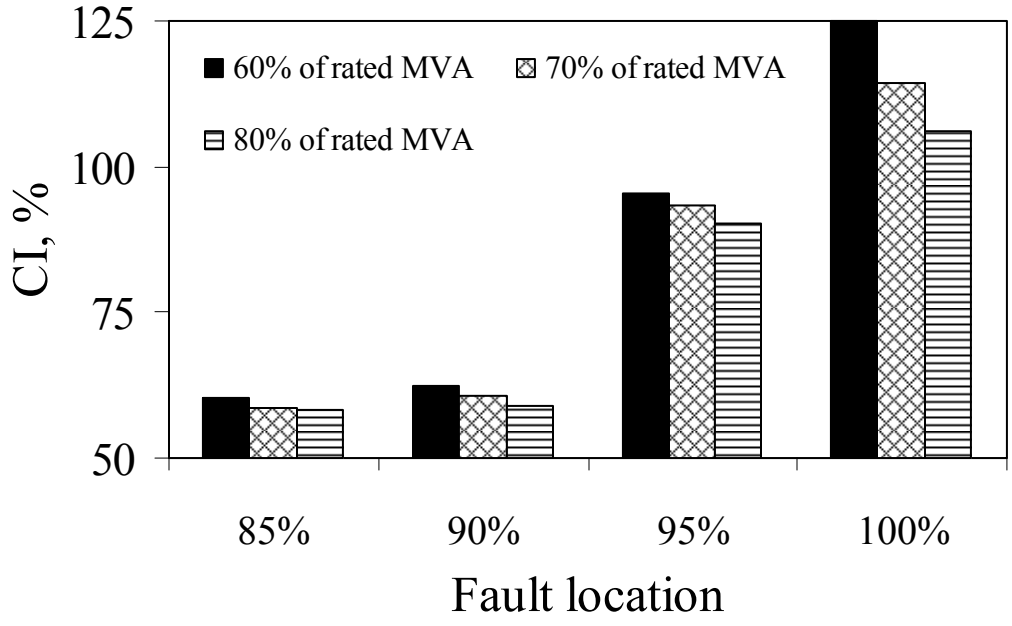

(b)

Figure 2.32. Coordination index, *CI* for line-to-line faults on Line 1 in System II: (a) with a midpoint STATCOM, (b) with a midpoint SVC.

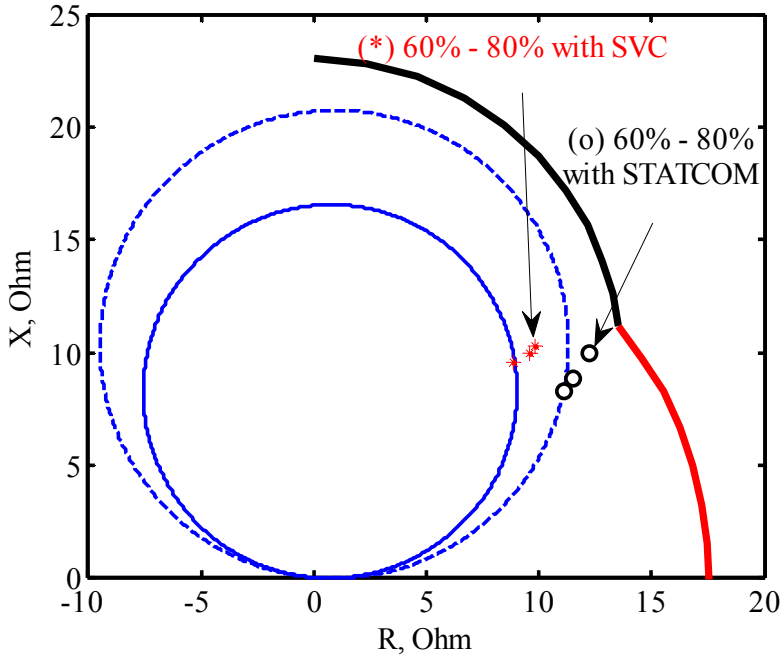

Figure 2.33. Impacts of the midpoint STATCOM and SVC on the coordination between Relay (21) and GOEC limit for three-phase faults on Line 1 in System II at the relay reach (the percentages are the generator loading).

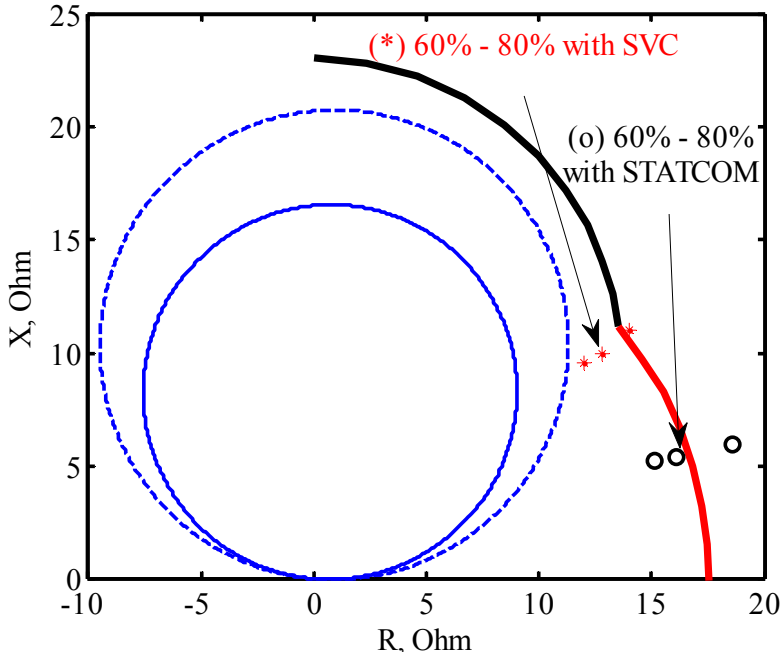

Figure 2.34. Impacts of the midpoint STATCOM and SVC on the coordination between Relay (21) and GOEC limit for line-to-line faults on Line 1 in System II at the relay reach (the percentages are the generator loading).

Table 2.6 shows a comparison between the impacts of the midpoint STATCOM and SVC on the performance and coordination efficiencies of Relay (21) (defined by Eqs. 2.34 and 2.35 respectively) of System II for all case studies.

Table 2.6. Relay (21) of System II performance and coordination efficiencies for all case studies.

Fault type	Relay (21) performance efficiency		Relay (21) coordination efficiency	
	With a midpoint STATCOM	With a midpoint SVC	With a midpoint STATCOM	With a midpoint SVC
Three-phase	66.67%	88.89%	83.33%	100%
Line-to-line	33.33%	77.78%	66.67%	83.33%

As an example, with a midpoint STATCOM, the performance and coordination efficiencies of Relay (21) during line-to-line faults are calculated as follows

$$\eta_{21-perf},\% = \left(1 - \frac{12}{18}\right) \times 100 = 33.33\%$$

(total number of cases = 18 on Lines 1 and 2 and number of TUR cases = 12)

and

$$\eta_{21-Coord},\% = \left(1 - \frac{6}{18}\right) \times 100 = 66.67\%$$

(total number of cases = 18 on Lines 1 and 2 and number of loss of coordination cases = 6).

2.13 Summary

In this chapter, investigations are carried out to explore the impacts of midpoint STATCOM and SVC on the coordination between the generator distance phase backup protection and the generator steady-state overexcited capability (GOEC) limit. The results of these investigations which are conducted on Systems I and II have shown that both the midpoint STATCOM and the SVC have an adverse effect on Relay (21). Such an impact varies according to the fault type, fault location and generator loading. It has been found for Systems I and II that the reaches of the generator distance phase backup protection relay are 16.1 Ω at MTA of 85° and 16.8 Ω at MTA of 85° respectively. With the presence of the midpoint STATCOM and SVC, it has been shown that these reaches have been exceeded at some generator loadings and fault locations.

Moreover, it has been found that the adverse effect of the midpoint STATCOM and SVC extends to affect the coordination between Relay (21) and the GOEC limit. Such an impact

varies also according to the fault type, fault location and generator loading. It has also been found that the maximum settings of Relay (21), which can keep the coordination with the GOEC limits, are 27.54 Ω at MTA of 85° and 20.8 Ω at MTA of 85° for Systems I and II respectively. With the presence of the midpoint STATCOM and SVC, it has been shown that these limits have been exceeded at some generator loadings and fault locations.

The above discussion clearly identifies potential problems with the existing generator distance phase backup protection and highlights the need for the search for new methods to achieve better coordination when midpoint FACTS Controllers are in service. The use of the Support Vector Machines technique for achieving a better coordination between generator phase backup protection and GOEC limit is proposed and investigated in the next chapter.

3. ENHANCEMENT OF THE COORDINATION BETWEEN GENERATOR PHASE BACKUP PROTECTION AND GENERATOR CAPABLITY LIMITS IN THE PRESENCE OF A MIDPOINT STATCOM USING SUPPORT VECTOR MACHINES

3.1 Introduction

This chapter presents an in depth discussion on the principles of the support vector machines classification technique and its mathematical formulation for solving pattern classification problems. The application of the support vector machines classification technique to generator phase backup protection, aimed on enhancing the coordination between such a protection and the generator steady-state overexcited capability (GOEC) limit in the presence of a midpoint STATCOM, is also presented.

3.2 Support Vector Machines

Support Vector Machines (SVMs) are a set of related supervised learning methods that analyze data and recognize patterns, used for classification and regression analysis. The standard SVM takes a set of input data and predicts, for each given input, which of two possible classes the input is a member of, which makes the SVM a non-probabilistic binary linear classifier. Since an SVM is a classifier, then given a set of training examples, each marked as belonging to one of two categories, an SVM training algorithm builds a model that predicts whether a new example falls into one category or the other. Intuitively, an SVM model is a representation of the examples as points in space, mapped so that the examples of the separate categories are divided by a clear gap that is as wide as possible. New examples are then mapped into that same space and predicted to belong to a category based on which side of the gap they fall on. The simplest form of a prediction problem is binary classification trying to discriminate between objects that belong to one of two categories, positive (+1) or negative (-1). SVMs use two key

concepts to solve this problem, large-margin separation and Kernel functions as described in the following sections.

3.3 Large Margin Separation

The idea of large margin separation can be motivated by the classification of points in two dimensions as shown in Figure 3.1.

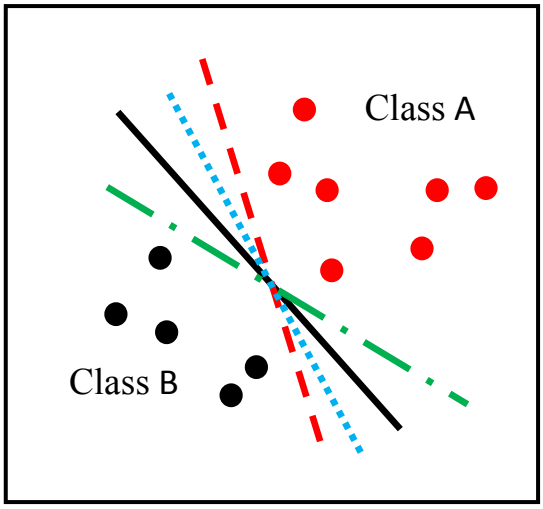

Figure 3.1. Large margin separation principle.

A simple way to classify the points is to draw a straight line and all the points which are lying on one side belong to Class A, otherwise, Class B. If the two sets are well separated, therefore, there exist many such separating hyperplanes that correctly classify all data points. However, there exists only one optimal separating hyperplane that it is as far as possible away from the points in both sets [29], [30]. The choice of the optimal hyperplane captures the idea of the large margin separation which is mathematically formulated in Subsection 3.3.2.

3.3.1 Linear separation with hyperplanes [31]-[39]

Consider the linear separable training data shown in Figure 3.1 which consist of a vector $\boldsymbol{x}$ with **N** components $\boldsymbol{x}_i$, where i = 1,2,…..**N**. The notation $\boldsymbol{x}_i$ will denote the i^{th} vector in a data set $\{(\boldsymbol{x}_i, y_i)\}_{i=1}^{N}$, where, y_i is the label associated with the vector $\boldsymbol{x}_i$, i.e. $\{\boldsymbol{x}_i, y_i\}$, and $y_i \in \{+1,-1\}$ corresponding to the class of $\boldsymbol{x}_i$ (y_i =1 for Class A, the red balls, y_i = -1 for Class B, the black balls). The concept for defining a linear classifier is based on the dot product between two vectors $\boldsymbol{w}$ and $\boldsymbol{x}$ as follows

$$\boldsymbol{x} \cdot \boldsymbol{w} = \sum_{i=1}^{N} x_i w_i. \tag{3.1}$$

In addition, a linear classifier is based on a linear discriminant function [30]-[33] of the following form

$$f(\boldsymbol{x}) = \boldsymbol{x} \cdot \boldsymbol{w} + b. \tag{3.2}$$

The discriminant function $f(\boldsymbol{x})$ assigns a value for the input $\boldsymbol{x}$, and is used to decide how to classify it. The vector $\boldsymbol{w}$ is known as the weight vector and it is a normal vector on the hyperplane. The scalar b is called the bias and it represents the distance from the origin to the hyperplane $\boldsymbol{H_P}$ as shown in Figure 3.2.

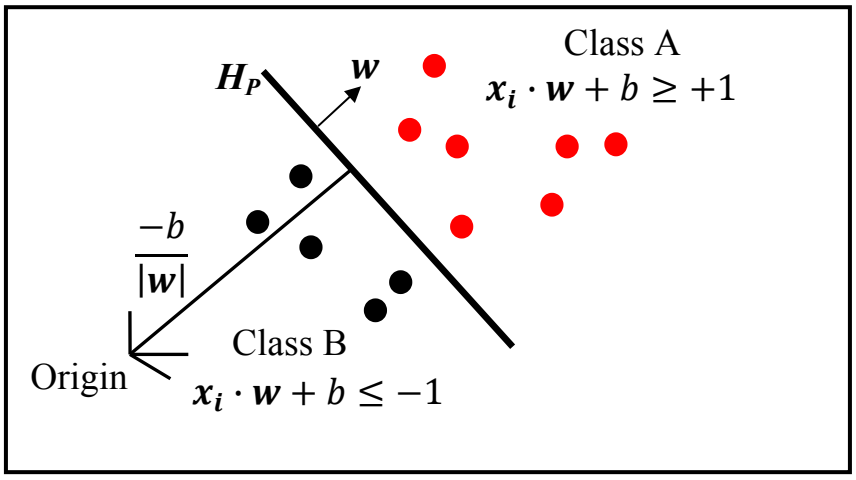

Figure 3.2. A linear separating hyperplane for linearly separable data.

The hyperplane shown in Figure 3.2 can be described as follows

$$\boldsymbol{x} \cdot \boldsymbol{w} + b = 0 \tag{3.3}$$

where this hyperplane $\boldsymbol{H_P}$ divides the space into two half spaces according to the sign of $f(\boldsymbol{x})$ which indicates the training data corresponding to Class A or B as follows

$$\text{Class A:} \quad \boldsymbol{x}_i \cdot \boldsymbol{w} + b \geq +1 \qquad \text{for } y_i = +1 \tag{3.4}$$

$$\text{Class B:} \quad \boldsymbol{x}_i \cdot \boldsymbol{w} + b \leq -1 \qquad \text{for } y_i = -1. \tag{3.5}$$

The boundary between the regions classified as positive and negative is called the decision boundary of the classifier. The decision boundary defined by a hyperplane (in the form of Eq. (3.2)) is said to be linear because it is linear in the input. Moreover, the classifier with a linear decision boundary is called a linear classifier. Furthermore, it will be shown in the next sections

how the principle of operation of a SVM linear classifier will be modified according to the type of the data samples.

3.3.2 Classification with large margin

3.3.2.1 Linearly separable data and the hard margin SVM [31]-[34]

In this section, the linearly separable data shown in Figure 3.1 are considered. As it is noted before, there exist many such separating hyperplanes that correctly classify all the data points but there exists only one optimal separating hyperplane. The optimal separating hyperplane is defined as the hard margin, which ensures that not only the training data, but also future data, unseen by the classifier at the training time, are classified correctly.

Therefore, the hard margin SVM, applicable to linearly separable data, is the classifier that not only separates the data correctly, but also does so with a large margin. The margin of a linear classifier is defined as the distance of the closest pattern to the decision boundary (m_r), as shown in Figure 3.3. The inequalities in Eqs. (3.4) and (3.5) can be combined as

$$y_i(\boldsymbol{x}_i \cdot \boldsymbol{w} + b) - 1 \geq 0 \quad \forall_i. \tag{3.6}$$

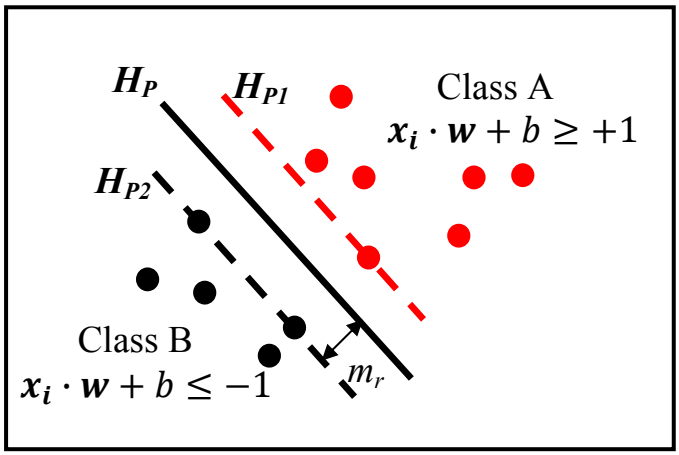

Figure 3.3. Optimal hyperplane through two linearly separable classes.

The inequalities of Eq. (3.6) can define hyperplanes $\boldsymbol{H_{P1}}$, and $\boldsymbol{H_{P2}}$ respectively. If $\boldsymbol{H}_{P1}$ and $\boldsymbol{H_{P2}}$ are parallel (they have the same normal) and no training data fall between them, any training data belong to Class A or Class B and lying on $\boldsymbol{H_{P1}}$ or $\boldsymbol{H_{P2}}$ are called support vectors (SVs) and described as follows

$$\boldsymbol{x}_i \cdot \boldsymbol{w} + b = +1 \qquad \text{for } \boldsymbol{H_{P1}} \tag{3.7}$$

$$\boldsymbol{x}_i \cdot \boldsymbol{w} + b = -1 \qquad \text{for } \boldsymbol{H_{P2}}. \tag{3.8}$$

Therefore, the aim of the SVM is to find a pair of hyperplanes which give the maximum margin m_r. From the vector geometry in Figure 3.3, the separating margin m_r of hyperplane $\boldsymbol{H_P}$ is equal to

$$m_r = \frac{1}{\|\boldsymbol{w}\|}. \tag{3.9}$$

Maximizing the separating margin m_r subject to the constraint in Eq. (3.6) is equivalent to

$$\text{Min}_{\boldsymbol{w},b} \ \|\boldsymbol{w}\| \quad \text{such that} \quad \text{y}_\text{i}(\boldsymbol{x}_i \cdot \boldsymbol{w} + b) - 1 \geq 0 \ \ \forall_\text{i}. \tag{3.10}$$

On the other hand, minimizing $\|\boldsymbol{w}\|$ is equivalent to minimizing $\frac{1}{2}\|\boldsymbol{w}\|^2$ and the use of this term makes it possible to perform Quadratic Programming (QP) optimization later on. Therefore, in order to compute $\boldsymbol{w}$ and b corresponding to the maximum margin hyperplane, the problem can be formulated as follows

$$\text{Min}_{\boldsymbol{w},b} \ \frac{1}{2}\|\boldsymbol{w}\|^2 \quad \text{such that} \quad y_i(\boldsymbol{x}_i \cdot \boldsymbol{w} + b) - 1 \geq 0 \quad \forall_i. \tag{3.11}$$

The above quadratic optimization problem is best solved using the Lagrangian formulation because the constraints in Eq. (3.6) will be replaced by constraints on the Lagrangian multipliers themselves, which will be much easier to handle. Also, in this formulation, the training data will only appear in the form of dot products between vectors. Thus, positive Lagrange multipliers α_i, i = 1,…, N are introduced with one Lagrangian multiplier for each of the inequality constraints in Eq. (3.6).

In order to form Lagrangian formulation, the following rule is considered; for constraints of the form $c_i \geq 0$, the constraint equations are multiplied by positive Lagrange multipliers and subtracted from the objective function. Taking into account that for the inequalities in Eq. (3.6), the Lagrangian multipliers are unconstrained, a Lagrangian expression is expressed as follows

$$\boldsymbol{L_P} \equiv \frac{1}{2}\|\boldsymbol{w}\|^2 - \boldsymbol{\alpha}[\text{y}_\text{i}(\boldsymbol{x}_i \cdot \boldsymbol{w} + b) - 1 \ ] \tag{3.12}$$

$$\equiv \frac{1}{2}\|\boldsymbol{w}\|^2 - \sum_{\text{i}=1}^{\text{N}} \alpha_i[y_i(\boldsymbol{x}_i \cdot \boldsymbol{w} + b) - 1 \ ] \tag{3.13}$$

$$\equiv \frac{1}{2}\|\boldsymbol{w}\|^2 - \sum_{\text{i}=1}^{\text{N}} \alpha_\text{i} y_i(\boldsymbol{x}_i \cdot \boldsymbol{w} + b) + \ \sum_{\text{i}=1}^{\text{N}} \alpha_i \, . \tag{3.14}$$

$\boldsymbol{L_P}$ will be minimized with respect to $\boldsymbol{w}$, b and all the derivatives of $\boldsymbol{L_P}$ with respect to all the Lagrangian multipliers, α_i will vanish. Where all of these multipliers are subjected to the following constraints

$$\alpha_i \geq 0 \ \forall_i. \tag{3.15}$$

By differentiating $\boldsymbol{L_P}$ with respect to $\boldsymbol{w}$ and b and setting the derivatives to zero

$$\frac{\partial \boldsymbol{L_P}}{\partial \boldsymbol{w}} = 0, \ \text{ therefore, } \ \boldsymbol{w} = \sum_{\mathrm{i}=1}^{\mathrm{N}} \alpha_i y_i \boldsymbol{x}_i \tag{3.16}$$

$$\frac{\partial \boldsymbol{L_P}}{\partial b} = 0, \ \text{ therefore, } \ \sum_{\mathrm{i}=1}^{\mathrm{N}} \alpha_i y_i = 0. \tag{3.17}$$

Now, this is a convex quadratic programming problem, since the objective function is itself convex, and those points which satisfy the constraints also form a convex set (any linear constraint defines a convex set and a set of N simultaneous linear constraints defines the intersection of N convex sets is also a convex set). This means that equivalently the dual formulation of the problem can be used. This implies maximizing $\boldsymbol{L_P}$ with respect to $\boldsymbol{\alpha}$, and subject to the constraints that all the derivatives of $\boldsymbol{L_P}$ with respect to $\boldsymbol{w}$ and b vanish, as well as the constraints in Eq. (3.15). Substituting Eqs. (3.16) and (3.17) into Eq. (3.14) gives a new formulation which is independent of $\boldsymbol{w}$, b**.** Therefore, it is required now to maximize

$$\boldsymbol{L_D} \equiv \sum_{\mathrm{i}=1}^{\mathrm{N}} \alpha_i - \frac{1}{2} \sum_{\mathrm{i,j}} \alpha_i \alpha_j y_i y_j \boldsymbol{x}_i \cdot \boldsymbol{x}_j \ \text{ such that } \ \alpha_i \geq 0 \ \forall_{\mathrm{i}}, \sum_{\mathrm{i}=1}^{\mathrm{N}} \alpha_i y_i = 0 \tag{3.18}$$

$$\equiv \sum_{\mathrm{i}=1}^{\mathrm{N}} \alpha_i - \frac{1}{2} \sum_{\mathrm{i,j}} \alpha_i H_{i,j} \alpha_j \ \text{ where } H_{i,j} = y_i y_j \boldsymbol{x}_i \cdot \boldsymbol{x}_j \tag{3.19}$$

$$\equiv \sum_{\mathrm{i}=1}^{\mathrm{N}} \alpha_i - \frac{1}{2} \boldsymbol{\alpha^T H \alpha} \ \text{ such that } \ \alpha_i \geq 0 \ \forall_{\mathrm{i}}, \sum_{\mathrm{i}=1}^{\mathrm{N}} \alpha_i y_i = 0 \tag{3.20}$$

where $\boldsymbol{L_P}$ refers to primal, $\boldsymbol{L_D}$ refers to dual and $\boldsymbol{H}$ is the Hessian matrix. As it is mentioned previously, the dual form requires only the dot product of each input vector $\boldsymbol{x_i}$ to be calculated. Having moved from minimizing $\boldsymbol{L_P}$ to maximizing $\boldsymbol{L_D}$

$$\mathrm{Max}_{\boldsymbol{\alpha}} \left[\sum_{\mathrm{i}=1}^{\mathrm{N}} \alpha_i - \frac{1}{2} \boldsymbol{\alpha^T H \alpha} \right] \ \text{ such that } \ \alpha_i \geq 0 \ \forall_{\mathrm{i}}, \sum_{\mathrm{i}=1}^{\mathrm{N}} \alpha_i y_i = 0. \tag{3.21}$$

Equation (3.21) is a convex quadratic optimization problem. This problem can be solved using a QP solver which returns $\boldsymbol{\alpha}$; in addition, $\boldsymbol{w}$ is obtained from Eq. (3.16). Any data point satisfying the inequalities in Eq. (3.6) is a Support Vector $\boldsymbol{x}_{\mathrm{s}}$, and this equality will have the following form

$$y_s(\boldsymbol{x}_s \cdot \boldsymbol{w} + b\ ) = 1. \tag{3.22}$$

Substituting Eq. (3.16) in Eq. (3.22) gives

$$y_s\left(\sum_{\mathrm{m}\in\mathrm{S}} \alpha_m y_m \boldsymbol{x}_m \cdot \boldsymbol{x}_s + b\right) = 1 \tag{3.23}$$

where S denotes the set of indices of the support vectors. S is determined by finding the indices i, where $\alpha_i > 0$. Finally, the scalar b is obtained by multiplying Eq. (3.23) by y_s and then using ${y_s}^2 = 1$ from Eqs. (3.4) and (3.5) results in

$${y_s}^2\left(\sum_{m\in S} \alpha_m y_m \boldsymbol{x}_m \cdot \boldsymbol{x}_s + b\right) = y_s \tag{3.24}$$

$$b = y_s - \left(\sum_{m\in S} \alpha_m y_m \boldsymbol{x}_m \cdot \boldsymbol{x}_s\right). \tag{3.25}$$

Instead of using an arbitrary Support Vector $\boldsymbol{x}_s$, it is better to take an average over all of the Support Vectors in S as follows

$$b = \frac{1}{N_s}\sum_{s\in S}\left(y_s - \left(\sum_{m\in S} \alpha_m y_m \boldsymbol{x}_m \cdot \boldsymbol{x}_s\right)\right). \tag{3.26}$$

After the values of $\boldsymbol{w}$ and b are obtained, any unknown sample can be classified as follows

$$y_{unknown} = sign(\boldsymbol{x}_{unknown} \cdot \boldsymbol{w} + b\ ). \tag{3.27}$$

The number of variables in Eq. (3.18) is the number of the training data. All the training data associated with the Lagrangian multipliers satisfying the inequality of Eq. (3.15) are the SVs. The number of SVs is considerably less than the number of the training data.

3.3.2.2 Classification problem and hard margin SVM

In order to use a SVM classifier to solve a linearly separable binary classification problem, the following steps are followed:

1. Create $\boldsymbol{H}$, where $H_{ij} = y_i y_j \boldsymbol{x}_i \cdot \boldsymbol{x}_j$.

2. Find $\boldsymbol{\alpha}$ so that

$\mathrm{Max}_{\boldsymbol{\alpha}}\left[\sum_{\mathrm{i}=1}^{\mathrm{N}} \alpha_i - \frac{1}{2}\boldsymbol{\alpha}^T \boldsymbol{H}\boldsymbol{\alpha}\right]$ subject to $\alpha_i \geq 0\ \forall_{\mathrm{i}}$, $\sum_{\mathrm{i}=1}^{\mathrm{N}} \alpha_i y_i = 0$, using a QP solver.

3. Calculate $\boldsymbol{w} = \sum_{\mathrm{i}=1}^{\mathrm{N}} \alpha_i y_i \boldsymbol{x}_i$.

4. Determine the set of Support Vectors S by finding the indices such that $\alpha_i \geq 0$.

5. Calculate $b = \frac{1}{N_s}\sum_{s\in S}\left(y_s - \left(\sum_{m\in S}\alpha_m y_m \boldsymbol{x}_m \cdot \boldsymbol{x}_s\right)\right)$.

6. Each new unknown pattern is classified using $y_{unknown} = \text{sign}(\boldsymbol{x}_{unknown} \cdot \boldsymbol{w} + b)$.

Appendix C illustrates an example of a classification problem with hard limit Support Vector Machines.

3.3.2.3 Linearly non-separable data (noisy data) and the soft margin SVM [35]-[39]

In practice, data are often not fully linearly separable. In order to extend the linear SVMs methodology to handle data that are not fully linearly separable (noisy data), the constraints in Eqs. (3.4) and (3.5) are relaxed slightly to obtain a greater margin by allowing some patterns to be in the margin or to be misclassified. This is performed by introducing a positive slack variable ξ_i as shown in Figure 3.4 and Eqs. (3.28) to (3.30). This formulation is called the soft margin SVM.

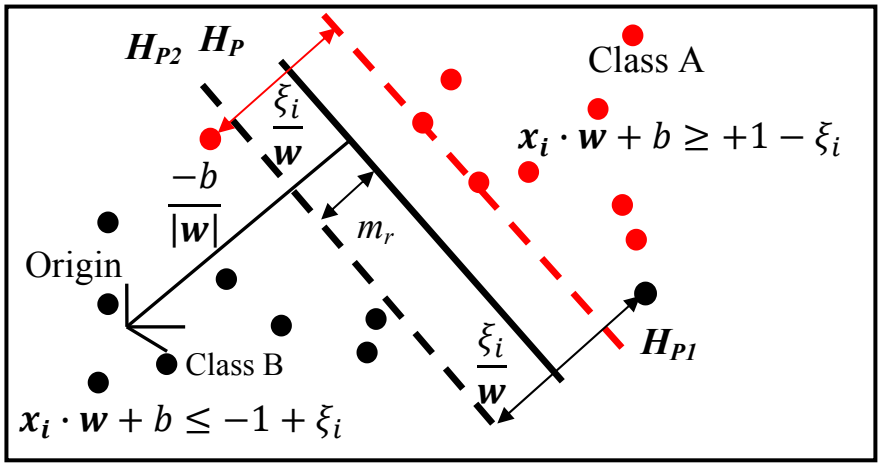

Figure 3.4. Optimal hyperplane through two linearly non-separable (noisy) classes.

$$\text{Class A:}\quad \boldsymbol{x}_i \cdot \boldsymbol{w} + b \geq +1 - \xi_i \qquad \text{for } y_i = +1 \tag{3.28}$$

$$\text{Class B:}\quad \boldsymbol{x}_i \cdot \boldsymbol{w} + b \leq -1 + \xi_i \qquad \text{for } y_i = -1 \tag{3.29}$$

$$\xi_i \geq 0 \quad \forall_i. \tag{3.30}$$

The slack variable ξ_i defines the distance between the input vector $\boldsymbol{x}_i$ lying on the wrong side of the margin (m_r) and the margin boundary of the class of that input vector $\boldsymbol{x}_i$, i =1,…., N.

Equations (3.28) to (3.30) can be combined as

$$y_i(\boldsymbol{x}_i \cdot \boldsymbol{w} + b) - 1 + \xi_i \geq 0 \qquad \text{and } \xi_i \geq 0 \quad \forall_i. \tag{3.31}$$

In this soft margin SVM, data points on the incorrect side of the margin boundary have a penalty that increases with the distance from it. In order to reduce the number of misclassified patterns, a term is added to Eq. (3.11) as

$$\text{Min}_{\boldsymbol{w},b}\ \frac{1}{2}\|\boldsymbol{w}\|^2 + C\sum_{i=1}^{N}\xi_i \quad \text{subject to} \quad y_i(\boldsymbol{x}_i \cdot \boldsymbol{w} + b) - 1 + \xi_i \geq 0 \quad \forall_i \qquad (3.32)$$

where the parameter C controls the trade-off between the slack variable penalty and the size of the margin (maximizing the margin and minimizing the value of the slack variable).

The effect of the choice of C is illustrated using Figures 3.4 and 3.5. As C decreases, the hyperplane's orientation changes to $\boldsymbol{H_{P\_new}}$ and the margin increases. This leads the closest points to the separating hyperplane to move inside the margin as shown in Figure 3.5(a). On the other hand, as C increases, the margin decreases and the SVMs successfully separate the two classes as shown in Figure 3.5(b).

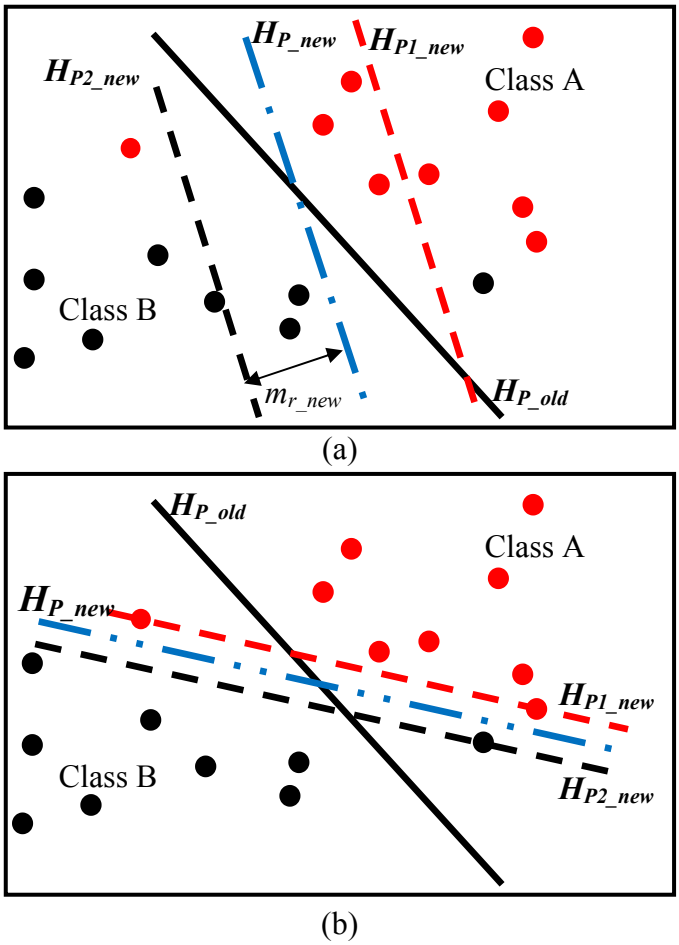

Figure 3.5. Effect of the soft margin parameter C on the decision boundary through two linearly non-separable (noisy) classes.

Reformulating Eq. (3.32) as a Lagrangian, as previously explained, in addition, minimizing with respect to $\boldsymbol{w}$, b and ξ_i and maximizing with respect to $\boldsymbol{\alpha}$ and $\boldsymbol{\mu}$ yield

$$\boldsymbol{L_P} \equiv \frac{1}{2}\|\boldsymbol{w}\|^2 + C\sum_{i=1}^{N}\xi_i - \sum_{i=1}^{N}\alpha_i[y_i(\boldsymbol{x}_i \cdot \boldsymbol{w} + b) - 1 + \xi_i] - \sum_{i=1}^{N}\mu_i\xi_i \quad (3.33)$$

Where μ_i are Lagrangian multipliers introduced to enforce positivity of ξ_i.

$$\alpha_i \geq 0, \mu_i \geq 0 \ \forall_i. \quad (3.34)$$

By differentiating $\boldsymbol{L_P}$ with respect to $\boldsymbol{w}$, b and ξ_i and setting the derivatives to zero

$$\frac{\partial \boldsymbol{L_P}}{\partial \boldsymbol{w}} = 0, \ \text{therefore,} \ \boldsymbol{w} = \sum_{i=1}^{N}\alpha_i y_i \boldsymbol{x}_i \quad (3.35)$$

$$\frac{\partial \boldsymbol{L_P}}{\partial b} = 0, \ \text{therefore,} \ \sum_{i=1}^{N}\alpha_i y_i = 0 \quad (3.36)$$

$$\frac{\partial \boldsymbol{L_P}}{\partial \xi_i} = 0, \ \text{therefore,} \ C = \alpha_i + \mu_i. \quad (3.37)$$

Substituting Eqs. (3.35) to (3.37) in $\boldsymbol{L_D}$ which has the same form as Eq. (3.20). Here again using Eq. 3.21 as follows

$$\text{Max}_{\boldsymbol{\alpha}}\left[\sum_{i=1}^{N}\alpha_i - \frac{1}{2}\boldsymbol{\alpha}^T\boldsymbol{H}\boldsymbol{\alpha}\right] \ \text{subject to} \ 0 \leq \alpha_i \leq C \ \forall_i, \ \text{and} \ \sum_{i=1}^{N}\alpha_i y_i = 0. \quad (3.38)$$

b is then calculated as in Eq. (3.25), where the set of Support Vectors used to calculate b is determined by finding the indices i, and $0 \leq \alpha_i \leq C$.

3.3.2.4 Classification problem and soft margin SVM

In order to use a SVM to solve binary classification problem for data that are not fully linearly separable the following steps are followed:

1. Create $\boldsymbol{H}$, where $H_{ij} = y_i y_j \boldsymbol{x}_i \cdot \boldsymbol{x}_j$.
2. Choose how significantly misclassifications should be treated by selecting a suitable value for the parameter C.
3. Find $\boldsymbol{\alpha}$, so that

$\text{Max}_{\boldsymbol{\alpha}}\left[\sum_{i=1}^{N}\alpha_i - \frac{1}{2}\boldsymbol{\alpha}^T\boldsymbol{H}\boldsymbol{\alpha}\right]$ subject to $0 \leq \alpha_i \leq C \ \forall_i$, and $\sum_{i=1}^{N}\alpha_i y_i = 0$, using a QP solver.

4. Calculate $\boldsymbol{w} = \sum_{i=1}^{N}\alpha_i y_i \boldsymbol{x}_i$.

5. Determine the set of Support Vectors S by finding the indices subject to $0 \leq \alpha_i \leq C \ \forall_i$.

6. Calculate $b = \frac{1}{N_s} \sum_{s \in S} \left(y_s - \left(\sum_{m \in S} \alpha_m y_m \boldsymbol{x}_m \cdot \boldsymbol{x}_s \right) \right)$.

7. Each new unknown pattern is classified using $y_{unknown} = sign(\boldsymbol{x}_{unknown} \cdot \boldsymbol{w} + b)$.

3.3.3 Nonlinear data and the usage of Kernel functions [40]-[45]

In many cases, data are of nonlinear nature. For such cases, the use of a nonlinear classifier would provide better accuracy. Therefore, in order to extend the linear SVM methodology to generate non-linear decision boundaries, there is a straightforward way consists of mapping the data vector into a higher dimension space, using a function $\emptyset$ as shown in Figure 3.6.

Therefore, the discriminant function defined by Eq. (3.2) is modified as

$$f(\boldsymbol{x}) = \boldsymbol{w} \cdot \emptyset(\boldsymbol{x}) + b. \tag{3.39}$$

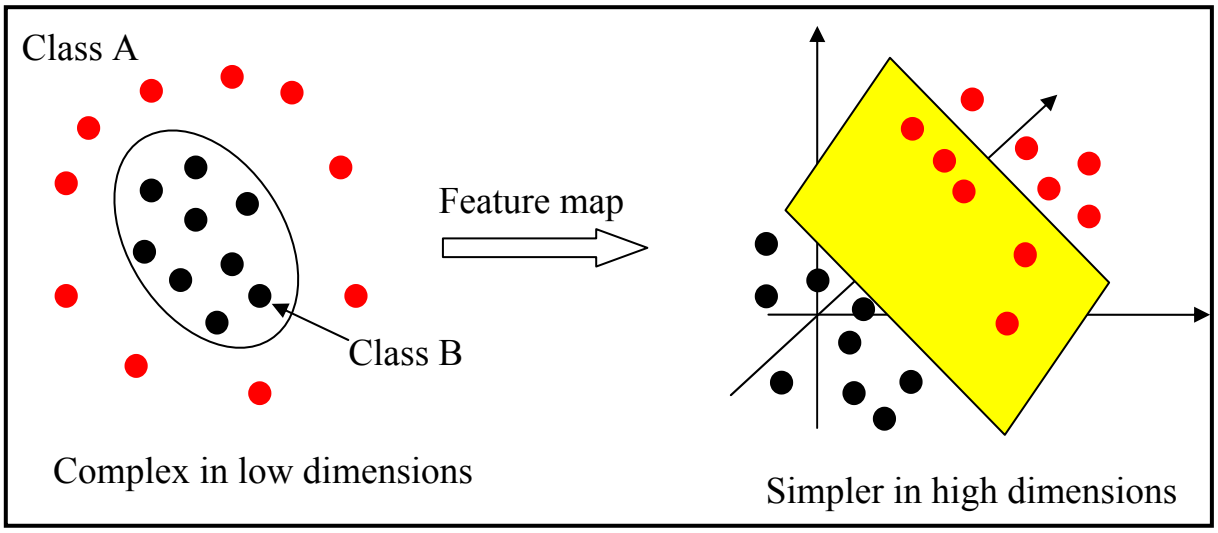

Figure 3.6. Projecting data that are not linearly separable into a higher dimensional space can make them linearly separable.

It can be noticed that the only way in which the data appear in the training algorithm is in the form of dot products as in Eq. (3.18). This means that the training algorithm would only depend on the data through dot products in the higher dimension space, i.e. on functions of the form $\emptyset(x_i) \cdot \emptyset(x_j)$. Kernel functions are defined as

$$\boldsymbol{K}(\boldsymbol{x}_i, \boldsymbol{x}_j) = \emptyset(\boldsymbol{x}_i) \cdot \emptyset(\boldsymbol{x}_j). \tag{3.40}$$

In such a representation, the Kernel will be only used in the training algorithm and there will be no need to explicitly know what $\emptyset$ is. Therefore, by replacing every $\boldsymbol{x}_i \cdot \boldsymbol{x}_j$ by $\boldsymbol{K}(\boldsymbol{x}_i, \boldsymbol{x}_j)$ in the training algorithm, the algorithm will produce a support vector machine in the higher dimension space. Furthermore, this is processed in roughly the same amount of time it would take to train on the unmapped data. The same manner introduced in all the previous sections is still considered, since a linear separation is still being used, but in the higher dimension space.

The SVM can then be used by modifying Eq. (3.16) which results in

$$\boldsymbol{w} = \sum_{\mathrm{i}=1}^{\mathrm{N}} \alpha_i y_i \emptyset(\boldsymbol{x}_i). \tag{3.41}$$

Substituting Eq. (3.41) into Eqs. (3.2) gives

$$f(\boldsymbol{x}) = \sum_{i=1}^{N} \alpha_i y_i \emptyset(\boldsymbol{x}_i) \cdot \emptyset(\boldsymbol{x}_j) + b = \sum_{\mathrm{i}=1}^{\mathrm{N}} \alpha_i y_i \boldsymbol{K}(\boldsymbol{x}_i, \boldsymbol{x}_j) + b. \tag{3.42}$$

Moreover, the dual form of the problem is also applied and Eq. (3.20) is modified as follows

$$\boldsymbol{L_D} \equiv \sum_{\mathrm{i}=1}^{\mathrm{N}} \alpha_i - \frac{1}{2} \sum_{\mathrm{i,j}} \alpha_i \alpha_j y_i y_j \emptyset(\boldsymbol{x}_i) \cdot \emptyset(\boldsymbol{x}_j), \quad \alpha_{\mathrm{i}} \geq 0 \; \forall_{\mathrm{i}} \, , \sum_{\mathrm{i}=1}^{\mathrm{N}} \alpha_i y_i = 0. \tag{3.43}$$

Here again, $\boldsymbol{\alpha}$ is obtained from Eq. (3.38) using a quadratic programming (QP) solver. Finally, the scalar b is obtained by modifying Eq. (3.26) as follows

$$b = \frac{1}{N_s} \sum_{s \in S} \left[y_s - \left(\sum_{m \in S} \alpha_m y_m \emptyset(\boldsymbol{x}_m) \cdot \emptyset(\boldsymbol{x}_s) \right) \right]. \tag{3.44}$$

Substituting $\boldsymbol{w}$, b in the following equation allows the classification of any unknown sample

$$y_{unknown} = \mathrm{sign}(\boldsymbol{w} \cdot \emptyset \, (\boldsymbol{x}_{unknown}) + b \,). \tag{3.45}$$

3.3.3.1 Classification problem and Kernel functions

In order to use a SVM to solve a classification problem on data that are not linearly separable, a Kernel and relevant parameters which could map the non-linearly separable data into a feature space where they are linearly separable should be first selected. This is more of an art than an exact science and can be achieved empirically, i.e. by trial and error. In order to use a SVM to solve binary classification problem for data that are non-linearly separable, the following steps are followed

1. Choose the Kernel and create $\boldsymbol{H}$, where $H_{ij} = y_i y_j \emptyset(\boldsymbol{x}_i) \cdot \emptyset(\boldsymbol{x}_j)$.

2. Choose how significantly misclassifications should be treated, by selecting a suitable value for the parameter *C*.

3. Find $\boldsymbol{\alpha}$ so that

$\text{Max}_{\boldsymbol{\alpha}} \left[\sum_{i=1}^{N} \alpha_i - \frac{1}{2}\boldsymbol{\alpha}^T \boldsymbol{H}\boldsymbol{\alpha}\right]$ subject to $0 \leq \alpha_i \leq C \ \forall_i$, and $\sum_{i=1}^{N} \alpha_i y_i = 0$, using a QP solver.

4. Calculate $\boldsymbol{w} = \sum_{\text{i}=1}^{\text{N}} \alpha_i y_i \emptyset(\boldsymbol{x}_i)$.

5. Determine the set of Support Vectors S by finding the indices subject to $0 \leq \alpha_i \leq C \ \forall_{\text{i}}$.

6. Calculate $b = \frac{1}{N_s}\sum_{s \in S}\left[y_s - \left(\sum_{m \in S} \alpha_m y_m \emptyset(\boldsymbol{x}_m) \cdot \emptyset(\boldsymbol{x}_s)\right)\right]$.

7. Each new unknown pattern is classified using

$$y_{unknown} = \text{sign}(\boldsymbol{w} \cdot \emptyset\ (\boldsymbol{x}_{unknown}) + b\ ).$$

3.3.3.2 Applications of SVM and Kernel functions in power systems

During the last decade, several reported studies have proposed the use of the support vector machines (SVMs) for power system applications [46]-[50]. In [46], a new learning-based nonlinear classifier, SVM-ANN (Artificial Neural Network), suitable for power system transient stability analysis (TSA) is presented. It is proposed as a different approach to cope with the problem of high dimensionality due to its fast training capability which can be combined with existing feature extraction techniques. The SVM's theoretical motivation is conceptually explained and applied to the IEEE 50-generator and the 2684-bus Brazilian systems. The aspects of model adequacy, training time and classification accuracy are discussed and compared to stability classifications obtained by Multi-Layer Perceptrons (MLPs).

In [47], a novel technique based on SVM for the classification of transient phenomena in three-phase power transformers is presented. This technique neither depends on the equivalent circuit model nor on the harmonic contents of the differential currents, rather makes the decision based on current signature verification.

The results presented in [48] show a fast, accurate and robust approach for distance relaying of transmission lines using SVM. The proposed SVM technique is used for faulty phase selection and ground detection in different fault situations that occur on large power transmission networks.

In [49], a two-phase algorithm combined from wavelet and SVM techniques for fault zone identification in series capacitor compensated transmission lines is presented. In this technique, the detailed coefficients of the three-phase currents are extracted by discrete wavelet transform (DWT) and are provided at the input of a SVM, which in turn determines the faulted zone.

Reference [50] presented a scheme for transmission line distance relaying coordination based on SVM as a pattern classifier. The scheme utilizes the apparent impedance values observed during the fault as inputs. SVM is used to build the underlying concept between the reach of different zones and the impedance trajectory during the fault. The improved performance with the use of SVM, keeping the reach when faced with different conditions as well as line flow changes is illustrated.

A close examination of the previous reported studies reveals that the two most commonly used Kernel functions in power system applications are the Polynomial and the Gaussian Kernels. A Polynomial Kernel of degree n is defined as

$$\boldsymbol{K}_{n,k}^{polynomial}(\boldsymbol{x_i}, \boldsymbol{x_j}) = \left(\boldsymbol{x_i} \cdot \boldsymbol{x_j} + k\right)^n \tag{3.46}$$

where k is often chosen to be 0 (homogeneous) or 1 (inhomogeneous, which is the case used in the investigations in this chapter). The feature space for the inhomogeneous Kernel consists of all monomials with degree up to n. And yet, its computation time is linear in the dimensionality of the input-space. A Kernel with $n = 1$ and $k = 0$, denoted by k^{linear}, is a linear Kernel leading to a linear discriminant function.

The degree of the Polynomial Kernel controls the flexibility of the resulting classifier as shown in Figure 3.7 [51]. The lowest degree polynomial is the linear Kernel, which is not sufficient when a non-linear relationship between features exists. For the data in Figure 3.7(a), the degree 2 polynomial is already flexible enough to discriminate between the two classes with a good margin. The degree 5 polynomial yields a similar decision boundary, with a greater curvature as shown in Figure 3.7(b).

The other very widely used Kernel is the Gaussian Kernel defined by

$$\boldsymbol{K}_{\boldsymbol{\gamma}}^{Gaussian}(\boldsymbol{x_i}, \boldsymbol{x_j}) = exp^{\left(-\frac{1}{2\gamma^2}\|\boldsymbol{x_i}-\boldsymbol{x_j}\|^2\right)} \tag{3.47}$$

where $\gamma > 0$ is a parameter that controls the width of the Gaussian. It has a similar role as the

degree of the Polynomial Kernel in controlling the flexibility of the resulting classifier as shown in Figure 3.8. The Gaussian Kernel is essentially zero if the squared distance $\|\boldsymbol{x_i} - \boldsymbol{x_j}\|^2$ is much larger than γ; i.e. for a fixed $\boldsymbol{x_j}$, there is a region around $\boldsymbol{x_j}$ with high Kernel values. The discriminant function in Eq. (3.42) is, thus, a sum of Gaussian "bumps" centered around each support vector (SV). When γ is large, as shown in Figure 3.8(a) [51], a given data point *x* has a non-zero Kernel value relative to any example in the set of patterns. Therefore, the whole set of SVs affects the value of the discriminant function at $\boldsymbol{x}$ leading to a smooth decision boundary. As γ is decreased, the Kernel becomes more local, leading to greater curvature (more flexibility) of the decision surface as shown in Figure 3.8(b) [51].

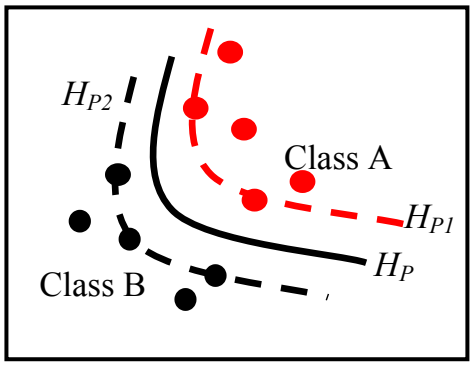

(a)

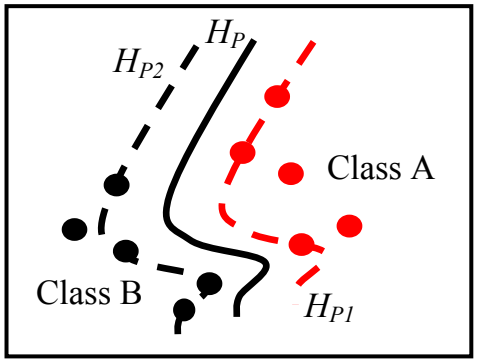

(b)

Figure 3.7. Effect of the degree of a Polynomial Kernel on the flexibility of the decision boundary: (a) Kernel with a degree 2 polynomial, (b) Kernel with a degree 5 polynomial.

As it is seen from Figures 3.7 and 3.8, the degree of the Polynomial Kernel and the width parameter of the Gaussian Kernel determine the flexibility of the resulting SVM in fitting the data. An extremely large degree or an extremely small width values can lead to overfitting and suboptimal performance as shown in Fig. 3.9 [51], [52].

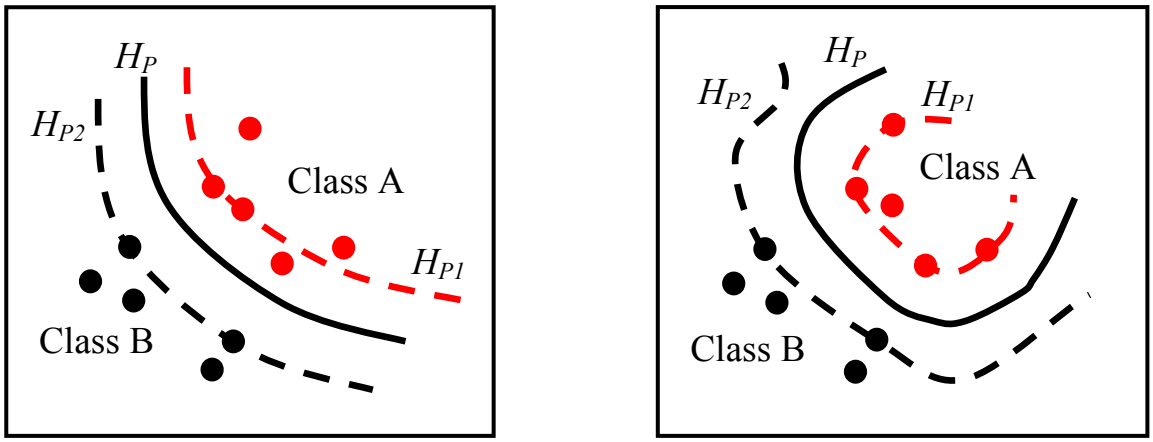

(a) (b)

Figure 3.8. Effect of the width parameter of the Gaussian Kernel γ on the decision boundary: (a) for large values of γ (5), the decision boundary is nearly linear, (b) as γ decreases (0.1), the flexibility of the decision boundary increases.

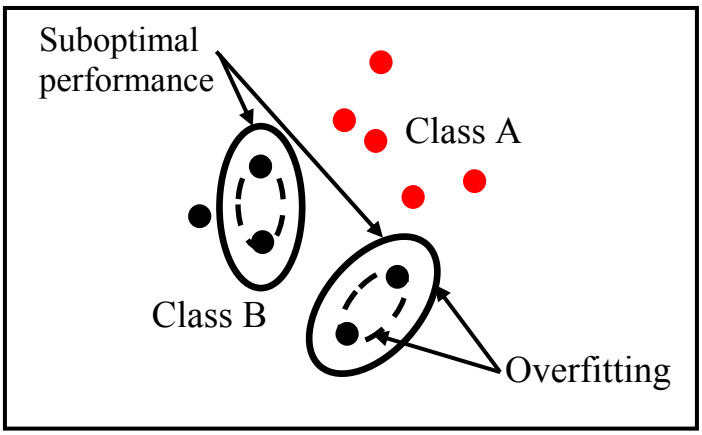

Figure 3.9. An extremely large Polynomial degree (n) or an extremely small Gaussian width (γ) leads to overfitting.

3.4 Enhancement of the Coordination between Generator Phase Backup Protection and Generator Capability Limits in the Presence of a Midpoint STATCOM in System II using SVM

In this section, the generalization of SVM classification technique to generator phase backup protection is investigated. As it has been shown in Chapter 2, the midpoint STATCOM has a stronger impact on the performance of Relay (21) as well as on the coordination between such a relay and the GOEC limit during line-to-line faults than during three-phase faults. Based on this conclusion and from the SVM classification technique point of view, the detection of a three-phase fault on a transmission line (incorporating a midpoint STATCOM) is more difficult than the detection of a line-to-line fault on the same line. Therefore, in order to obtain the best SVM

classifiers (SVM with optimum parameters), the SVM classification technique is implemented first (trained and tested) for the worst-case scenario (from the SVM point of view, during a three-phase fault). The best classifiers are then generalized for line-to-line faults.

3.4.1 Generation of the training, testing and generalization cases for System II

During three-phase faults, the main set of training cases (Set_1) is generated considering four generator loading conditions (50%, 60%, 70% and 80% of the rated MVA), three values of fault resistance (0, 10 Ω, 20 Ω) and nine fault locations (10%, 20%, 30%, 40%, 60%, 70%, 80%, 90%, 100%) on each of the three transmission lines of System II. The two groups of testing and generalization cases (Set_t during three-phase faults and Set_g during line-to-line faults) are generated considering three generator loading conditions (55%, 65%, 75% of the rated MVA), two values of fault resistance (5 Ω, 15 Ω) and eight fault locations of (5%, 15%, 25%, 35%, 65%, 75%, 85%, 95%) on each of the three transmission lines.

The main training data set (Set_1) contains a total number of training cases of 4×3×9×3 = 324, while each of the testing and generalization data sets (Set_t and Set_g) contains a number of testing cases of 3×2×8×3 = 144. Here again, all the training, testing and generalization simulations are carried out using the PSCAD/EMTDC simulation package [23]. The input feature vectors (training /testing/generalization) are normalized to [-1, +1] before entering the SVM module using [25], [27]

$$x_{norm} = 2\left(\frac{(x-min_i)}{max_i-min_i}\right) - 1 \tag{3.48}$$

where max_i and min_i are the maximum and minimum values of the i^{th} attributes.

3.4.2 Description of the proposed SVM scheme

The proposed SVM scheme uses the phasor values of the phase voltages and currents measured at the relaying point, which are formed using discrete Fourier transform (DFT) at a sampling frequency of 1.2 kHz (20 samples per cycle). It consists of two stages (two SVM modules). Stage_1 contains the fault detection module (SVM_D) while Stage_2 contains the protective zone identification module (SVM_Reach). A data window of 3 cycles (form the fault inception time) is used for the fault detection and protective zone identification. The outputs of

the two SVM modules are combined to provide the decision for the generator phase backup protection as shown in the block diagram in Figure 3.10.

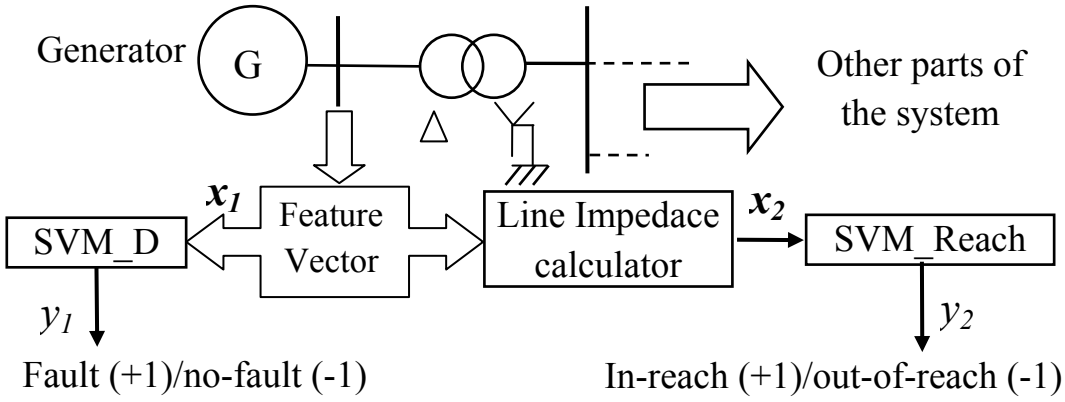

Figure 3.10. Block diagram of the proposed SVM scheme for generator phase backup protection.

3.4.2.1 Fault detection module (SVM_D)

The training technique presented in [48] is adopted in the training of SVM_D. Sixty samples of voltages and currents from the fault inception are retrieved at the relaying point and their corresponding normalized values are directly used as the input features (vector $\boldsymbol{x_1}$ of 120 points) for SVM_D. The corresponding output y_1 for SVM_D is (-1 for a no-fault condition and +1 for a fault condition).

3.4.2.2 Protective zone identification module (SVM_Reach)

It has been concluded, based on the nature of the results in Chapter 2, that the training technique presented in [50] would be suitable to use for protective zone identification (training SVM_Reach). SVM_Reach identifies the protective zone based on the connectivity of the lines. The protective zone includes all faults that occur on Lines 1 and 2 that are within the reach of 16.8 Ω at MTA=85°.

The samples of the phase voltages and currents, which are used in Section 3.4.2.1, are fed to a line impedance calculator. The output from this calculator is the input feature vector (vector $\boldsymbol{x_2}$ of 60 points) for SVM_Reach. The corresponding output y_2 for SVM_Reach is (-1 for fault out-of-reach condition and +1 for fault in-reach condition).

3.4.3 Design of the proposed SVM scheme

SVM_D and SVM_Reach modules are designed during the training process using trial and error. The training process involves different Kernel functions as well as several values of each Kernel parameters in order to obtain the SVM classifier with the best performance. The "SVM and Kernel Methods MATLAB Toolbox" [52] is used for the SVM training, testing and generalization.

3.4.3.1 Selection of the Kernel function

The SVM classification technique is generalized to the generator phase backup protection by testing two different Kernel functions during the training process namely, the Polynomial and the Gaussian Kernel functions of Eqs. (3.46) and (3.47). According to the performance of these Kernel functions, the suitability of the SVM as an intelligent generator phase backup protection is judged.

3.4.3.2 Selection of the Kernel parameters

The selection of the optimum parameters for SVM is done during the training process using Set_1 (obtained during three-phase faults). The SVM classifier with the best performance is obtained by testing different values of the Kernel parameters. These parameters are varied in the following manner; γ = 0.1, 0.2, 0.3, 0.5, 1, 3, 5. The order of the Polynomial Kernel n is varied in the range [2, 10] with steps of 2. The penalty due to the error C = 1, 10, 100, 500 and 1000. The tolerance for the QP solver is 0.00001. The performances of the two SVM modules are assessed for each of these values by calculating the training performance efficiency defined by

$$\eta_{training}\% = \frac{Number\ of\ samples\ correctly\ classified\ during\ training}{Total\ number\ of\ training\ samples} \times 100. \qquad (3.49)$$

From these results, the SVM classifier with the highest training percentage performance efficiency is selected. The testing and the generalization processes are then performed (using Set_t and Set_g).

3.4.3.3 Reducing the size of the training data

The main training data set (Set_1 for three-phase faults) of the 324 cases is reduced to 124 cases in order to obtain a new training data set (Set_2), which is also used for training the

proposed classifiers. After training all the SVM classifiers using these two sets, they are tested with Set_t (obtained during three-phase faults) of 144 cases in order to evaluate the efficiency of the proposed scheme when subjected to a reduced size of training data.

3.4.4 Training and testing results

Figures 3.11 to 3.14 show the performance of the Kernel functions during the training process of Set_1 obtained during three-phase faults for both SVM_D and SVM_Reach respectively. The performance is introduced in terms of the percentage training efficiency defined by Eq. (3.49) with respect to the variation of the Kernel parameters γ, and *n* as well as the parameter C (the penalty due to the error). From the results illustrated in Figure 3.11 to 3.14, the following observations are worth noting:

3.4.4.1 Effect of the penalty due to the error (C)

- For the Kernel functions, the best performance is obtained at high values of C (500 and 1000). Moreover, as C increases, the training efficiency increases while the training time decreases (this observation is based on all values C, i.e. C = 1 which is not shown in Figures 3.11 to 3.14 is included).
- The maximum training efficiency is 95.1% and 95.67% at *C* = 1000 for SVM_D and SVM_Reach respectively.

3.4.4.2 Effect of the Kernel parameters

- For the polynomial Kernel, as n increases, the training efficiency increases while the training time decreases. This is also true for n = 6 which is not shown in Figures 3.11 to 3.14. The best performance for the Polynomial Kernel function is 94.8% and 95.3% (*C* = 1000, n = 10) for SVM_D and SVM_Reach respectively.
- For the Gaussian Kernel, as γ decreases, the training efficiency increases, while the training time decreases (this observation is based on all values γ, i.e. γ = 0.3, 0.5 and 3 which are not shown in Figures 3.11 to 3.14 are included). The best performance for the Gaussian Kernel function is 95.1% and 95.67% (*C* = 1000, γ = 0.1) for SVM_D and SVM_Reach respectively.

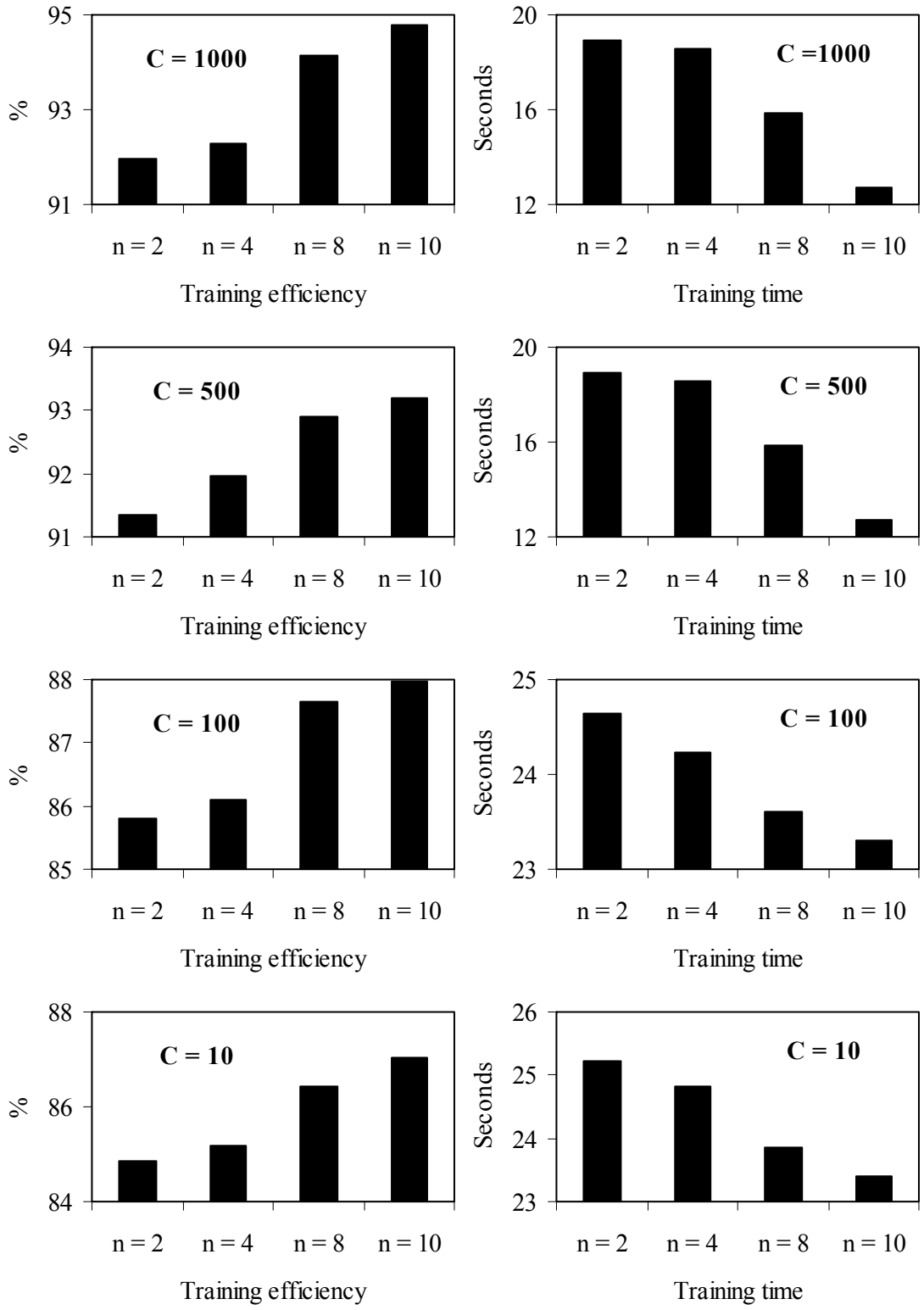

Figure 3.11. Training of SVM_D with Set_1 data for different values of Polynomial Kernel parameters for three-phase faults.

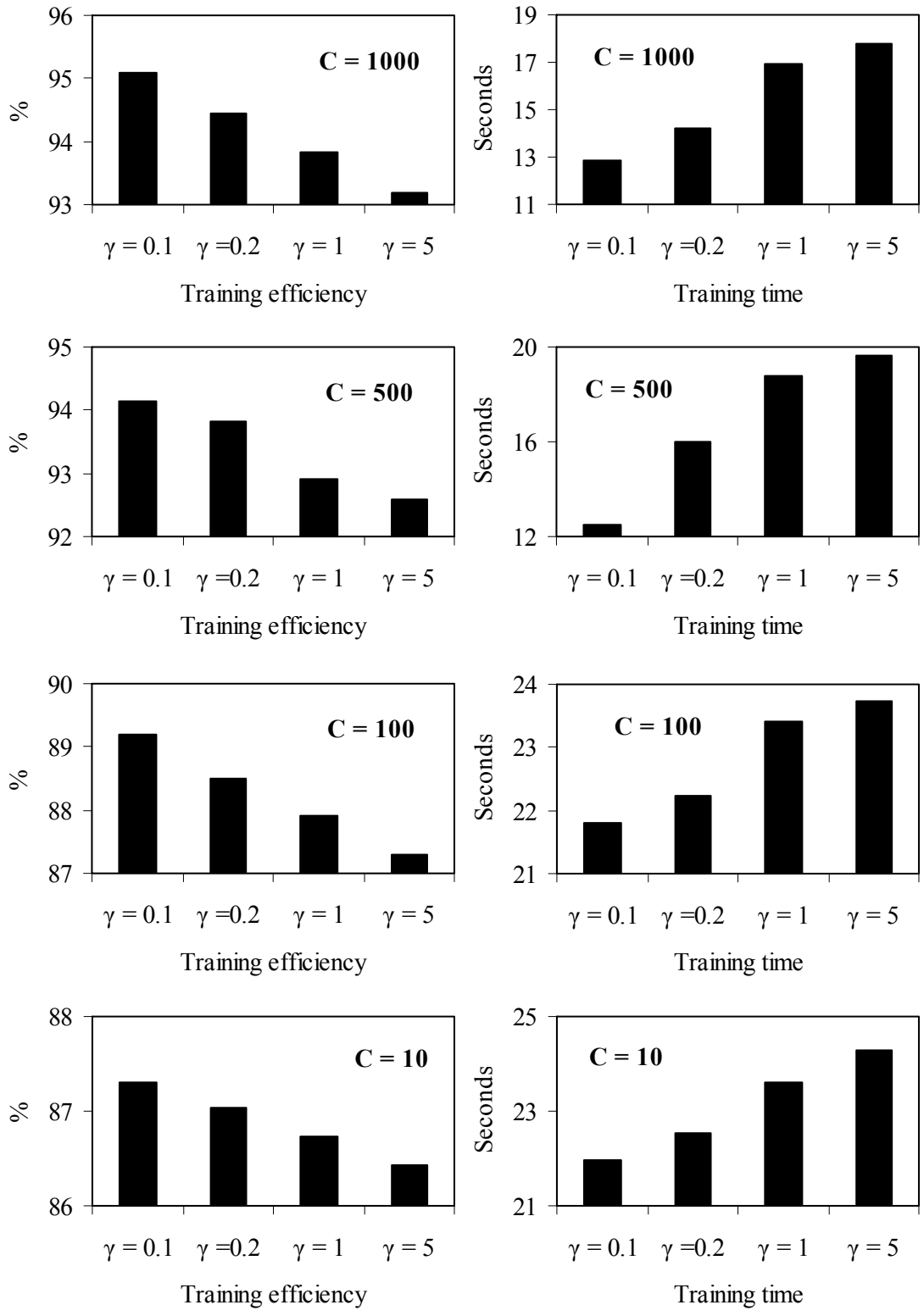

Figure 3.12. Training of SVM_D with Set_1 data for different values of Gaussian Kernel parameters for three-phase faults.

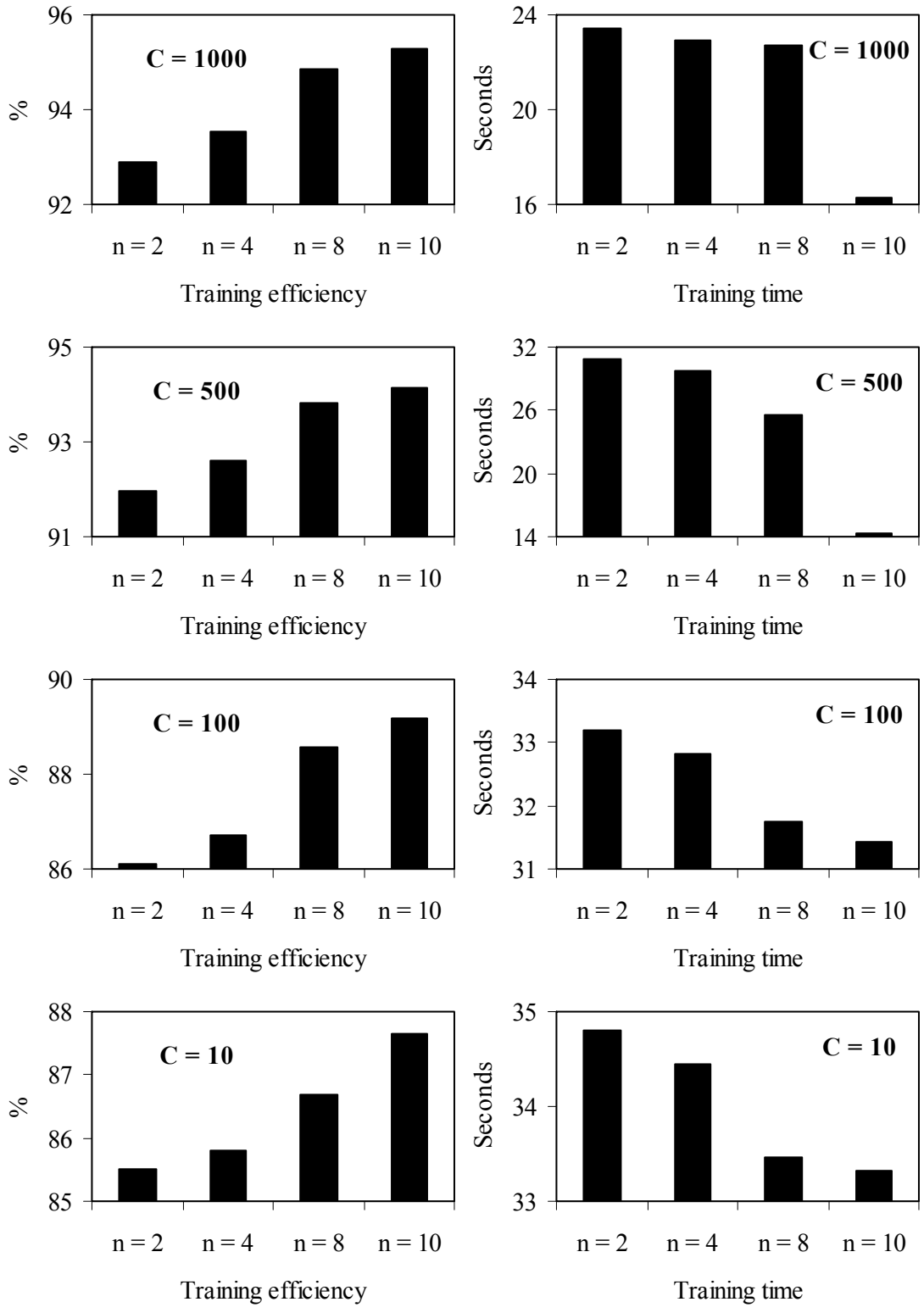

Figure 3.13. Training of SVM_Reach with Set_1 data for different values of Polynomial Kernel parameters for three-phase faults.

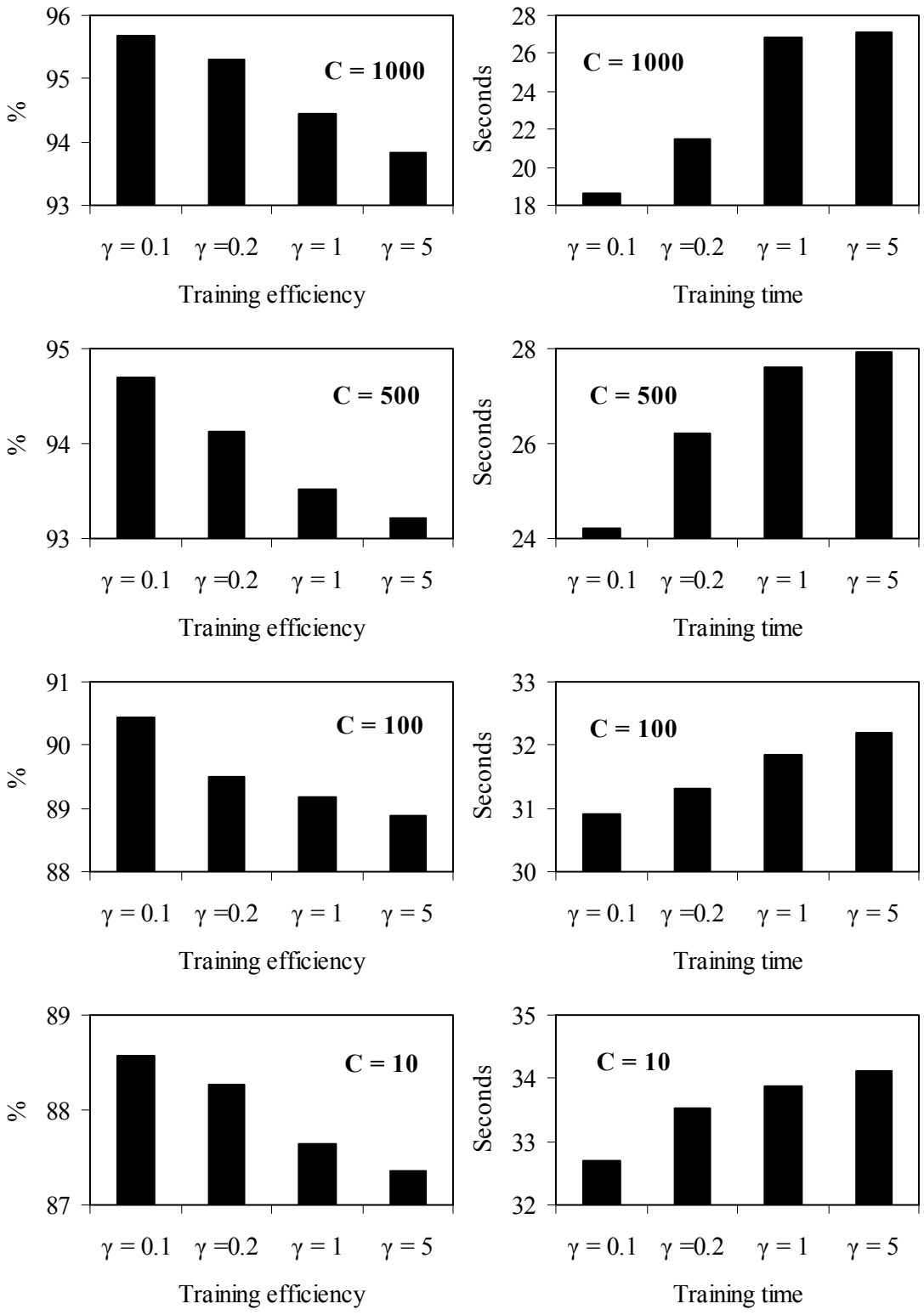

Figure 3.14. Training of SVM_Reach with Set_1 data for different values of Gaussian Kernel parameters for three-phase faults.

3.4.4.3 Effect of the type of the Kernel function

- The best training efficiency is obtained with the Gaussian Kernel function (95.67% during SVM_Reach training).
- The shortest training time is obtained for the Polynomial Kernel function (12.7 seconds) during SVM_D training.

Tables 3.1 and 3.2 depict the testing performance of the best classifiers obtained during the training process using Set_1 and Set_2. The testing performance is introduced in terms of the testing efficiency (defined by Eq. (3.50) using Set_t) for both SVM_D and SVM_Reach modules.

$$\eta_{testing}\% = \frac{Number\ of\ samples\ correctly\ classified\ during\ testing}{Total\ number\ of\ testing\ samples} \times 100. \qquad (3.50)$$

From the results of these two tables, the following are worth noting:

1- The best testing performance efficiencies of the fault detection module (SVM_D) during three-phase faults are 95.14% (Gaussian, $\gamma = 0.1$, $C = 1000$) and 94.44% (Polynomial, $n = 10$, $C = 1000$).

2- The best performance efficiencies of the protective zone identification module ((SVM_Reach) during three-phase faults are 96.53% (Gaussian, $\gamma = 0.1$, $C = 1000$) and 95.14% (Polynomial, $n = 10$, $C = 1000$).

3- When the training data set size is reduced from Set_1 to Set_2, the testing efficiency is also reduced. For Set_1, the maximum testing efficiencies are 95.14% and 96.53 % for SVM_D and SVM_Reach respectively, while they are 93.75% and 94.44% for Set_2 for SVM_D and SVM_Reach respectively. This shows the ability of the proposed SVM classifier in learning with small size of data patterns and demonstrates the computational efficiency of the proposed approach.

Table 3.3 shows a comparison between the performance efficiency of Relay (21) and the proposed SVM_D module (Polynomial/Gaussian) for generator phase backup protection during three-phase faults. The performance efficiency of Relay (21) is obtained from Table 2.6, while the efficiencies of the SVM_D module (Polynomial/Gaussian) are obtained from Table 3.1.

Table 3.1. SVM_D testing performance for three-phase faults.

Kernel function	Kernel parameters	% Testing efficiency	
		Train Set_1 Test Set_t	Train Set_2 Test Set_t
Polynomial	n = 10, C = 1000	94.44	91.67
	n = 10, C = 500	90.97	89.6
	n = 8, C = 1000	91.67	90.28
	n = 8, C = 500	90.97	88.9
Gaussian	γ = 0.2, C = 1000	93.75	92.36
	γ = 0.2, C = 500	91.67	90.28
	γ = 0.1, C =1000	95.14	93.75
	γ = 0.1, C = 500	93.03	91.67

Table 3.2. SVM_Reach testing performance for three-phase faults.

Kernel function	Kernel parameters	% Testing efficiency	
		Train Set_1 Test Set_t	Train Set_2 Test Set_t
Polynomial	n = 10, C = 1000	95.14	93.05
	n = 10, C = 500	91.67	90.28
	n = 8, C = 1000	93.05	91.67
	n = 8, C = 500	90.97	89.6
Gaussian	γ = 0.2, C = 1000	95.14	93.75
	γ = 0.2, C = 500	93.05	91.67
	γ = 0.1, C = 1000	96.53	94.44
	γ = 0.1, C = 500	93.75	92.36

Table 3.3. Performance efficiencies of Relay (21) and SVM_D module during three-phase faults for all case studies.

Generator Phase Backup Protection	Performance Efficiency
Relay (21)	$\eta_{21-perf} = 66.67\%$
SVM_D (Polynomial Kernel)	$\eta_{SVM\_D} = 94.44\%$
SVM_D (Gaussian Kernel)	$\eta_{SVM\_D} = 95.14\%$

Table 3.4 shows a comparison between the coordination efficiencies of Relay (21) as well as the proposed SVM_Reach module (Polynomial/Gaussian) with the GOEC limit. The coordination efficiency between Relay (21) with the GOEC limit is obtained from Table 2.6 while the coordination efficiency of the SVM_Reach module (Polynomial/Gaussian) are obtained from Table 3.2. The overall testing efficiency of the proposed scheme during three-phase faults, which is defined by Eq. (3.51), is shown in Table 3.5.

$$\eta_{overall-testing}\% = \frac{\mathrm{N}_{correct-testing}}{Total\ number\ of\ testing\ samples} \times 100 \tag{3.51}$$

where $\mathrm{N}_{\text{correct-testing}}$, is the number of cases where SVM_D and SVM_Reach produced simultaneously correct decisions during testing.

The comparisons illustrated in Tables 3.3 and 3.4 demonstrate satisfactory accuracy for the proposed technique during three-phase faults. The significant improvement in the efficiencies reflects an appreciable enhancement in the coordination between such protection and the GOEC limit.

Table 3.4. Coordination efficiencies of Relay (21) and SVM_Reach module during three-phase faults for all case studies.

Generator Phase Backup Protection	Coordination Efficiency
Relay (21)	$\eta_{21-coord} = 83.33\%$
SVM_Reach (Polynomial Kernel)	$\eta_{SVM\_Reach} = 95.14\%$
SVM_Reach (Gaussian Kernel)	$\eta_{SVM\_Reach} = 96.53\%$

Table 3.5. Overall testing efficiency of the proposed SVM scheme for generator phase backup protection during three-phase faults for all case studies.

SVM proposed scheme for Generator Phase Backup Protection	Overall Efficiency
Proposed scheme (Polynomial Kernel)	$\eta_{overall-testing} = 94.44\%$
Proposed scheme (Gaussian Kernel)	$\eta_{overall-testing} = 95.14\%$

3.4.5 Generalization of the proposed SVM scheme during line-to-line faults

The best classifiers which are shown in Tables 3.1 and 3.2 are generalized against line-to-line faults. Tables 3.6 and 3.7 depict the generalization performance of the best classifiers using Set_g. Here again, the generalization performance is introduced in terms of the generalization efficiency (defined by Eq. (3.52) using Set_g) for both SVM_D and SVM_Reach.

$$\eta_{generalization}\% = \frac{Number\ of\ samples\ correctly\ classified\ during\ generalization}{Total\ number\ of\ generalization\ samples} \times 100. \quad (3.52)$$

Table 3.6. SVM_D generalization performance for line-to-line faults.

Kernel function	Kernel parameters	% Generalization efficiency (Set_g)
Polynomial	n = 10, C = 1000	94.44
	n = 10, C = 500	92.36
	n = 8, C = 1000	93.05
	n = 8, C = 500	92.36
Gaussian	γ = 0.2, C = 1000	95.14
	γ = 0.2, C = 500	93.05
	γ = 0.1, C =1000	96.53
	γ = 0.1, C = 500	93.75

Table 3.7. SVM_Reach generalization performance for line-to-line faults.

Kernel function	Kernel parameters	% Generalization efficiency (Set_g)
Polynomial	n = 10, C = 1000	95.83
	n = 10, C = 500	93.75
	n = 8, C = 1000	94.44
	n = 8, C = 500	93.05
Gaussian	γ = 0.2, C = 1000	96.52
	γ = 0.2, C = 500	94.44
	γ = 0.1, C = 1000	97.91
	γ = 0.1, C = 500	95.14

From the results of these two tables, the following are worth noting:

1- The best generalization performance efficiencies of the fault detection module (SVM_D) during line-to-line faults are 96.53% (Gaussian, $\gamma = 0.1$, $C = 1000$) and 94.44% (Polynomial, $n = 10$, $C = 1000$).

2- The best generalization performance efficiencies of the protective zone identification module (SVM_Reach) during line-to-line faults are 97.91% (Gaussian, $\gamma = 0.1$, $C = 1000$) and 95.83% (Polynomial, $n = 10$, $C = 1000$).

Table 3.8 shows a comparison between the performance of Relay (21) and the proposed SVM_D module (Polynomial/Gaussian) for generator phase backup protection during line-to-line faults. The performance efficiency of Relay (21) is obtained from Table 2.6 while the generalization efficiencies of the SVM_D module (Polynomial/Gaussian) are obtained from Table 3.6.

Table 3.8. Performance efficiencies of Relay (21) and SVM_D module during line-to-line faults for all case studies.

Generator Phase Backup Protection	Performance Efficiency
Relay (21)	$\eta_{21-perf} = 33.33\%$
SVM_D (Polynomial Kernel)	$\eta_{SVM\_D} = 94.44\%$
SVM_D (Gaussian Kernel)	$\eta_{SVM\_D} = 96.53\%$

Table 3.9 shows a comparison between the coordination efficiencies of Relay (21) as well as the proposed SVM_Reach module (Polynomial/Gaussian) with the GOEC limit during line-to-line faults. Here again, the coordination efficiency between Relay (21) with the GOEC limit is obtained from Table 2.6 while the coordination efficiencies of the SVM_Reach module (Polynomial/Gaussian) are obtained from Table 3.7.

Table 3.9. Coordination efficiencies of Relay (21) and SVM_Reach module during line-to-line faults for all case studies.

Generator Phase Backup Protection	Coordination Efficiency
Relay (21)	$\eta_{21-coord} = 66.67\%$
SVM_Reach (Polynomial Kernel)	$\eta_{SVM\_Reach} = 95.83\%$
SVM_Reach (Gaussian Kernel)	$\eta_{SVM\_Reach} = 97.91\%$

The overall generalization efficiency of the proposed scheme during line-to-line faults, which is defined by Eq. (3.53), is shown in Table 3.10.

$$\eta_{overall-generalization}\% = \frac{\mathrm{N}_{correct-generalization}}{Total\ number\ of\ generalization\ samples} \times 100 \qquad (3.53)$$

where $\mathrm{N}_{\text{correct-generalization}}$, is the number of cases where SVM_D and SVM_Reach produced simultaneously correct decisions during generalization.

Table 3.10. Overall generalization efficiency of the proposed SVM scheme for generator phase backup protection during line-to-line faults for all case studies.

SVM proposed scheme for Generator Phase Backup Protection	Overall Efficiency
Proposed scheme (Polynomial Kernel)	$\eta_{overall-generalization} = 94.44\%$
Proposed scheme (Gaussian Kernel)	$\eta_{overall-generalization} = 96.53\%$

3.5 Summary

In this chapter, the Support Vector Machines (SVMs) classification technique is proposed to enhance the performance of the generator phase backup protection as well as the coordination between such protection and the generator steady-state overexcited capability (GOEC) limit with the presence of a midpoint STATCOM.

The proposed SVM scheme is trained and tested for 324 and 144 data samples respectively obtained during three-phase faults for different fault locations and generator loadings. After obtaining the best classifiers during three-phase faults, the proposed scheme is then generalized to 144 data samples obtained during line-to-line faults.

The results presented in this chapter demonstrate that the proposed SVM scheme is fast and reliable with a performance efficiency of 95.14% and 96.53% for three-phase and line-to-line faults respectively. In comparison to the performance of Relay (21) during three-phase and line-to-line faults (66.67% and 33.33% respectively), the proposed SVM scheme reflects an appreciable enhancement in the coordination between generator SVM phase backup protection and the generator steady-state overexcited capability limit.

4. IMPACT OF THE COORDINATION BETWEEN GENERATOR DISTANCE PAHSE BACKUP PROTECTION AND GENERATOR STEADY-STATE OVEREXCITED CAPABILITY ON GENERATOR OVEREXCITATION THERMAL CAPABILTY IN THE PRESENCE OF A MIDPOINT STATCOM

4.1 Introduction

In this chapter, investigations are carried out on System I to explore the impact of the coordination between generator distance phase backup protection (Relay (21)) and generator steady-state overexcited capability on the generator overexcitation thermal capability. These investigations are focused on the performance of Relay (21) when it is set to provide thermal backup protection for the generator during two common system disturbances, namely a system fault and a sudden application of a large system load while the overexcitation limiter (OEL) is in service. Moreover, the performance of Relay (21) is also evaluated during these disturbances with the presence of a midpoint STATCOM.

4.2 Generator Overexcitation Thermal Capability

In response to system voltage drops caused by high reactive power requirements, switching manipulations or faults, the generator field winding is allowed for short time overexcitation levels [53], [54]. These short time overexcitation levels are based on the principles of thermodynamic heat balance; that is higher levels are allowed for shorter periods of time, and lower levels for longer periods of time. With regard to these overexcitation levels in the standards, the IEEE C50.13 [53] is related to turbogenerators, while the IEEE C50.12 [54] covers hydrogenerators generators and does not give specific overexcitation guidelines. For this reason, IEEE C50.13 is used for hydrogenerators although its interpretation of overexcitation allowable may be quite conservative [55].

According to the IEEE C50.13, the generator field winding shall be capable of operating at a field current of 125% of its rated value for at least 1 minute starting from stabilized temperatures

at rated conditions. The permissible field current, in the range of 5 s to 120 s, based on the same increment of heat storage, is given by the following equation

$$I_{FD} = I_{FD\_RATED} \times \sqrt{\frac{33.75}{time} + 1},\ time > 0 \quad (4.1)$$

where I_{FD} and I_{FD_RATED} are in p.u. and the time is in seconds. Ten points in the permissible range are listed in Table 4.1 and plotted in Figure 4.1. It is recognized that the field winding temperatures under these conditions will exceed the rated load values. Therefore, the machine construction is based on the assumption that the number of such operations at field currents to the limits specified will occur not more than two times per year.

Table 4.1. Generator overexcitation thermal capability.

Time, s	5	10	15	20	30	45	60	90	100	120
Field current, p.u.	2.78	2.09	1.8	1.64	1.46	1.32	1.25	1.17	1.15	1.13

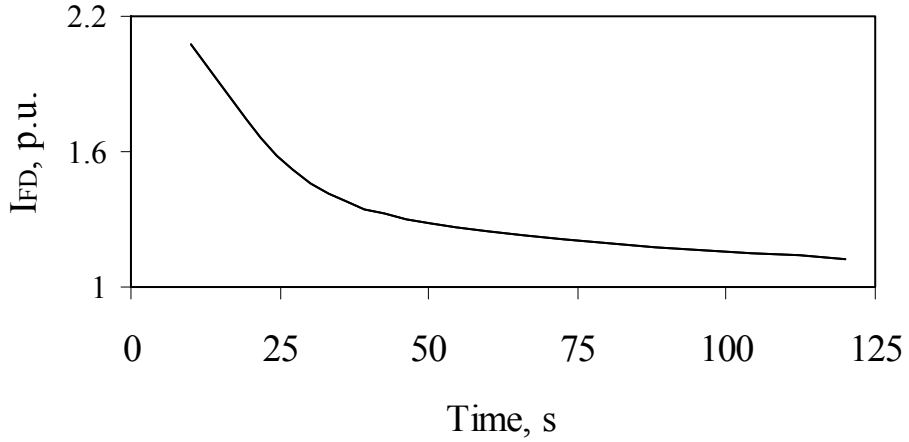

Figure 4.1. Generator overexcitation thermal capability.

4.3 Overexcitation Limiters (OEL)

4.3.1 Types of overexcitation limiters

A simple form of OEL has a fixed pickup point, a fixed time delay and instantly reduces the excitation set point to a safe value. A more common type of overexcitation limiter provided by many manufacturers combines instantaneous and inverse-time pickup characteristics and switches from an instantaneous limiter with a setting of about 160% of the rated field current (I_{FD_RATED}) to a timed limiter with a setting of about 105% of the rated field current. The field current set point is not ramped down, but decreases almost instantly when this type of limiter

switches. The inverse-time curve, the instantaneous limiter value and the timed limiter value are all adjustable on this type of limiter [56].

Other manufacturers provide overexcitation limiters that ramp down the limiter set point from the instantaneous value to the timed limiter setting. The ramp rate can be constant [25] or proportional to the level of overexcitation [57].

Some, typically older, excitation systems do not have continuously acting overexcitation limiters. These systems switch from automatic voltage regulation to a fixed field set point if the excitation is high for too long. The excitation set point may be positioned to produce the maximum continuous field current or it may be positioned near the normal unity power factor position. In these types of systems, the AVR output signal is permanently overridden. [58].

4.3.2 Operation of overexcitation limiters

The main function of the OEL is to prevent excessive heating in the generator field winding. OEL must offer proper protection from overheating due to high field current levels while simultaneously allowing maximum field forcing for power system stability enhancement purposes. All of the different types of OELs operate with the same sequence of events: detect the overexcitation condition, allow it to persist for a defined time-overload period and then reduce the excitation to a safe level [55], [59]-[64]. During such events, the field current or the field voltage is typically the monitored variable that is compared with a predefined pickup level. The variation in the OEL designs appears in two main aspects; the allowed overexcitation period which may be fixed or vary inversely with the excitation level and the excitation level reduction characteristic. Figure 4.2 shows a flow chart describing the operation of an OEL during a system disturbance.

As shown in Figure 4.2, during a system disturbance, the field current I_{FD} is compared to a predefined pickup value I_{pickup}. If I_{FD} is greater than I_{pickup} (typically 1.05 I_{FD_RATED}), the OEL timer starts. A field forcing period T_{FF} (ranges from 0.1 to 1 s) is allowed, where I_{FD} is permitted to levels above a predefined maximum value, I_{FF} (1.4 to 1.6 I_{FD_RATED}). After the field forcing is timed out, the overexcitation limiting function observes the field current level. If I_{FD} is greater than I_{FF}, the OEL restores the field current to safe value I_{safe} (1.0 to 1.25 I_{FD_RATED}) by either one of the following ways:

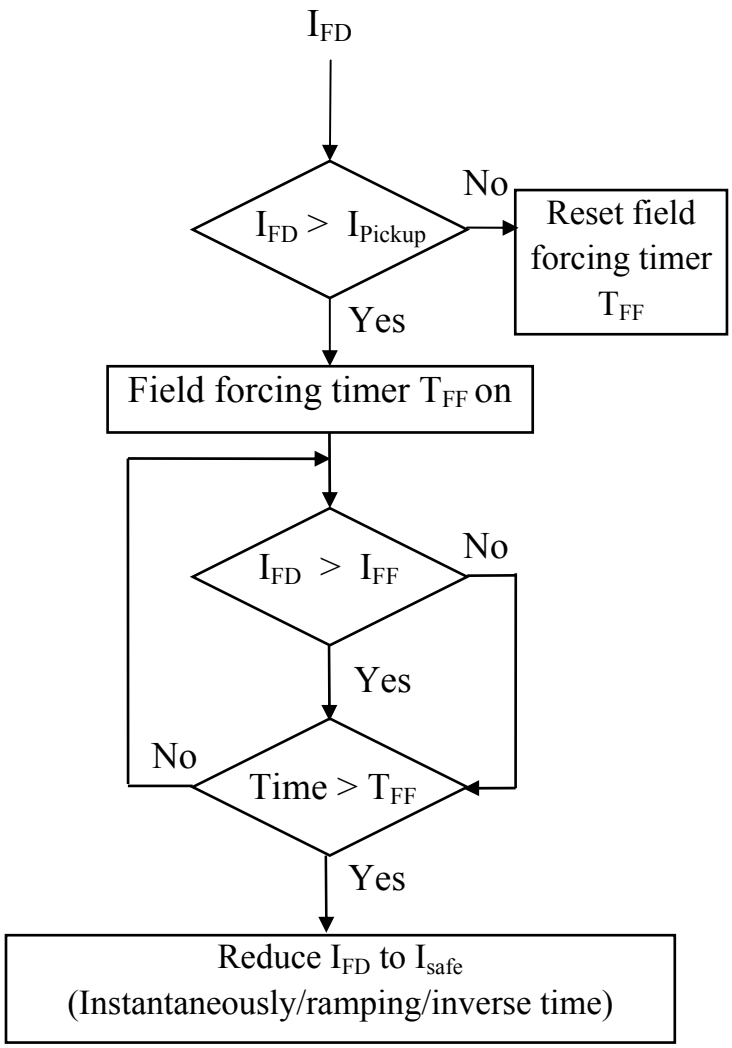

Figure 4.2. A flow-chart of OEL operation during system disturbances.

1. Ramping down the set point from the instantaneous setting point I_{FF} to a timed setting where the ramp rate can be constant or proportional to the level of overexcitation.
2. Reducing the field current level instantaneously with an instantaneous setting of I_{FF} to a timed setting, where this timed setting may be a fixed or an inverse-pickup characteristic.
3. A combination of instantaneous and inverse-time pickup characteristic can also be used where the OEL switches from an instantaneous limiter with a setting around I_{FF} to a timed limiter with a setting of about 1.05 I_{FD_RATED}. The field current set point is decreased almost instantly when the OEL switches.

The inverse-time curve, the instantaneous limiter and the timed limiter values are all adjustable on these types of limiters. On the other hand, if I_{FD} is less than I_{FF}, the existing field

current level will be allowed to continue for a time delay according the timed setting characteristic of the OEL [55], [56], [62], [63].

4. 4. Setting of Relay (21) for Generator Thermal Backup Protection

As it is mentioned in Chapter 2, Relay (21) is set within the generator steady-state overexcited capability (GOEC) with adequate margin overload and stable power swings. In this context, Relay (21) element is typically set at the smallest of the three criteria listed in Section 2.7.2.4 [26]. In particular cases when the generator distance phase backup protection is mainly required to provide thermal backup protection for the generator against transmission lines faults which are not cleared by transmission line relays, Relay (21) is set directly according to the second criterion in Section 2.7.2.4 which states "50% to 67% of the generator load impedance (Z_{load}) at the rated power factor angle (RPFA) of the generator. This provides a 150% to 200% margin over the generator full load". In order to achieve a correct operation with such a setting, the following considerations must be taken into account:

1. Coordination with transmission line primary and backup protection. In this regard, the time delay for Relay (21) should be set longer than the transmission lines backup protection (0.8 to 1 s) with an appropriate margin for proper coordination.
2. Coordination with the OEL. The time delay for Relay (21) should also be set longer than that of the field forcing time (0.1 to 1 s).

In order to satisfy these two requirements, a delay time of 2 s is considered in the investigations of this chapter.

4.5. Impact of Relay (21) on Generator Overexcitation Thermal Capability

4.5.1 Coordination of Relay (21) and GOEC limit of System I

In order to provide thermal backup protection for the generator, Relay (21) reach is set at 67% of the generator load impedance at RPFA = 19.95° which yields $Z_{21} = 23.25\ \Omega$ at MTA = 85° (Appendix C). The generator steady-state overexcited capability limit (GOEC of Fig. 2.19(a)) and Relay (21) characteristic are plotted in Figure 4.3.

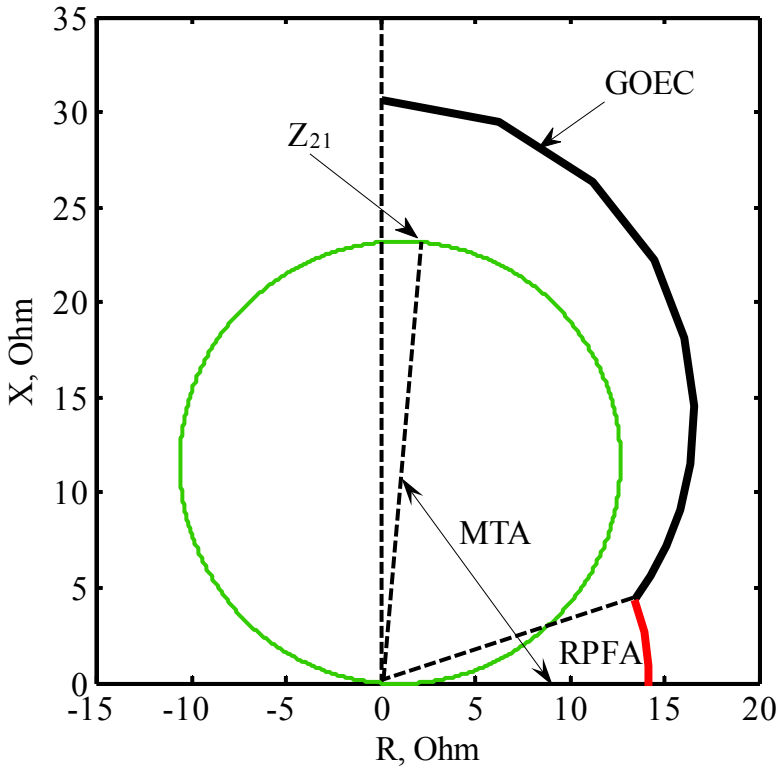

Figure 4.3. Coordination between Relay (21), when it is set for generator thermal backup protection and G_1 steady-state overexcited capability limit (System I).

4.5.2 Case studies and simulation results

The performance of Relay (21) is examined during the five system disturbances described in Table 4.2 while the overexcitation limiter (OEL) is in service (I_{FF} is assumed to be 1.5 I_{FD_RATED} where I_{FD_RATED} = 1.57 p.u.). The generator pre-disturbance loading conditions considered in the investigations of this chapter are selected in accordance with the recommendation of [65]. Such a recommendation states that "in order to perform an OEL test (typically for a hydrogenerators), the generator should be loaded to at least 80% of its rated MVA".

4.5.2.1 OEL response during and after Disturbance 1

Figure 4.4 shows the generator terminal voltage and field current transient time responses during and after Disturbance 1. The trip signal of Relay (21) is also shown in the same figure. In response to the sudden drop in the generator terminal voltage due to the fault, the field current I_{FD} exceeds I_{pickup} (1.05 I_{FD_RATED}) and causes the field forcing timer T_{FF} to start. During the permissible time of the field forcing (1 s), the field current increases and reaches 2.4 p.u. which is higher than the maximum limit I_{FF} (1.5 × 1.57 = 2.355 p.u.). After the field forcing timer is

timed out at t = 6 s, the OEL would ramp down the field current to its rated value. As the fault is cleared at t = 5.07 s, a stable power swing is observed in the oscillations of the generator terminal voltage and field current. Relay (21) trip signal shown in Figure 4.4 indicates, however, that Relay (21) tripped during this stable power swing at 7.0043 s.

Table 4.2. Coordination of Relay (21) and GOEC with OEL case studies.

Generator output power (pre-disturbance loading), p.u.	Disturbance number	Description
P = 0.8, Q = 0.27 (Without a midpoint STATCOM)	1	A three-phase fault 50 km from bus A. Fault inception: t = 5 s, fault duration = 0.07 s.
	2	A sudden application of an inductive load (Q_L = 0.47 p.u.) at the generator terminals at t = 3 s, duration = 7 s.
P = 0.8, Q = 0.135 (With a midpoint STATCOM)	3	A three-phase fault 50 km from bus A. Fault inception: t = 5 s, fault duration = 0.07 s.
	4	A sudden application of an inductive load (Q_L = 0.47 p.u.) at the generator terminals at t = 3 s, duration = 7 s
	5	A three-phase fault 5 km from the midpoint M (145 km from bus A). Fault inception: t = 5 s, fault duration = 0.07 s.

4.5.2.2. Impedance trajectory measured by Relay (21) during and after Disturbance 1

Figure 4.5 depicts the impedance trajectory measured by Relay (21) during and after Disturbance 1. As a result of fault occurrence at t = 5 s, the impedance trajectory jumps into the relay characteristic at t = 5.0043 s and Relay (21) timer starts. After the fault is cleared at t = 5.07, the impedance trajectory jumps outside the relay characteristic at t = 5.09 s. The oscillations in the generator voltages and currents due to the disturbance result, however, in that the impedance trajectory moves again in and out of Relay (21) characteristic twice during the 2 s timer (5.177 s - 6.109 s and 6.869 s - 7.653 s) as shown in Figure 4.5. Relay (21) issued a trip signal at t = 7.0043 s as shown in Figure 4.4.

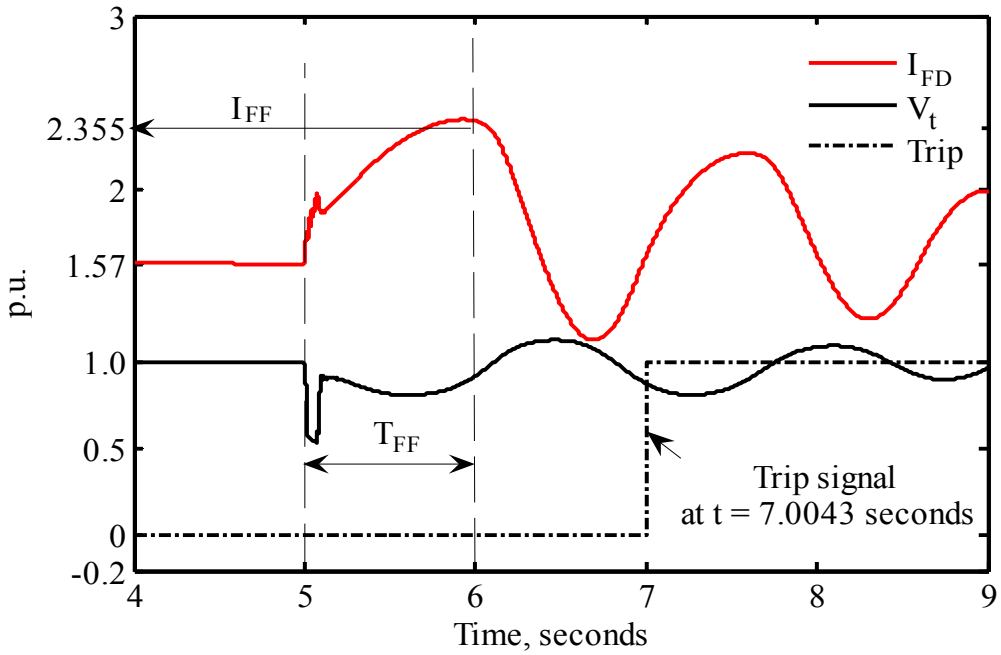

Figure.4.4. Generator terminal voltage and field current transient time responses as well as Relay (21) trip signal during and after Disturbance 1.

4.5.2.3. OEL response during and after Disturbance 2

Figure 4.6 shows the generator terminal voltage and field current transient time responses during and after Disturbance 2. The trip signal of Relay (21) is also shown in the same figure. Similar to the case of Disturbance 1, the sudden application of the large load results in a sudden drop in the generator terminal voltage that causes the field current to increase and exceed $I_{pickup.}$ During the permissible time of the field forcing (1 s), the field current reaches 2.278 p.u. which is below the maximum limit I_{FF} (2.355 p.u.). After the field forcing timer is timed out at t = 4 s, the field current oscillates around 1.95 p.u. (1.242 × 1.57 p.u.) and the OEL would allow it to continue at this level until the overload condition is removed. Figure 4.6 shows that after the removal of the load, the generator field current returns back to its pre-disturbance value. Despite the fact that the generator field winding is not at a thermal risk during Disturbance 2, Relay (21) issued a trip signal at 5.014 s.

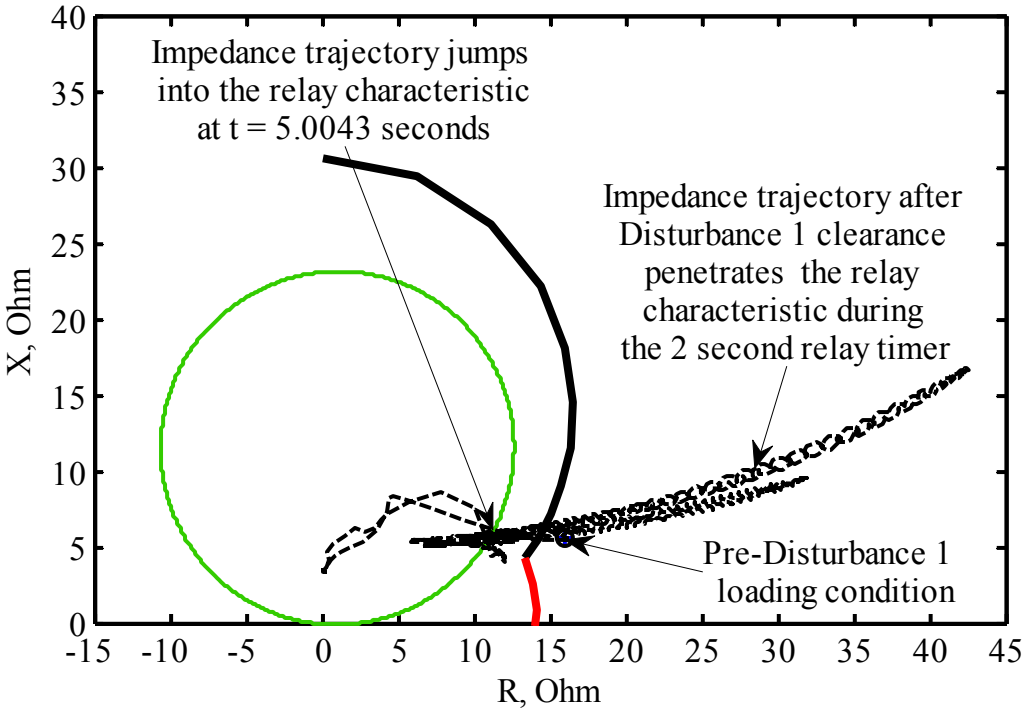

(a)

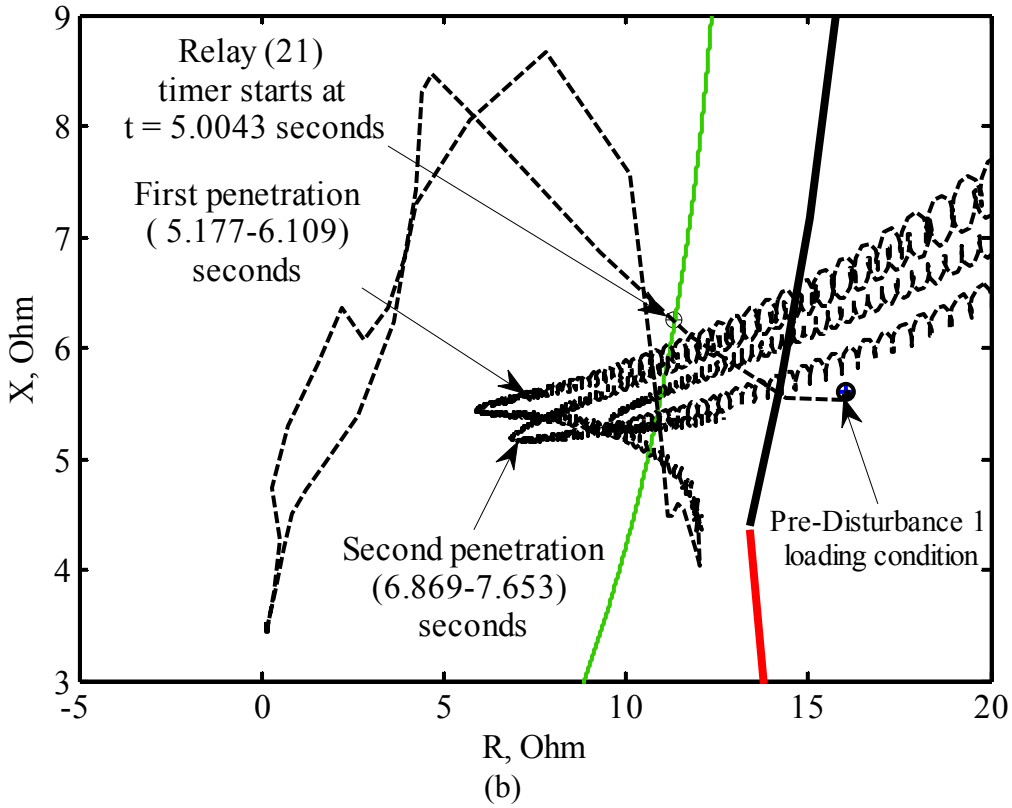

(b)

Figure 4.5. Impedance trajectory measured by Relay (21) during and after Disturbance 1: (a) total overview, (b) a zoom in on the impedance trajectory penetrations.

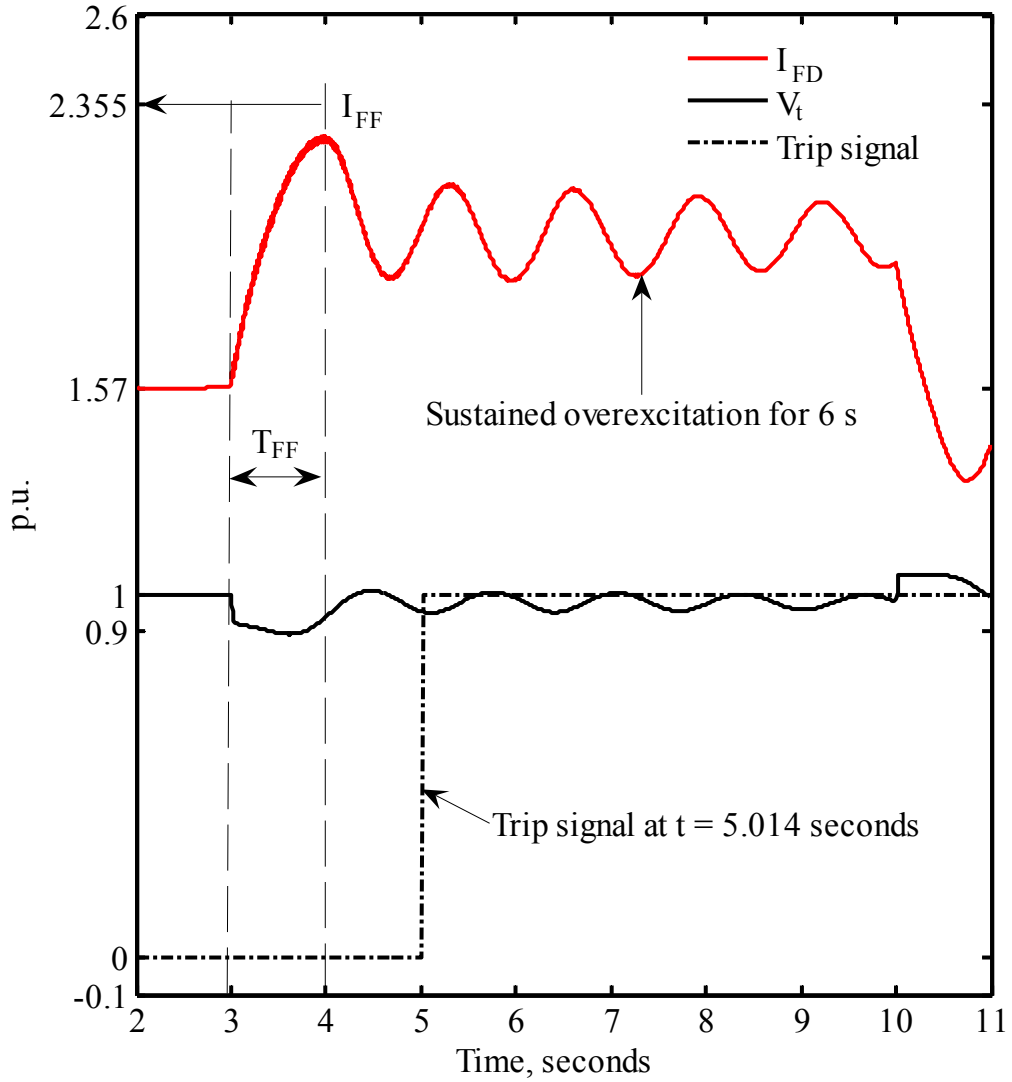

Figure 4.6. Generator terminal voltage and field current transient time responses as well as Relay (21) trip signal during and after Disturbance 2.

4.5.2.4 Impedance trajectory measured by Relay (21) during and after Disturbance 2

Figure 4.7 depicts the impedance trajectory measured by Relay (21) during and after Disturbance 2. The sudden application of the load at t = 3 s forces the impedance trajectory to penetrate the relay characteristic at 3.014 s and stay inside it. Once the impedance trajectory penetrates Relay (21) characteristic, Relay (21) timer starts but the relay would not trip until its delay timer (2 s) is timed out. During this duration, the impedance trajectory reflects the result of several cycles of generator oscillations after the disturbance. At t = 5.014 s, Relay (21) issued a trip signal as shown in Figure 4.6.

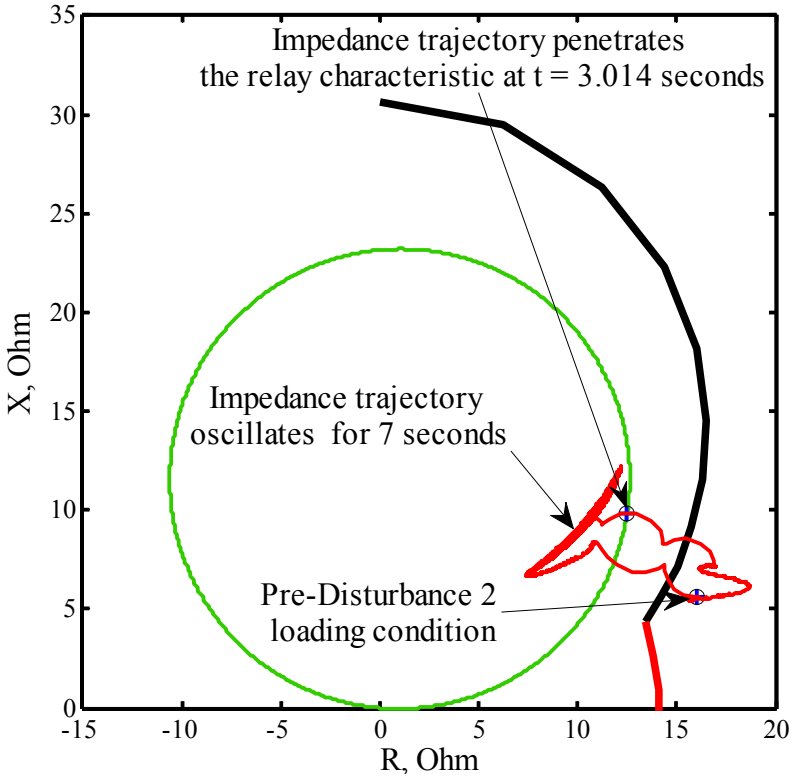

Figure 4.7. Impedance trajectory measured by Relay (21) during and after Disturbance 2.

4.5.2.5. OEL response during and after Disturbance 3

Figure 4.8 shows the generator terminal and the midpoint M voltages as well as the generator field current transient time responses during and after Disturbance 3. The fault results in sudden drops in the generator terminal and the transmission line midpoint voltages (to 0.52 p.u. and 0.38 p.u. respectively) as well as in a sudden increase in the generator field current. As it can be seen from Figure 4.8, during the permissible field forcing period, the field current I_{FD} reaches 1.765 p.u. which is less than I_{FF}. After fault clearance, Figure 4.8 shows that the generator field current I_{FD} returns to its pre-disturbance value and the oscillations in the generator terminal voltage indicate a stable power swing. No trip signal is received from Relay (21).

4.5.2.6. Impedance trajectory measured by Relay (21) during and after Disturbance 3

Figure 4.9 shows the impedance trajectory measured by Relay (21) during and after Disturbance 3. Due to the presence of the midpoint STATCOM, the impedance trajectory starts at ($R = 18.2\ \Omega$, $X = j2.98\ \Omega$) corresponding to the pre-fault loading condition in the P-Q plane. As a result of the fault at t = 5 s, the impedance trajectory jumps into the relay characteristic at t

= 5.004 s and Relay (21) timer starts. After the fault is cleared at t = 5.07, the impedance trajectory jumps outside the relay characteristic at t = 5.089 s and stabilizes at its pre-disturbance loading condition. No trip signal occurred during the 2 s of Relay (21) timer.

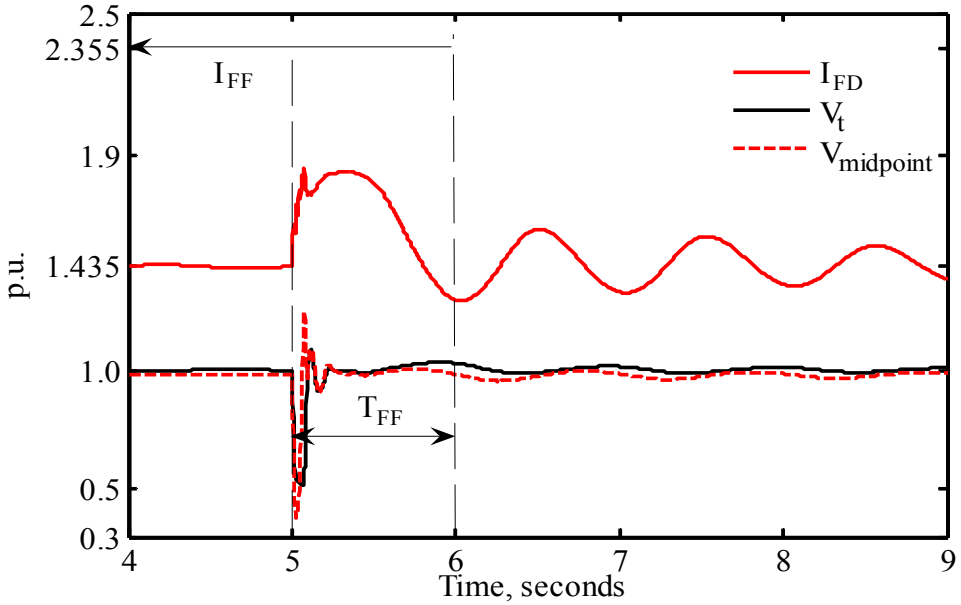

Figure 4.8. Generator terminal voltage, transmission line midpoint voltage and generator field current transient time responses during and after Disturbance 3 (with a midpoint STATCOM).

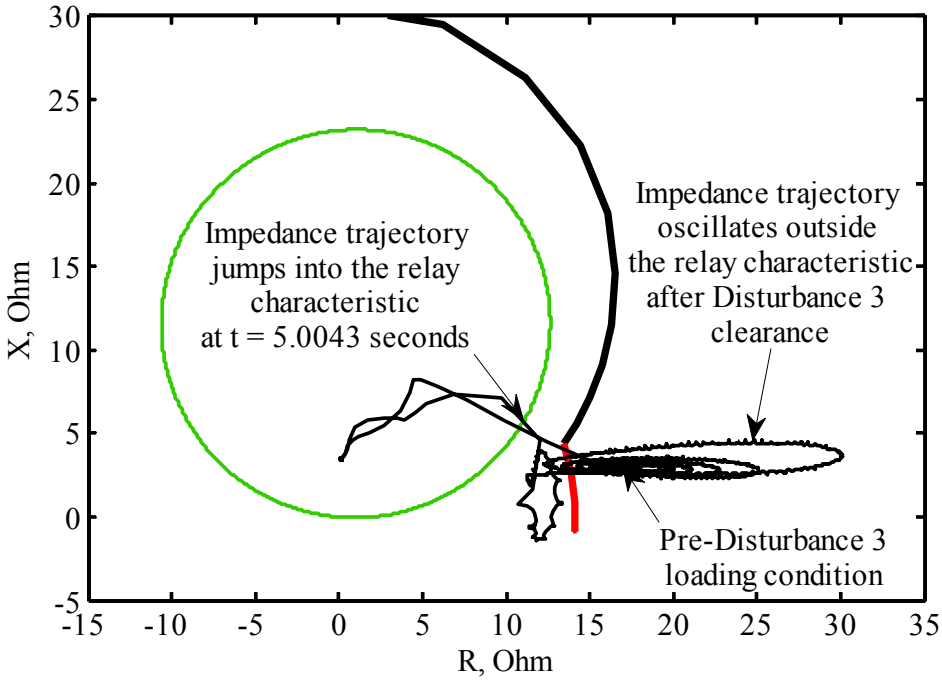

Figure 4.9. Impedance trajectory measured by Relay (21) during and after Disturbance 3 (with a midpoint STATCOM).

4.5.2.7. OEL response during and after Disturbance 4

Figure 4.10 shows the generator terminal and the midpoint M voltages as well as the generator field current transient time responses during and after Disturbance 4. Similar to the case of Disturbance 2, the sudden application of the large load results in a sudden drop in the generator terminal voltage that causes the field current to increase above I_{pickup}. During the permissible time of the field forcing (1 s), the field current reaches 1.8 p.u. which is below the maximum limit I_{FF} (2.355 p.u.). After the field forcing timer is timed out at t = 4 s, the field current oscillates around 1.774 p.u. (1.13 × 1.57 p.u.) and the OEL would allow it to continue at this level until the overload condition is removed. Figure 4.10 shows that after the removal of the load, the generator field current is returning back to its pre-disturbance value. No trip signal is obtained from Relay (21).

4.5.2.8. Impedance trajectory measured by Relay (21) during and after Disturbance 4

Figure 4.11 shows the impedance trajectory measured by Relay (21) during and after Disturbance 4. Similar to Disturbance 3, due to the presence of the midpoint STATCOM, the impedance trajectory starts at ($R = 18.2\ \Omega$, $X = j2.98\ \Omega$) corresponding to the pre-disturbance loading condition in the P-Q plane. The sudden application of the inductive load at t = 1 s forces the impedance trajectory to move towards the relay characteristic. The reduction in the generator reactive power output due to the presence of the midpoint STATCOM results in a reduction in the generator overexcitation level during Disturbance 4. As a result, the impedance measured by Relay (21) stays outside its characteristic at ($R = 12.5\ \Omega$, $X = j7.7\ \Omega$) for the 6 second duration and no trip signal is issued by the relay.

4.5.2.9. OEL response during and after Disturbance 5

Figure 4.12 shows the generator terminal and the midpoint M voltages as well as the generator field current transient time responses during and after Disturbance 5. As a result of the fault, the generator field current increases while the voltage of the transmission line midpoint drops below the threshold of the STATCOM self-protection (which is assumed to be 0.15 p.u.) and the STATCOM is disconnected during the 0.07 s fault duration (the VSC will stop gating until the voltage rises above 0.15 p.u). During the permissible field forcing period, the field current I_{FD} reaches 1.7 p.u., which is less than I_{FF}. As the fault is cleared at t = 5.07 s, a stable

power swing is observed in the oscillations of the generator terminal voltage. No trip signal is issued by Relay (21).

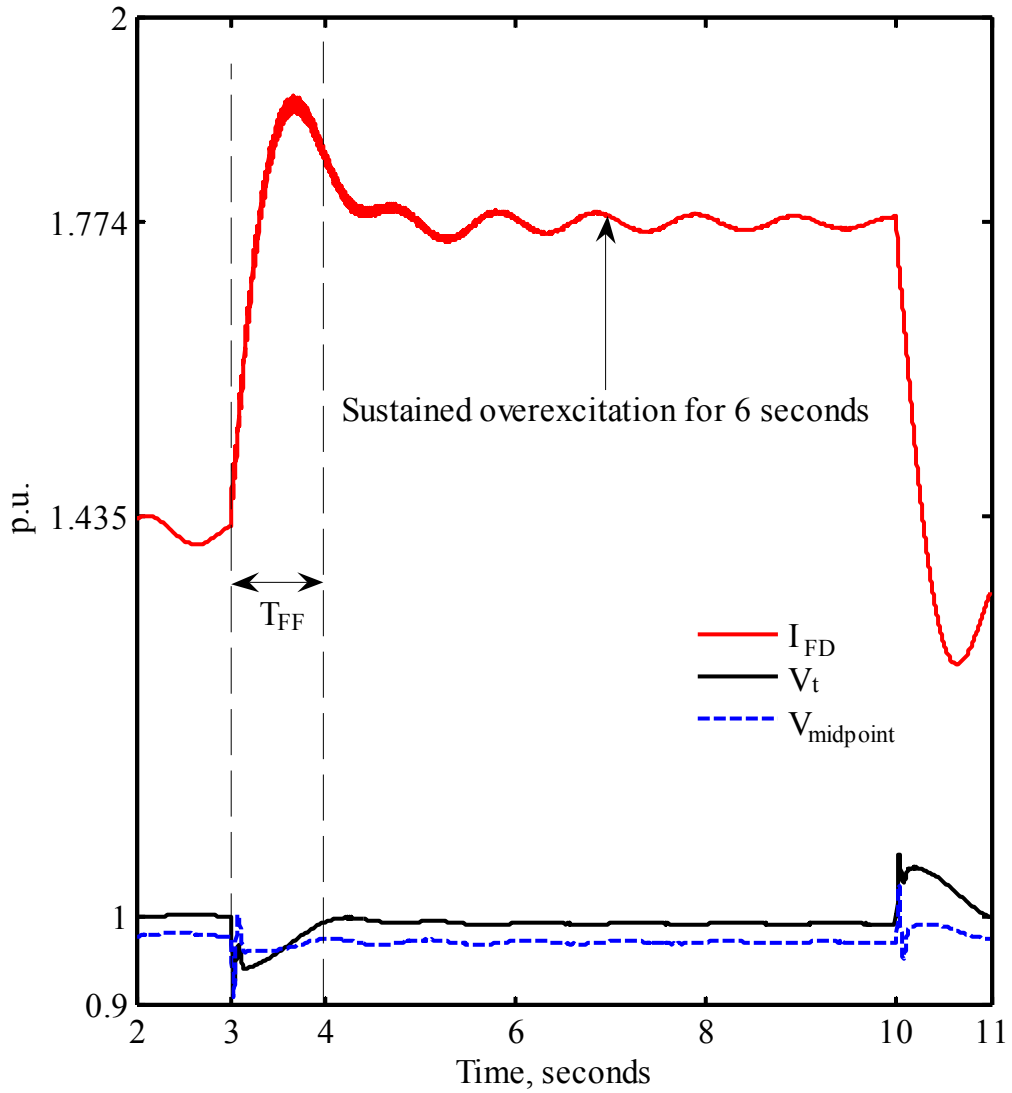

Figure 4.10. Generator terminal voltage, transmission line midpoint voltage and generator field current transient time responses during and after Disturbance 4 (with a midpoint STATCOM).

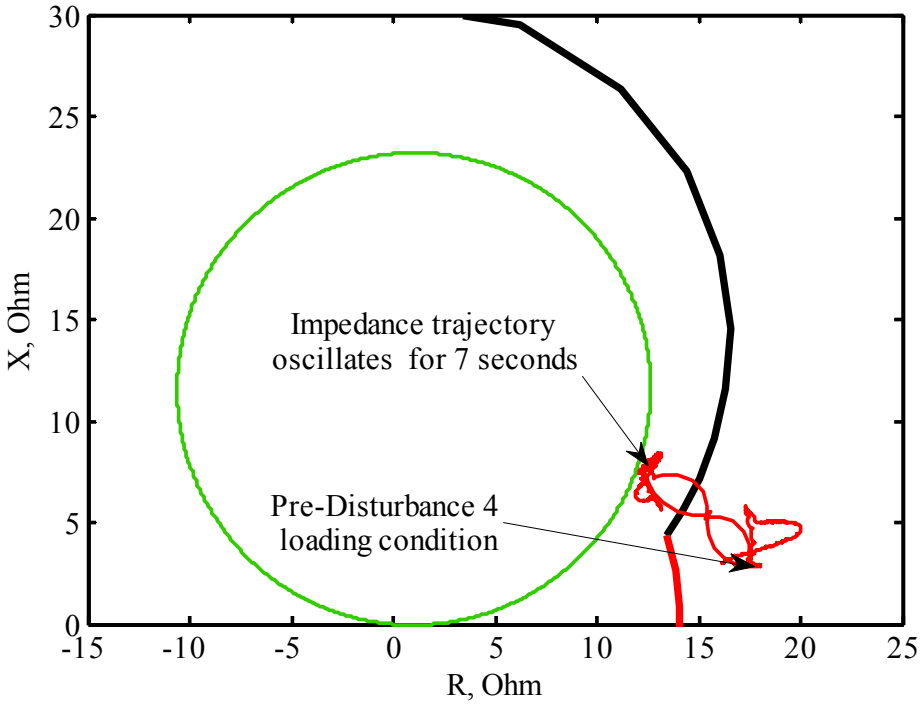

Figure 4.11. Impedance trajectory measured by Relay (21) during and after Disturbance 4 (with a midpoint STATCOM).

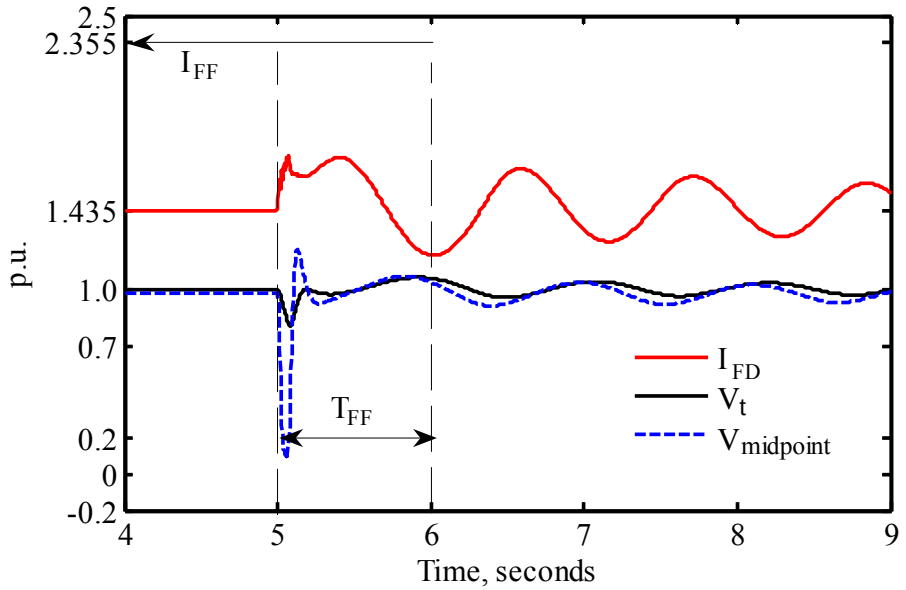

Figure 4.12. Generator terminal voltage, transmission line midpoint voltage and generator field current transient time responses during and after Disturbance 5 (with a midpoint STATCOM).

4.5.2.10. Impedance trajectory measured by Relay (21) during and after Disturbance 5

Figure 4.13 shows the impedance trajectory measured by Relay (21) during and after Disturbance 5. Similar to Disturbances 3 and 4, the impedance trajectory starts at ($R = 18.2\ \Omega$, $X = j2.98\ \Omega$) corresponding to the pre-disturbance loading condition. As a result of the fault occurrence at t = 5 s, the impedance trajectory jumps into the relay characteristic at 5.0043 s and the relay timer starts. After the fault is cleared at t = 5.07, the impedance trajectory jumps outside the relay characteristic at t = 5.089 s. At this time, however, the midpoint STATCOM is already back in service and the impedance trajectory stabilizes at its pre-disturbance loading condition. No trip signal is issued by Relay (21).

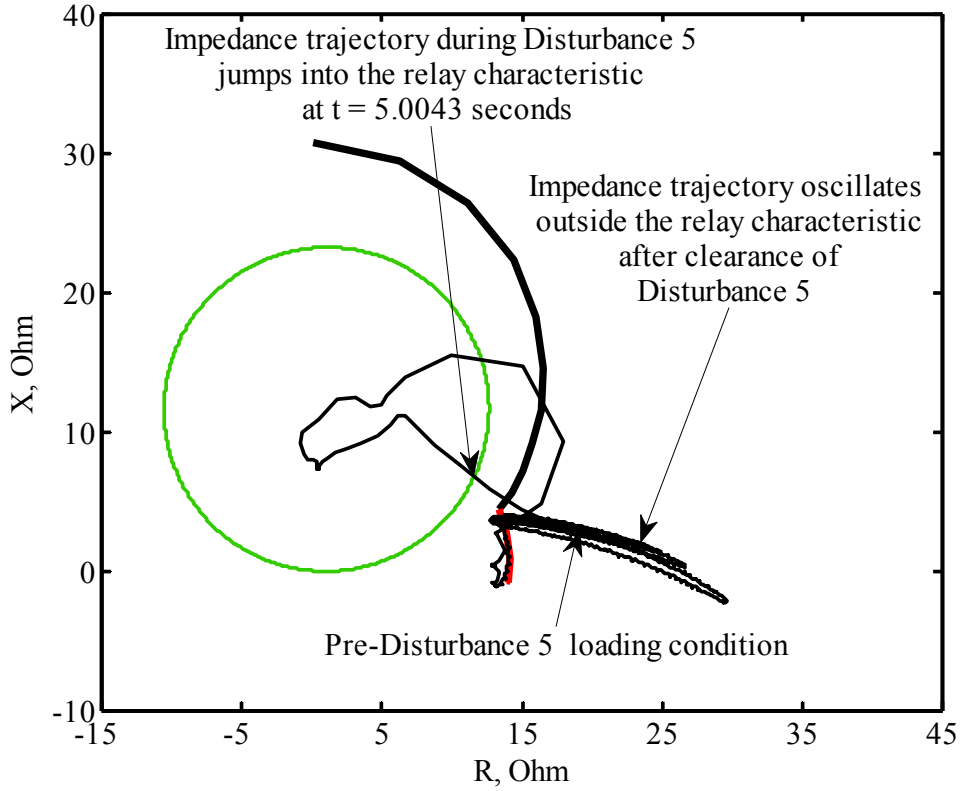

Figure 4.13. Impedance trajectory measured by Relay (21) during and after Disturbance 5 (with a midpoint STATCOM).

4.6. Discussion of Results and the Proposed Solution

The results of the investigations presented for the five disturbances show that the OEL is allowing some levels of field forcing in order to maintain the system stability as shown in Figures 4.4, 4.6, 4.8, 4.10 and 4.12. On the other hand, Relay (21) is set for generator thermal

backup protection against transmission line uncleared faults with a reach of 23.25 Ω at MTA of 85°. This setting, however, leads the generator to be over-protected. In other words, Relay (21) issued trip signals during a stable power swing (Disturbance 1) as well as when the generator is not at a thermal risk (and during a stable power swing too, Disturbance 2).

The presence of a midpoint STATCOM significantly enhances Relay (21) performance during system disturbances. This enhancement is due to the fact that the STATCOM maintains the voltage of the midpoint bus at "almost" 1 p.u. by injecting inductive current which reduces the levels of the generator output reactive power and the oscillations in the impedance trajectory of Relay (21). Therefore, an existing midpoint STATCOM, installed in a transmission line for the purpose of increasing its power transfer capability, would alleviate the problem caused by Relay (21). This is, however, not an economical solution (installing a midpoint STATCOM) for generators that are connected to uncompensated (no midpoint shunt compensation) transmission lines. In this case, the proposed solution in this thesis is to reduce Relay (21) reach in order to provide a more secure performance during system disturbances. This would allow the generator to supply its maximum reactive power during such events. In this regard, Relay (21) (of System I) reach is reduced from $Z_{21} = 23.25$ Ω at MTA = 85° to $Z_{21} = 9.6$ Ω at MTA = 85° as shown in Figure 4.14.

4.7. Summary

In this chapter, investigations are carried out to explore the impact of generator distance phase backup protection (Relay (21)) of System I on the generator overexcitation thermal capability. These investigations have included the performance of Relay (21) when it is set to provide thermal backup protection for the generator during two common system disturbances, namely a system fault and a sudden application of a large system load while the overexcitation limiter (OEL) is in service. Moreover, the performance of Relay (21) is also evaluated during these disturbances without/with the presence of a midpoint STATCOM. The results of these investigations have shown that, in the absence of a midpoint STATCOM, the current setting of Relay (21) for generator thermal backup protection restricts the overexcitation thermal capability of the generator. Such a restriction does not allow the generator to supply its maximum reactive power during such events. This highlights the need to revise the setting of the generator distance phase backup protection relay in order to allow the generator to fulfill the system

requirements during major disturbances to ensure adequate level of voltage stability. In this regard, the reduction of Relay (21) reach is proposed as a simple and feasible solution.

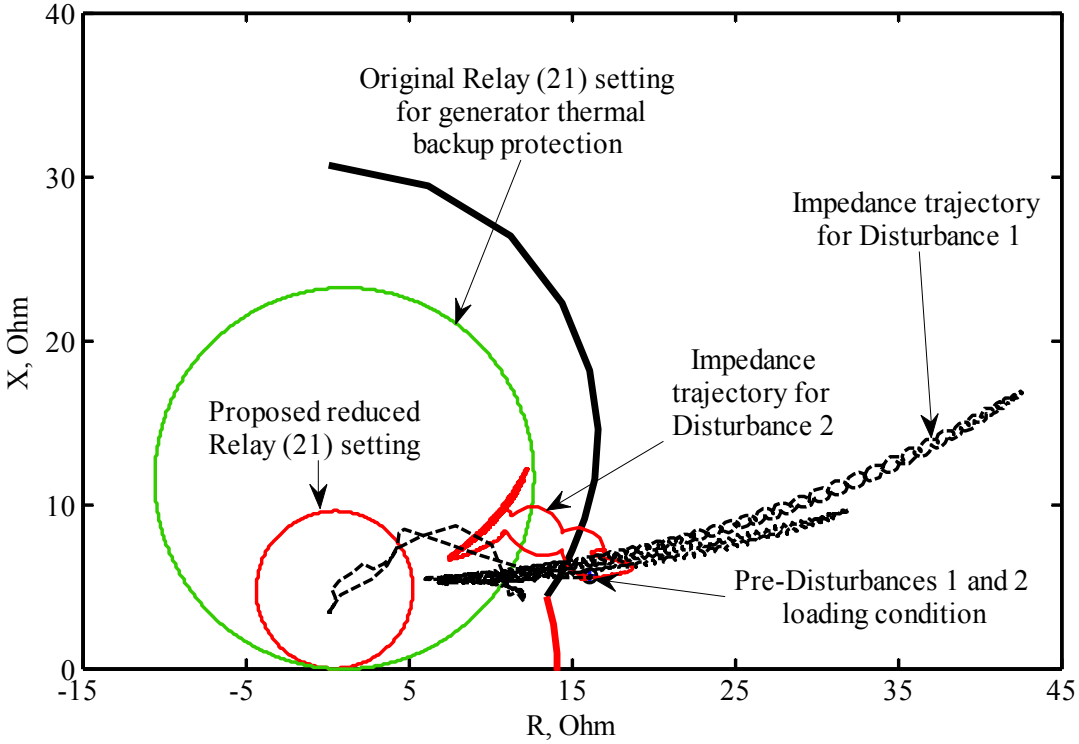

Figure 4.14. Impedance trajectories measured by Relay (21) during and after Disturbances 1 and 2 with the original and reduced Relay (21) reaches.

5. SUMMARY AND CONCLUSIONS

5.1 Summary

As a result of the Flexible AC Transmission Systems (FACTS) initiative, considerable effort has been spent in the last two decades on the development of power electronic-based power flow controllers. The potential benefits of these FACTS Controllers are now widely recognized by the power system engineering and the transmission and distribution communities. The ability of FACTS Controllers, however, to rapidly change system voltages, currents and impedances may affect the performance of the power system protection system. It is, therefore, important to investigate the impact of FACTS Controllers on the power system protective system.

A literature review has shown that virtually, no research work has been reported on the impact of midpoint FACTS Controllers on the performance of generator distance phase backup protection. The objective of this research was to carry out extensive studies to explore the impacts of midpoint STATCOM as well as the early generation of midpoint static shunt compensation controllers, namely the Static Var Compensator (SVC) on generator distance phase backup protection in order to identify the important issues that protection engineers need to consider when designing and setting the generator protection system. In addition, practical, feasible and simple solutions to mitigate the adverse impact of midpoint FACTS Controllers on generator distance phase backup protection need to be explored. The research objective has been accomplished through the completion the following three studies:

1. Investigating the impact of midpoint FACTS Controllers on the coordination between generator distance phase backup protection and generator capability limits.
2. The use of the Support Vector Machines pattern classification technique for enhancing the coordination between generator phase backup protection and generator capability limits in the presence of midpoint FACTS controllers.

3. Investigating the impact of generator distance phase backup protection on generator overexcitation thermal capability in the presence of a midpoint STATCOM and proposing a feasible and practical solution for any potential existing problem.

Chapter 1 provides a brief introduction on the concept and application of FACTS Controllers with emphasis on their role in transmission line midpoint compensation. A brief introduction on distance relaying and generator protection is also included. Important conclusions and the objectives of the research were drawn from the literature review on the impact of FACTS Controllers on the performance of distance protection of transmission lines.

The principle of operation and control of SVC and STATCOM are presented in Chapter 2. The capability curves for different turbine driven generators and the distance phase backup protection are also discussed. The remainder of Chapter 2 is devoted to reporting the studies conducted to explore the impact of midpoint FACTS Controllers on the performance of generator phase backup protection as well as on the coordination between generator distance phase backup protection and generator capability limits.

Chapter 3 presents comprehensive studies on the use of the Support Vector Machines pattern classification technique to enhance the coordination between generator backup protection and generator capability limits. In this context, the performance of the two commonly used Kernel functions in power system applications, namely the Polynomial and the Gaussian Kernel functions were tested to assess the suitability of the SVM as an intelligent generator phase backup protection relay.

Chapter 4 presents the studies concerned with the impact of generator distance phase backup protection on generator overexcitation thermal capability. The impact of a midpoint STATCOM on the behavior of this protection is also investigated.

5.2 Conclusions

The studies conducted in this thesis yield the following conclusions for the systems under study:

1. Both the midpoint STATCOM and the SVC have an adverse effect on the generator distance phase backup protection. This impact varies according to the fault type, fault

location and generator loading. It has been found for Systems I and II that the reaches of the generator distance phase backup protection relay are 16.1 Ω at MTA of 85° and 16.8 Ω at MTA of 85° respectively. With the presence of a midpoint STATCOM or an SVC, it has been shown that these reaches are exceeded at some generator loadings and fault locations.

2. The underreaching effect of a midpoint STATCOM is more severe compared to that of an SVC, which results in more cases of relay mal-operation. This is attributed to the distinct V-I characteristic of the STATCOM that maintains the injection of the STATCOM full-load current even at much reduced bus voltages.

3. In the case of three-phase and line-to-line faults, the highest error in the measured impedance by Relay (21) occurred at the lowest generator loadings in both Systems I and II.

4. For the same fault location, the responses of midpoint STATCOM and SVC to the variation in the generator loading cause the error in the measured impedance by Relay (21) to increase as the generator loading decreases.

5. As the midpoint STATCOM and SVC control circuits always operate in a balanced mode (i.e. injecting three-phase balanced current), the severest impact of the midpoint STATCOM and SVC (TUR) occurs during line-to-line faults, at all the generator loading and fault locations in both Systems I and II.

6. In all fault case studies, the error in the measured impedance by Relay (21) increases as the fault location varies from the midpoint of the shunt compensated line to the end of the relay reach.

7. The midpoint STATCOM and SVC have no impact on Relay (21) for faults occurring on the midpoint shunt compensated line from its end near the generator to its midpoint regardless of generator loading or fault type.

8. The adverse effect of the midpoint STATCOM and SVC extends to affect the coordination between generator distance phase backup protection and the GOEC limit.

Such an impact varies also according to the fault type, fault location and generator loading. It has also been found that the maximum settings of Relay (21), which can keep the coordination with the GOEC limits, are 27.54 Ω at MTA of 85° and 20.8 Ω at MTA of 85° for Systems I and II respectively. With the presence of the midpoint STATCOM and SVC, it has been shown that these limits have been exceeded at some generator loadings and fault locations.

9. For the same fault location and in the presence of a midpoint STATCOM or SVC, the coordination index increases as the generator loading decreases. This is true for both three-phase and line-to-line faults. Moreover, the ratio of the loss of coordination cases due to line-to-line faults to that due to three-phase faults is always greater than 1 in Systems I and II.

10. A midpoint STATCOM or SVC has no impact on the coordination between Relay (21) and the generator capability limits for faults occurring on the midpoint shunt compensated line from its end near the generator to its midpoint regardless of generator loading or fault type.

11. The Support Vector Machines classification technique, which is proposed as a replacement of Relay (21) in order to enhance the coordination between generator phase backup protection and the generator steady-state overexcited capability (GOEC) limit in the presence of midpoint FACTS Controllers, is a very promising solution. In this regard, it has been demonstrated that the SVMs classification technique is fast and reliable with a performance efficiency of 95.14% and 96.53% for three-phase and line-to-line faults respectively. In comparison to the performance of Relay (21), the proposed SVM technique reflects an appreciable enhancement in the coordination between generator phase backup protection and generator steady-state overexcited capability limit.

12. The setting of Relay (21) of System I (in accordance to the current Standard) for generator thermal backup protection against system uncleared faults is 23.25 Ω at MTA of 85°. With such a setting, it has been shown that in the absence of a midpoint STATCOM, the generator is over-protected and that Relay (21) restricts the generator overexcitation thermal capability during system disturbances. This restriction does not

allow the supply of the maximum reactive power of the generating unit during such events.

13. The presence of a midpoint STATCOM significantly enhances Relay (21) performance during system disturbances. This enhancement is due to the fact that the STATCOM maintains the voltage of the midpoint bus at "almost" 1 p.u. by injecting inductive current which reduces the levels of the generator output reactive power and the oscillations in the impedance trajectory of Relay (21). Therefore, an existing midpoint STATCOM, installed in a transmission line for the purpose of increasing its power transfer capability, would alleviate the problem caused by Relay (21). This is, however, not an economical solution (installing a midpoint STATCOM) for generators that are connected to uncompensated (no midpoint shunt compensation) transmission lines. In this case, the proposed solution in this thesis is to reduce Relay (21) reach in order to provide a more secure performance during system disturbances. This would allow the generator to supply its maximum reactive power during such events. In this regard, Relay (21) (of System I) reach is reduced from $Z_{21} = 23.25\ \Omega$ at MTA = 85° to $Z_{21} = 9.6\ \Omega$ at MTA = 85°.

6. REFERENCES

[1] Y.H. Song and A.T. Johns, *Flexible AC Transmission Systems (FACTS)*, Institution of Electrical Engineers, London, 1999.

[2] N.G. Hingorani and L. Gyugyi, *Understanding FACTS: Concepts and Technology of Flexible AC Transmission Systems*, IEEE Press, New York, 2000.

[3] K.K. Sen and M.L. Sen, *Introduction to FACTS Controllers*, John Wiley & Sons, Inc., Hoboken, NJ, 2009.

[4] R.M. Mathur and R.K. Varma, *Thyristor-Based FACTS Controllers for Electrical Transmission Systems*, IEEE, Piscataway, NJ, 2002.

[5] P.M. Anderson and R.G. Farmer*, Series Compensation of Power Systems*, PBLSH! Inc., 1996.

[6] J.L. Blackburn and T.J. Domin, *Protective Relaying: Principles and Applications*, CRC Press, 3rd edition, 2007.

[7] T.S. Sidhu and M. Khederzadeh, "TCSC Impact on Communication – Aided Distance Protection Schemes and its Mitigation," IEE Proceedings: Generation, Transmission and Distribution, Vol. 152, Issue 5, September 2005, pp. 714 – 728.

[8] P.K. Dash, A.K. Pradhan, G. Panda and A.C. Liew, "Digital Protection of Power Transmission Lines in the Presence of Series Connected FACTS Devices," Proceedings of the IEEE Power Engineering Society Winter Meeting, Singapore, January 23-27 2000, Vol. 3, pp. 1967 - 1972.

[9] P. K. Dash, A. K. Pradhan and G. Panda, "Distance Protection in the Presence of Unified Power Flow Controller," Electric Power Systems Research, Vol. 54, No. 3, June 2000, pp. 189-198.

[10] P.K. Dash, A.K. Pradhan, G. Panda and A.C. Liew, "Adaptive Relay Setting for Flexible AC Transmission Systems (FACTS)," IEEE Transactions on Power Delivery, Vol. 15, No. 1, January 2000, pp. 38 – 43.

[11] X. Zhou, H. Wang, R.K. Aggarwal, and P. Beaumont, "Performance Evaluation of a Distance Relay as Applied to a Transmission System with UPFC," IEEE Transactions on Power Delivery, Vol. 21, No. 3, July 2006, pp. 1137-1147.

[12] J. Lim and J.N. Jiang, "A Refined Differential Current Protection Method in the FACTS-Compensated Line," Proceedings of the IEEE Power and Energy Society General Meeting, Pittsburgh, PA, July 20-24, 2008, pp. 1-6.

[13] K. El-Arroudi, G. Joos and D.T. McGillis," Operation of Impedance Protection Relays with the STATCOM," IEEE Transactions on Power Delivery, Vol. 17, No. 2, April 2002, pp. 381-387,

[14] T. S. Sidhu, R.K. Varma, P.K. Gangadharan, F.A. Albasri and G.R. Ortiz, "Performance of Distance Relays on Shunt-FACTS Compensated Transmission Lines," IEEE Transactions on Power Delivery, Vol. 20, No. 3, July 2005, pp. 1837-1845.

[15] F.A. Albasri, T.S. Sidhu and R.K. Varma, "Performance Comparison of Distance Protection Schemes for Shunt-FACTS Compensated Transmission Lines," IEEE Transactions on Power Delivery, Vol. 22, No. 4, October 2007, pp. 2116 – 2125.

[16] W. Elmore, *Protective Relaying Theory and Applications*, CRC Press, second edition, 2004.

[17] D. Reimert, *Protective Relaying for Power Generation Systems*, CRC Press, 2006.

[18] P.M. Anderson, *Power System Protection*, IEEE Press-McGraw-Hill, 1999.

[19] G. Ziegler, Numerical distance Protection principle and Applications, Publics Corporate Publishing, Erlangen, Germany, Publicis Corporate Publishing, Erlangen, third edition, 2008.

[20] C.J. Mozina, M. Reichard and Z. Bukhala, "Coordination of Generator Protection with Generator Excitation Control and Generator Capability," Working Group J-5 of the Rotating Machinery Subcommittee of the Power System Relay Committee, Proceedings of the IEEE Power Engineering Society General Meeting, Tampa, FL, June 24-28, 2007, pp. 1-17.

[21] S. Patel, K. Stephan, M. Bajpai, R. Das, T.J. Domin, E. Fennell, J.D. Gardell, I. Gibbs, C. Henville, P.M. Kerrigan, H.J. King, P. Kumar, C.J. Mozina, M. Reichard, J. Uchiyama, S. Usman, D. Viers, D. Wardlow and M. Yalla, "Performance of Generator Protection during Major System Disturbances," IEEE Transactions on Power Delivery, Vol. 19, No. 4, October 2004, pp. 1650-1662.

[22] D. Tziouvaras, "Relay Performance during Major System Disturbances," Proceedings of the 60th Annual Conference for Protective Relay Engineers, College Station, TX, March 27-29, 2007, pp. 251-270.

[23] PSCAD/EMTDC User's Manual, Manitoba HVDC Research Centre, 2003.

[24] IEEE Special Publication 08TP200 "Voltage Sourced Converter (VSC) Applications in Power Transmission" November 2007.

[25] P. Kundur, *Power System Stability and Control*, McGraw-Hill, 1994.

[26] IEEE Std. C37.102, "IEEE Guide for AC Generator Protection," 2006.

[27] IEEE Tutorial PES Tutorial 95 TP 102 "IEEE Tutorial on the Protection of Synchronous Generators," 1995.

[28] Charles Mozina, "Power Plant Protection and Control Strategies for Blackout Avoidance," Proceedings of the IEEE Power Systems Conference: Advanced Metering,

Protection, Control, Communication, and Distributed Resources, Clemson, SC, March 14-17, 2006, pp. 200-218.

[29] T. Hastie, R Tibshirani, J. Friedman, *The Elements of Statistical Learning, Data mining, Inference, and Prediction,* 2nd Edition, Springer, Inc., New York, NY, USA, 2009.

[30] C. Bishop, *Pattern Recognition and Machine Learning*, Springer, Inc., New York, NY, USA, 2007.

[31] R.O. Duda, P.E. Hart, and D.G. Stork*, Pattern Classification*, John Wiley and Sons, 2nd Edition, 2001.

[32] C.J. Burges, "A Tutorial on Support Vector Machines for Pattern Recognition," Journal of Data Mining and Knowledge Discovery, Vol. 2, No. 2, June 1998, pp. 121-167.

[33] S.R. Gunn, Support Vector Machines for Classification and Regression, Technical report, Faculty of Engineering, Science and Mathematics, School of Electronics and Computer Science, University of Southampton, May 1998.

[34] N. Cristianini, "Support Vectors and Kernel Machines," Proceedings of the 18th International Conference on Machine Learning (ICML 2001), Williamstown, MA, USA, June 28-July 1, 2001.

[35] T. Fletcher, "Support Vector Machines Explained," Tutorial paper, Centre of Computational Statistics and Machine Learning, University College London (UCL), March 2009.

[36] S. Boyd S, L. Vandenberghe, *Convex Optimization*, Cambridge University Press, 2004.

[37] R. Fletcher, *Practical Methods of Optimization*, Wiley, 2nd edition, 2000.

[38] L. Kaufman, "Solving the quadratic programming problem arising in support vector classification," an Article published in a book 'Advances in Kernel Methods' MIT Press, Cambridge, MA, USA, 1999.

[39] B.E. Boser, I.M. Guyon and V. Vapnik, "A Training Algorithm for Optimal Margin Classifiers," Proceedings of the 5th Annual Workshop on Computational Learning Theory (COLT '92), Pittsburgh, PA, July 27-29, 1992, pp. 144-152.

[40] B. Scholkopf, C.J.C. Burges, and S. Mika, *Advances in Kernel Methods*, MIT Press Cambridge, MA, 1998.

[41] K.R. Muller, S. Mika, G. Ratsch, K. Tsuda and B. Scholkopf, "An introduction to Kernel-Based Learning Algorithms," IEEE Transactions on Neural Network, Vol. 12, issue 2, March 2001, pp. 181–201.

[42] S.T John and N. Cristianini, *Kernel Methods for Pattern Analysis*, Cambridge University Press, 2004.

[43] B Scholkopf, A. Smola, *Learning with Kernels*, MIT Press, 2002.

[44] V. Vapnik, *The Nature of Statistical Learning Theory*, Springer, 2nd edition, 1999.

[45] B. Scholkopf, K Sung, C. Burges, F. Girosi, P. Niyogi, T. Poggio and V. Vapnik, "Comparing Support Vector Machines With Gaussian Kernels to Radial Basis Function Classifiers," IEEE Transactions on Signal Processing, Vol. 45, issue 11, November 1997, pp. 2758–2765.

[46] L.S. Moulin, A.P.A. da Silva, M.A. El-Sharkawi and R.J. Marks, " Support Vector Machines for Transient Stability Analysis of Large-Scale Power Systems," IEEE Transactions on Power Systems, Vol. 19, No. 2, May 2004, pp. 818-825.

[47] V. Malathi and N.S. Marimuthu, "Support Vector Machine for Discrimination Between Fault and Magnetizing Inrush Current in Power Transformer," Journal of Computer Science, Vol. 3, issue 11, November 2007, pp. 894-897.

[48] S.R. Samantaray and P.K. Dash, "Transmission Line Distance Relaying Using Machine Intelligence Technique," IET Generation, Transmission, and Distribution, Vol. 2, No. 1, 2008, pp. 53-61.

[49] U.B. Parikh, D. Biswarup and R.P. Maheshwari, "Combined Wavelet-SVM Technique for Fault Zone Detection in a series Compensated Transmission line," IEEE Transactions on Power Delivery, Vol. 23, No. 4, October 2008, pp. 1789-1794.

[50] B. Ravikumar, D. Thukaram and H.P. Khincha, "An Approach Using Support Vector Machines for Distance Relay Coordination in Transmission System," IEEE Transactions on Power Delivery, Vol. 24, No. 1, January 2009, pp. 79-88.

[51] B. Scholkopf, K. Tsuda and J.P. Vert, *Kernel methods in computational biology*, MIT Press, 2004.

[52] "SVM and Kernel Methods MATLAB Toolbox" available @ misc{SVM-KM Toolbox}, 2008.

[53] IEEE Std. C50.13, " IEEE Standard for Cylindrical-Rotor 50 Hz and 60 Hz Synchronous Generators Rated 10 MVA and Above," 2005.

[54] IEEE Std. C50.12, "IEEE Standard for Salient-Pole 50 Hz and 60 Hz Synchronous Generators/Motors for Hydraulic Turbine Applications Rated 5 MVA and Above," 2005.

[55] A. Murdoch, G.E. Boukarim, B.E. Gott, M.J D'Antonio and R.A. Lawson, "Generator Overexcitation Capability and Excitation System Limiters," Proceedings of the IEEE Power Engineering Society Winter Meeting, Columbus, OH, January 28 –February 1, 2001, Vol. 1, pp. 215-220.

[56] IEEE Std. 421.5, "IEEE Recommended Practice for Excitation System Models for Power System Stability Studies," 2005.

[57] G.K. Morison, B. Gao and P. Kundur, "Voltage Stability Analysis using Static and Dynamic Approaches," IEEE Transactions on Power Systems, Vol. 8, No. 3, August 1993, pp. 1159-1171.

[58] C.W. Taylor, Power System Voltage Stability, McGraw-Hill, New York, 1994.

[59] IEEE Task Force on Excitation Limiters, Excitation System Subcommittee, Performance and Modeling Working Group, Energy Development and Power Generation Committee, "Recommended Models for Overexcitation Limiting Devices," IEEE Transactions on Energy Conversion, Vol. 10, No. 4, December 1995, pp. 706-712.

[60] C.R. Mummert, " Excitation System Limiter Models for use in System Stability Studies," Proceedings of the IEEE Power Engineering Society Winter Meeting, New York, NY, January 31 - February 4, 1999, Vol. 1, pp. 187-192.

[61] A. Murdoch, R.W. Delmerico, S. Venkataraman, R.A. Lawson, J.E. Curran and W.R. Pearson, "Excitation System Protective Limiters and Their Effect on Volt/Var Control-Design, Computer Modeling, and Field Testing," IEEE Transactions on Energy Conversion, Vol. 15, No. 4, December 2000, pp. 440-450.

[62] A. Murdoch and M.J. D'Antonio, "Generator Excitation Systems Performance Specification to Meet Interconnection Requirements," Proceedings of the IEEE International Electric Machines and Drives Conference (IEMDC 2001), Cambridge, MA, June 17-20, 2001, pp. 317-322.

[63] M.J. Basler, "Excitation Systems: The Current State of the Art," Proceedings of the IEEE Power Engineering Society General Meeting, Montreal, Quebec, June 18-22, 2006, pp. 1-7.

[64] S. Patterson, "Overexcitation Limiter Modeling for Power System Studies," Proceedings of the IEEE Power Engineering Society General Meeting, San Francisco, CA, June 12-16, 2005, Vol. 1, pp. 985-988.

[65] Western Systems Coordinating Council (WSCC), "Guidelines for Over Excitation System Limiter (OEL) and Over Excitation Protection (OEP) Testing," 2000.

[66] N. Mohan, T.M. Undeland and W.P. Robbins, *Power Electronics: Converters, Applications, and Design,* Wiley, New York, 1995.

7. APPENDICES

APPENDIX A

DATA OF THE SYSTEMS UNDER STUDY

A.1 Synchronous Generators

Table A.1. Synchronous generators data.

	G_1	G_2
Rating, MVA	300	492
Rated voltage, kV	23	20
Armature resistance, r_a, p.u.	0.0045	0.003
Leakage reactance, x_l, p.u.	0.16	0.12
Direct-axis synchronous reactance, x_d, p.u.	1.15	1.888
Quadrature-axis synchronous reactance, x_q, p.u.	0.75	1.82
Direct-axis transient reactance, $x_d^{'}$, p.u.	0.314	0.205
Quadrature-axis transient reactance, $x_q^{'}$, p.u.	-	0.42
Direct-axis subtransient reactance, $x_d^{''}$, p.u.	0.25	0.178
Quadrature-axis subtransient reactance, $x_q^{''}$, p.u.	0.28	0.175
Direct-axis transient open-circuit time constant, $T_{do}^{'}$, s	4.7	6.5
Quadrature-axis transient open-circuit time constant, $T_{qo}^{'}$, s	-	0.55
Direct-axis subtransient open-circuit time constant, $T_{do}^{''}$, s	0.03	0.04
Quadrature-axis subtransient open-circuit time constant, $T_{qo}^{''}$, s	0.08	0.09
Inertia constant, H, s	4	3
Rated power factor	0.94	0.76

A.2 Excitation System

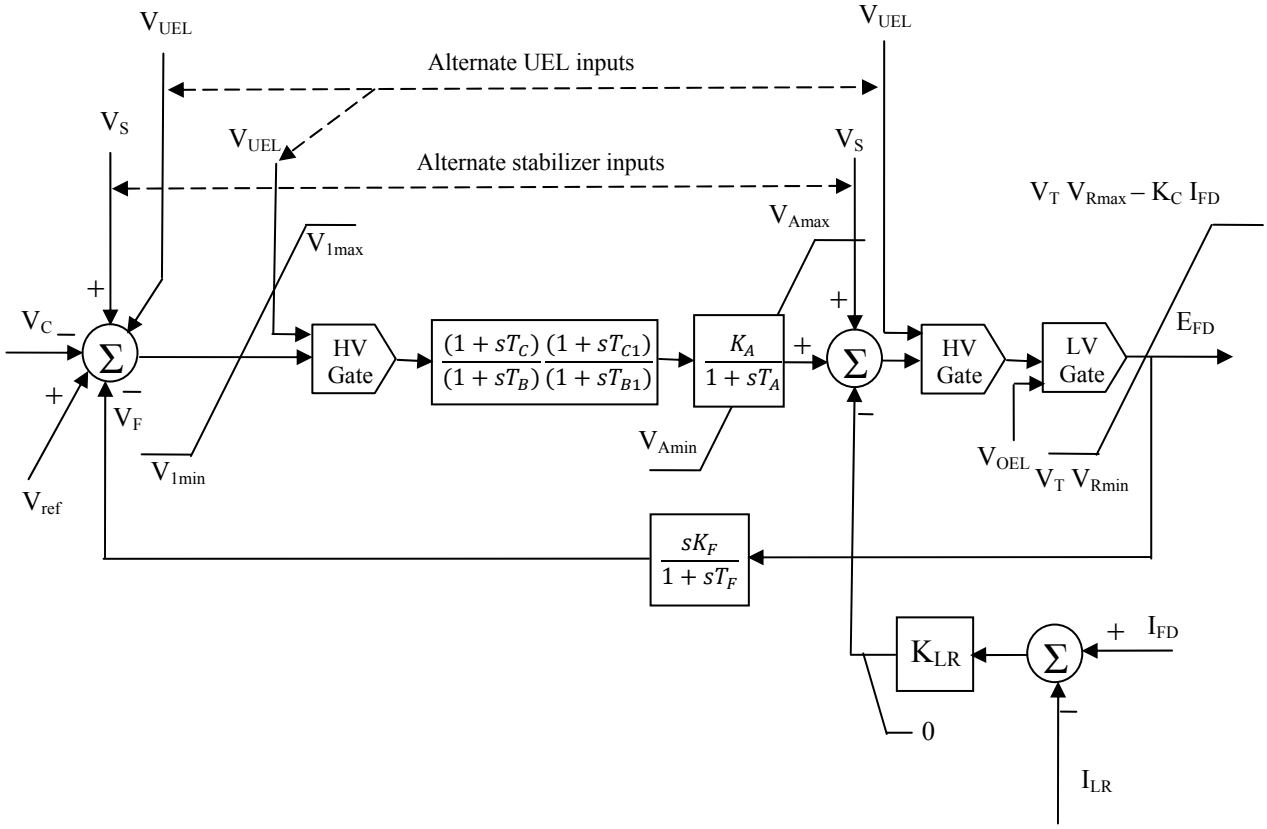

Figure A.1. Excitation system type ST1A [56].

Table A.2. Excitation system (Type: ST1A) data.

K_A = 210	T_R = *0.02, s*
Tc = T_B = *1.0, s*	T_A = *0*
V_{AMAX} = *15*	V_{AMIN} = *-15*
V_{RMAX} = *6.43 p.u.*	V_{RMIN} = *-6.0 p.u*
K_C = *0.038*	K_F, T_F not used = 0
K_{LR} = *4.54*	T_B, T_C, T_{B1}, T_{C1} not used = 0

A.3 Transformers

Table A.3. Transformers data.

	System I	System II
Rating, MVA	300	492
Winding connection	Δ / Yg	Δ / Yg
Voltage ratio	23/230 kV	20/230 kV
Leakage reactance, x_T, p.u.	0.1	0.1

A.4 Transmission Lines

All the transmission lines in Systems I and II have the same series impedance and shunt admittance per unit length.

Table A.4. Transmission lines data.

	Systems I and II
Transmission voltage	230 kV
Shunt admittance	3.2×10^{-6} S/km
Positive-sequence Impedance	$0.51 \angle 85.98°$ Ω/km
Zero-sequence Impedance	$1.378 \angle 74.69°$ Ω/km

A.5 Static Synchronous Compensators (STATCOM)

Table A.5. STATCOM data.

	System I	System II
STATCOM rating	± 100 MVA	± 100 MVA
Interfacing transformer	3 winding (Y/y/d)	3 winding (Y/y/d)
Transformer ratio	230/11/11 kV	230/11/11 kV
Transformer impedance	0.1 p.u	0.1 p.u
Capacitor	300 μF	500 μF

A.6 Static Var Compensators (SVC)

Table A.6. SVC data.

	System I	System II
Interfacing transformer	3 winding (Y/y/d)	3 winding (Y/y/d)
Transformer rating	200 MVA	300 MVA
Transformer ratio	230/11/11 kV	230/11/11 kV
Transformer impedance	0.1 p.u	0.1 p.u
SVC inductive rating	100 MVA	150 MVA
SVC capacitive rating	167 MVA	267 MVA
Number of capacitor stages	2	2

A.7 Large Systems: S_1, S_2, S_3 (System II)

The infinite bus system in System I is represented by a constant sinusoidal voltage source at the power frequency. The three large systems in Systems II are represented by constant sinusoidal voltage sources at 60-Hz behind source impedances.

Table A.7. Large systems data.

	System II
Rated voltage	230 kV
Positive-sequence impedance	$25.9 \angle 80°$ Ω
Zero-sequence impedance	$25.9 \angle 80°$ Ω

APPENDIX B

THE VOLTAGE SOURCE CONVERTER

B.1 Voltage-Source Converter

The Voltage-Source Converter (VSC) is the basic building block of many of the modern FACTS devices such as STATCOM, SSSC, and UPFC. The voltage-source converter uses switching gates that have turn-on and turn-off capability such as Gate Turn-Off Thyristor (GTO), Insulated Gate Bipolar Transistor (IGBT), MOS Turn-Off Thyristor (MTO) and Insulated Gate-Commutated Thyristor (IGCT). The voltage-sourced converter generates ac voltage from a dc voltage. With a voltage-source converter, the magnitude, the phase angle and the frequency of the output voltage can be controlled. It has the capability to transfer power in either direction by just reversing the polarity of the current. A typical topology of a GTO–based three-phase two level voltage-source converter is shown in Figure B.1 (also known as six-pulse converter). The voltage-source converter dc voltage is supported by capacitor(s) large enough to at least handle a sustained charge/discharge current without a significant change in the dc voltage.

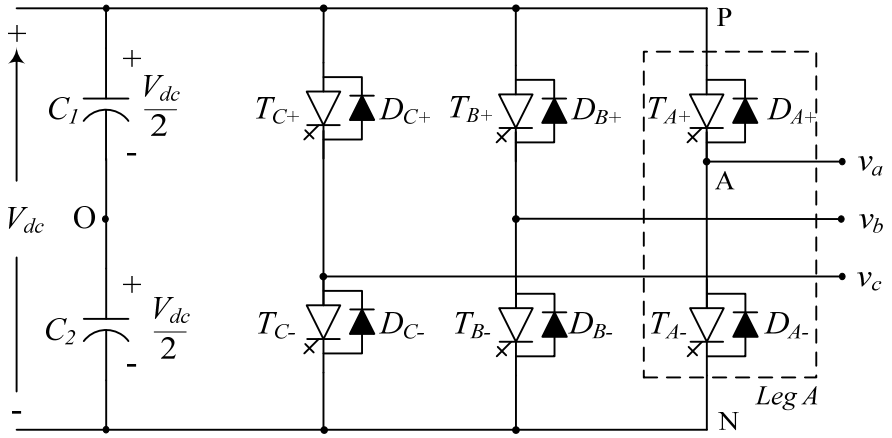

Figure B.1. Topology of a three-phase, two-level, voltage-source converter.

The operating principle of a converter can be explained with the help of GTO and diode switching operation. For example, when GTO T_{A+} is switched '*on*', the phase *a* ac voltage would jump to $+V_{dc}/2$. If the current happens to flow from P to A through GTO T_{A+} (shown in the dotted box in Figure B.1), the power would flow from the dc side to the ac side acting as an inverter. On the other hand, if the current happens to flow from A to P, it would flow through

diode D_{A+} even if GTO T_{A+} is switched '*on*', and the power would flow from the ac side to dc side acting as a rectifier.

There are many types of converter concepts within the voltage-sourced converter category for example: multi pulse, multi level, and cascade concept. As all the converter topologies operate by turn-on and turn-off of power electronic gates, they require some sort of switching circuitry. The inverter switching strategies used at present can be classified into two main categories [66]:

1. ***Fundamental frequency switching***: In this technique, the switching of each semiconductor device is limited to one turn-on and one turn-off per power cycle. The six-pulse converter shown in Figure B.1 produces a quasi-square-wave output with this method, which has an unacceptably high harmonic content. In practice, a number of six-pulse units are combined in series and/or parallel to achieve a better waveform quality and higher power ratings.
2. ***Pulse-Width Modulation* (*PWM*)**: In this technique, the semiconductor switches are turned '*on*' and '*off*' at a rate considerably higher than the power frequency. The output waveform has multiple pulses per half-cycle. This shifts the undesirable harmonics in the output to higher frequencies and filtering is possible with smaller components. This method suffers, however, from higher switching losses compared to the previous switching technique. The PWM method is described in detail in the following section.

B.1.1 Pulse Width Modulation

The Pulse Width Modulation based switching scheme creates a train of switching pulses by comparing a reference wave "v_{ref}" and a carrier wave "$v_{carrier}$". The *ac* output voltage of the converter consists of multiple pulses per half-cycle and the width of the pulses can be varied to change the amplitude of the fundamental frequency of the output voltage. The PWM converter related basic terms that are used throughout this thesis are given below:

V_{ref} = Reference sinusoidal waveform peak magnitude, volts.

f_r = Reference sinusoidal wave frequency, Hz, 60 Hz in general.

$V_{carrier}$ = Triangular carrier wave peak magnitude, volts, generally kept constant.

f_c = Triangular carrier wave frequency, Hz.

MI = $V_{ref}/V_{carrier}$, amplitude modulation ratio, or modulation index.

$m_f = f_c/f_r$, frequency modulation ratio.

Figure B.2 shows one leg of a six-pulse converter and Figure B.3 shows the generation of the switching pulses by comparing the reference wave with the high frequency triangular carrier wave. The turn-on and turn-off of the GTOs takes place corresponding to the crossing points of the saw-tooth wave and the sine wave. For example, when the rising slope of the triangular wave crosses the sinusoidal wave, GTO T_{A+} switches '*on'* and GTO T_{A-} switches '*off*'. Similarly, when the negative slope of the triangular wave crosses the sine wave, GTO T_{A-} turns '*on'* and GTO T_{A+} turns '*off*'. The switching pair T_{A+} and T_{A-} are complement to each other.

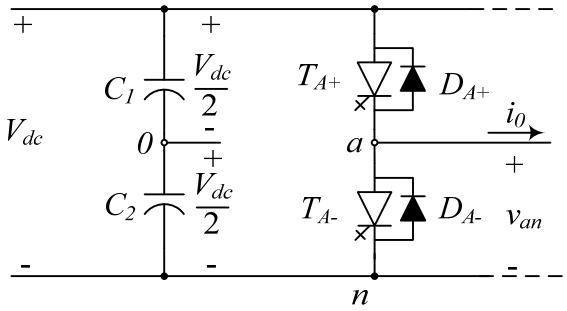

Figure B.2. One leg of a voltage-source converter.

The output voltage "v_{an}" of the PWM converter contains a fundamental frequency component "v_{a0}" and harmonics. Furthermore, the output voltage is symmetrical about the zero crossing of the sine wave (if the triangular wave frequency is chosen to be an odd multiple of the reference wave). In general, the magnitude of the triangular carrier wave is kept constant and the magnitude of the sinusoidal reference wave is either increased or decreased (i.e. increase or decrease of modulation index, *MI*), to increase or decrease the amplitude of the fundamental component of the ac output voltage. When the sinusoidal reference wave amplitude, V_{ref} is less than $V_{carrier}$, the *ac* output voltage changes linearly with modulation index, and when V_{ref} is greater than $V_{carrier}$, the output voltage tends to become a square wave.

The magnitude of the PWM converter output voltage can be controlled from zero to the maximum value and the phase angle and/or frequency can be controlled by controlling the reference wave phase and/or frequency almost instantaneously [2], [66]. The PWM method has certain advantages such as faster response and capability for harmonic elimination [2], [66] compared to the fundamental switching method. The PWM method is used to model the voltage-source converter in this research work.

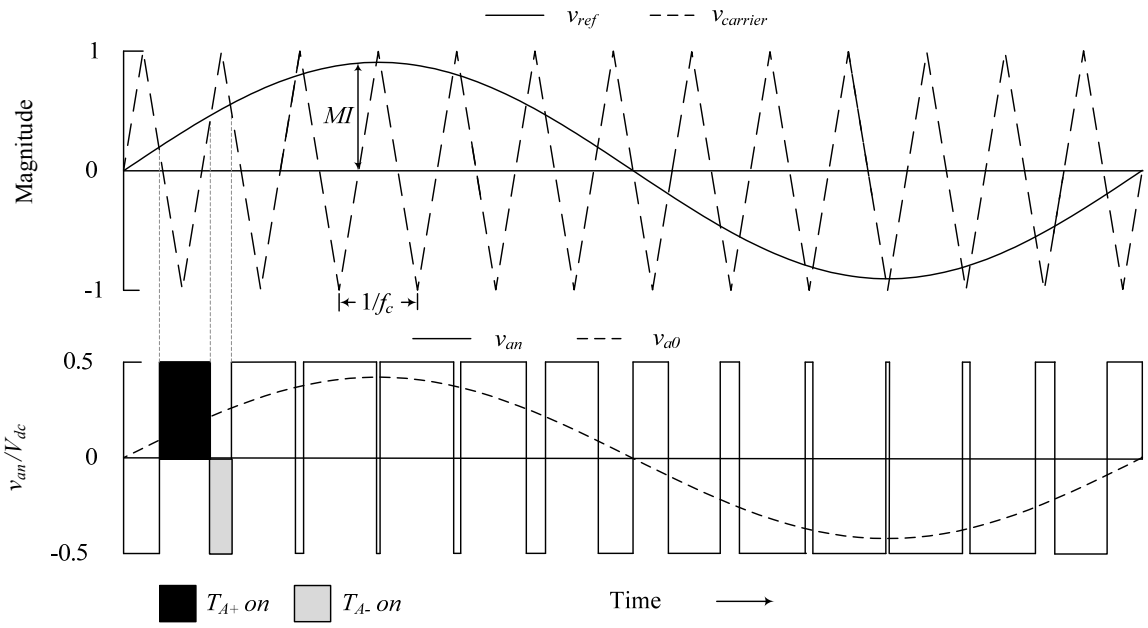

Figure B.3. Pulse-width modulation switching signal generation and output voltage.

B.2 Principle of Voltage Source Converter Operation

Consider a VSC connected to an AC system through a lossless reactor as illustrated in Figure B.4. The converter produces an AC voltage with a fundamental frequency equal to that of the AC reference voltage. The voltage at the supply bus is assumed to be $V_s \angle 0^0$, and the AC voltage produced by the VSC is taken to be $V_{sh} \angle \delta_{sh}$. X_l is the reactance of the converter reactor.

The active and the reactive power can be expressed respectively as

$$P = \frac{V_{sh} V_s}{X_l} \sin \delta_{sh} \tag{B.1}$$

$$Q = \frac{V_{sh} V_s}{X_l} \cos \delta_{sh} - \frac{V_s^{\,2}}{X_l} \ . \tag{B.2}$$

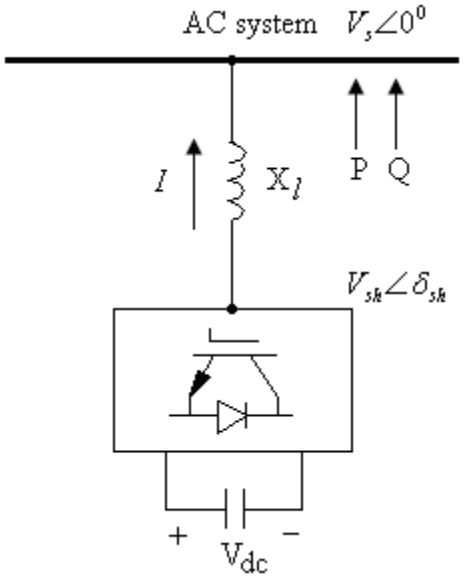

Figure B.4. A VSC connected to an AC system.

With respect to these two Equations, the following observations are noticed:

1. The active power flow between the AC source and the VSC is controlled by the phase angle δ_{sh}. The active power flows into the AC source from the VSC for $\delta_{sh} > 0$, and flows out of the AC source from the VSC for $\delta_{sh} < 0$,
2. The reactive power flow is determined mainly by the amplitude of the AC source voltage, V_s, and the VSC output fundamental voltage, V_{sh}, as the angle δ_{sh} is generally small. For $V_{sh} > V_s$, the VSC generates reactive power and while it consumes reactive power when $V_{sh} < V_s$.

Because of its key steady-state operational characteristics and impact on system voltage and power flow control, the VSC is becoming the basic building block employed in the new generation of FACTS Controllers.

APPENDEX C

CALCULATIONS OF RELAY (21) REACH

According to Section 2.7.2.4 (Relay (21) setting criteria), Relay (21) is set within the generator steady-state overexcited capability (GOEC) with adequate margin overload and stable power swings. Therefore, Relay (21) elements of G_1 and G_2 are, generally, set at the smallest of the following three criteria [26], [27]:

A. Hydrogenerator (G_1):

1. 120% of the longest line with system infeed currents (Transmission line trip dependability):

$$Z_{21} = \left[X_T + \left(1.2 \times z_{line\_prim\_infeed}^{p.u}\right)\right] \times Z_{Base\_Relay} \quad \text{(C.1)}$$

$$z_{line\_prim} = 152.7058 \times \left(\frac{23}{230}\right)^2 = 1.527058\ \Omega \quad \text{(C.2)}$$

$$Z_{Base\_Gen} = \frac{23^2}{300} = 1.76333\ \Omega \quad \text{(C.3)}$$

$$z_{line\_prim}^{p.u} = \frac{1.527058}{1.76333} = 0.866\ p.u. \quad \text{(C.4)}$$

$$Z_{Base\_Relay} = \frac{\left[V_{ph\_Gen}/R_v\right]}{\left[I_{ph\_Gen}/R_c\right]} = \frac{\left[\left(\frac{23000}{\sqrt{3}}\right)/200\right]}{\left[7540/1600\right]} = 14.10589\ \Omega \quad \text{(C.5)}$$

$$\therefore Z_{21} = [0.1 + (1.2 \times 0.866)] \times 14.10589 = 16.1\ \Omega. \quad \text{(C.6)}$$

2. 50% to 67% of the generator load impedance (Z_{load}) at the rated power factor angle (RPFA) of the generator. This provides a 150% to 200% margin over the generator full load (Generator thermal backup protection):

$$Z_{21} = (0.5\ to\ 0.67) \times \frac{Z_{Max\ loading\ at\ RPF}}{\cos\ (Transmission\ line\ angle - RPFA)} \quad \text{(C.7)}$$

$$Z_{Max\ loading\ at\ RPF} = \frac{KV_{LL}^2}{Gen\_MVA} \times \frac{R_c}{R_v} = \frac{23^2}{300} \times \frac{1600}{200} = 14.10667\ \Omega \quad \text{(C.8)}$$

$$Z_{21\_2} = 0.67 \times \frac{14.10667}{cos\ (85.9732 - 19.95)} = 23.25\ \Omega. \quad \text{(C.9)}$$

3. 80% to 90% of the generator load impedance at the maximum torque angle (typically 85°) (Maximum setting allowable of Relay (21) (Z_{GCC}):

$$Z_{21} = (0.8\ to\ 0.9) \times\ Z_{GCC\_MTA} \quad \text{(C.10)}$$

$$Z_{GCC\_MTA} = \frac{KV_{LL}^2}{Gen\_MVA\_MTA} \times \frac{R_c}{R_v} = \frac{23^2}{138} \times \frac{1600}{200} = 30.6\ \Omega \quad \text{(C.11)}$$

$$Z_{21} = 0.9 \times\ Z_{GCC\_MTA} =\ 0.9\ \times 30.6\ = 27.54\ \Omega. \quad \text{(C.12)}$$

B. Turbogenerator (G_2):

1. 120% of the longest line with system infeed currents (Transmission line trip dependability):

$$Z_{21} =\ \left[X_T +\ \left(1.2 \times z_{line\_prim\_infeed}^{p.u}\right)\right] \times Z_{Base\_Relay} \quad \text{(C.13)}$$

$$z_{line\_prim} =\ 152.7058 \times \left(\frac{23}{230}\right)^2 = 1.527058\ \Omega \quad \text{(C.14)}$$

$$Z_{Base\_Gen} = \frac{23^2}{300} = 1.76333\ \Omega \quad \text{(C.15)}$$

$$z_{line\_prim}^{p.u} = \frac{1.527058}{1.76333} = 0.866\ p.u. \quad \text{(C.16)}$$

$$Z_{Base\_Relay} = \frac{\left[V_{ph\_Gen}/R_v\right]}{\left[I_{ph\_Gen}/R_c\right]} = \frac{\left[\left(\frac{20000}{\sqrt{3}}\right)/166.67\right]}{\left[14202.8/3600\right]} = 17.56\ \Omega \quad \text{(C.17)}$$

$$\therefore Z_{21} =\ [0.1 +\ (1.2 \times 1.88)] \times 17.56 = 41.4\ \Omega. \quad \text{(C.18)}$$

2. 50% to 67% of the generator load impedance (Z_{load}) at the rated power factor angle (RPFA) of the generator. This provides a 150% to 200% margin over the generator full load (Generator thermal backup protection):

$$Z_{21} = (0.5\ to\ 0.67) \times \frac{Z_{Max\ loading\ at\ RPF}}{\cos\ (Transmission\ line\ angle - RPFA)} \quad \text{(C.19)}$$

$$Z_{Max\ loading\ at\ RPF} = \frac{KV_{LL}^2}{Gen\_MVA} \times \frac{R_c}{R_v} = \frac{20^2}{492} \times \frac{3600}{166.67} = 17.65\ \Omega \quad \text{(C.20)}$$

$$Z_{21} = 0.67 \times \frac{14.10667}{cos\ (85.9732 - 40.54)} =\ 16.8\ \Omega. \quad \text{(C.21)}$$

3. 80% to 90% of the generator load impedance at the maximum torque angle (typically 85°) (Maximum setting allowable of Relay (21) (Z_{GCC}):

$$Z_{21} = (0.8\ to\ 0.9) \times\ Z_{GCC\_MTA} \quad \text{(C.22)}$$

$$Z_{GCC\_MTA} = \frac{KV_{LL}^2}{Gen\_MVA\_MTA} \times \frac{R_c}{R_v} = \frac{20^2}{373} \times \frac{3600}{166.67} = 23.16\ \Omega \quad \text{(C.23)}$$

$$Z_{21} = 0.9 \times\ Z_{GCC\_MTA} =\ 0.9\ \times 23.16\ = 20.8\ \Omega. \quad \text{(C.24)}$$

APPENDEX D

AN EXAMPLE OF A CLASSIFICATION PROBLEM WITH HARD LIMIT SVMs

The following example is provided in order to illustrate a classification problem with hard limit Support Vector Machines (SVMs). This example considers the linear separable training data which consist of a vector $\boldsymbol{x}$ with **N = 4** components $\boldsymbol{x}_i$, where i = 1,2,3 and 4 as follows

$$\boldsymbol{x}_1 = \begin{bmatrix}1\\0\end{bmatrix}, \boldsymbol{x}_2 = \begin{bmatrix}2\\2\end{bmatrix}, \boldsymbol{x}_3 = \begin{bmatrix}-2\\2\end{bmatrix}, \boldsymbol{x}_4 = \begin{bmatrix}-2\\0\end{bmatrix}.$$

y_i is the label associated with the vector $\boldsymbol{x}_i$ (y_i = 1 for Class A, the red balls, y_i = -1 for Class B, the black balls) as follows y_1 = 1, y_2 = -1, y_3 = -1 and y_4 = 1. The training data and the corresponding labels are plotted in the R-X plane as shown in Figure D.1.

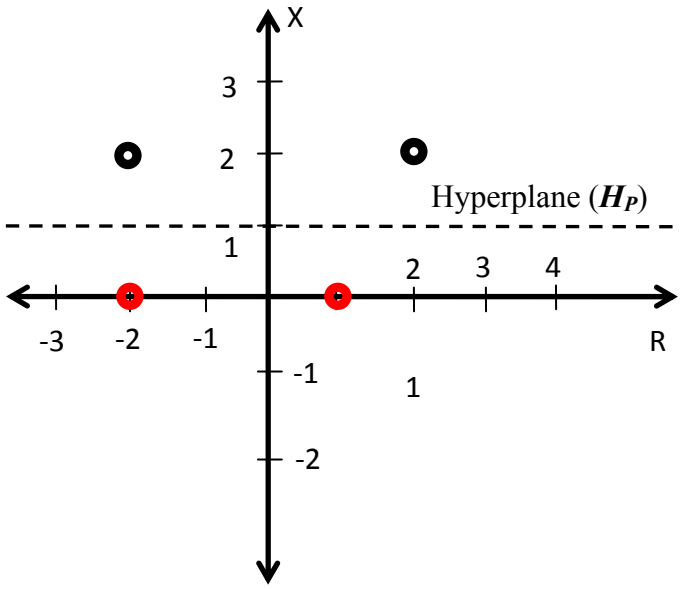

Figure D.1. A support vector machine numerical example.

The goal is to find the optimum hyperplane which verifies the largest margin m_r separates the two classes of data. The optimum hyperplane $\boldsymbol{H_P}$ is that maximizes the distance m_r and at the same time minimizes the magnitude of the weight vector $\|\boldsymbol{w}\|$.

Applying duality principle, yields to Eq. (3.20)

$$\boldsymbol{L_D} \equiv \sum_{\mathrm{i}=1}^{\mathrm{N}} \alpha_i - \frac{1}{2}\boldsymbol{\alpha^T H \alpha} \quad \text{subject to } \alpha_i \geq 0 \; \forall_{\mathrm{i}} \, , \sum_{\mathrm{i}=1}^{\mathrm{N}} \alpha_i y_i = 0,$$

which can be solved using Quadratic Programming. Using Eq. (3.19), the Hessian matrix $\boldsymbol{H}$ is obtained as follows

$$H_{i,j} = y_i y_j \boldsymbol{x}_i \cdot \boldsymbol{x}_j$$

This gives $\boldsymbol{H} = \begin{bmatrix} 1 & -2 & 2 & 2 \\ -2 & 8 & 0 & 4 \\ 2 & 0 & 8 & -4 \\ -2 & 4 & -2 & 4 \end{bmatrix}$.

Using Quadratic Programming, the Lagrangian multipliers are obtained as

$$\boldsymbol{\alpha} = \begin{bmatrix} 0 \\ 0 \\ 0.5 \\ 0.5 \end{bmatrix}.$$

Using Eq. (3.16) $\boldsymbol{w} = \sum_{\mathrm{i}=1}^{\mathrm{N}} \alpha_i y_i \boldsymbol{x}_i$, this results in $\boldsymbol{w} = \begin{bmatrix} 0 \\ -1 \end{bmatrix}$.

Applying Eq. (3.26), yields that $b = 1$.

Finally, any unknown sample is defined as follows

$$y_{unknown} = sign(\boldsymbol{x}_{unknown} \cdot \boldsymbol{w} + b \,).$$